2-4 Analysis Method

2-4-1 Data processing

The TDIP data processing involves the determination of 3 parameters, i.e., apparent resistivity, chargeability as well as metal factor. The first 2 parameters are calculated directly by the receiver unit during data acquisition. The third one is calculated as a simple relation between the first 2 parameters. These 3 parameters are calculated as follow:

a) Apparent resistivity (ρ)

$$\rho = K\frac{V_P}{I}$$

Where, $K = \pi an(n+1)(n+2)$ and ***Vp*** is the received voltage in volts, ***a*** is the A-spacing in meters, ***n*** is the N-spacing and ***I*** is the transmitted current in Amperes.

b) Chargeability (*M*)

$$M = \frac{1}{V_P}\int_{t_1}^{t_2} V_t dt$$

Where, ***Vp*** is the primary voltage in volts and ***Vs*** is the secondary voltage in volts.
Here, the secondary voltage is calculated from 55msec. to 1555msec.

c) Metal factor (*MF*)

$$MF = \frac{M}{\rho} \times 100$$

Where, M is the chargeability (mV/V) and ρ the apparent resistivity (Ω-m)

2-4-2 Topographic corrections

Since the apparent resistivity is calculated here as a function of the location of the current and potential electrodes on a half-infinite plane, it is affected by topography depending on the location of the electrodes. For the case of a dipole-dipole configuration, the apparent resistivity appears to be high beneath a hill and low beneath a valley. On the other hand, the chargeability values are less affected by topography.

In order to make the appropriate corrections for the present survey; a 2D analysis that takes into account the topographical elevation of the surveyed points was applied to each line of the survey. The corrected apparent resistivity values are then used to construct the related sections and contour maps.

2-4-3 Two-dimensional analysis

For the TDIP data analysis and according to the standard model, the apparent resistivity and chargeability distributions are used in combination to make a quantitative analysis of the pseudo-sections and plan maps. The resultant underground model is inferred by making use of the theoretical results given by the model. This is called in general a model simulation.

In the present survey, according to the limitations of the results of the forward modeling and to match the field results, it was used a 2D inversion model which combines the FEM forward calculations with a non-linear least square method. The inconveniences presented by the 1D analysis to make a layer analysis of the underground structure are best solved by the approximation made by the 2D model.

In order to make the model calculations, the underground structure is divided into many small blocks, each of them having initially assigned their own chargeability and resistivity value. The blocks are designed so that small blocks are placed close to the surface and increased in size as the blocks are located at deeper levels.

2-5 Survey Results

2-5-1 Electrical measurements of rock samples

Representative rock samples from the survey area were analyzed in order to investigate whether the contrast in resistivity between the target mineralization and the volcanic rocks is enough to discriminate between these units in terms of electrical properties.

In general, resistivity and IP measurements in rocks may not reflect in a direct way the intrinsic resistivity or chargeability because of different degree of alteration and water content over the survey area, however clear ideas can be obtained related to the relative variations between rocks units and mineralization.

(1) Measurement method

Measurement of the electrical properties of rock samples, such as resistivity and IP chargeability were carried out on some samples selected from the survey area. 21 pieces of the rocks collected from boreholes and 12 from outcrops located all within the survey area, were formed into a cylindrical shape and thereafter, soaked into water for a reasonable amount of days but not less than 48 hours. Apparent resistivity as well as chargeability values were measured according to the IP time domain procedures in the laboratory. For this purpose, it was used a Lab Downhole Transmitter LDT-10 made by Zonge.

(2) Results

Results of the electrical properties of rocks measured in the laboratory are indicated in Table II-2-3. The resistivity values measured in the laboratory ranged from 25 to 34,600 Ω-m. In general the core samples showed relatively low resistivities and those from the outcrop showed high resistivities. Among core samples the resistivities of volcanics V1-1 and V1-2 ranged from 25 to 307 Ω-m and dykes from 39 to 862 Ω-m, especially the samples including fine cracks indicated low resistivity. The samples

Table II-2-3 Resistivity and chargeability of rock samples

No.	Sample Name	Resistivity (Ωm)	Chargeability (mV/V)	Rock Name and Formation	Alteration and Mineralization
1	H1-34.10m	52	2.2	Ba, Pb (V2)	
2	H1-78.00m	154	1.1	Ba, Pw (V1-2)	Sili, Py diss(sl)
3	H1-131.50m	216	74.9	Ba, Pw (V1-2)	Sili, Py diss, Py-Epi vein
4	H1-185.50m	79	10.7	Ba, Pw (V1-2)	Sili(sl), Py diss
5	H1-269.30m	103	9.4	Ba, Pw (V1-2)	Sili
6	H2-31.50m	219	0.5	Ba, Pw (V2)	
7	H2-87.20m	25	19.2	Ba, Hy (V1-2)	Py diss
8	H2-139.40m	56	38.1	Ba, Pw (V1-2)	Sili(sl), Argi, Py diss(in)
9	H2-157.60m	49	4.2	Ba, Pw (V1-2)	Sili(in), Argi, Py diss(in)
10	H2-204.10m	154	6.9	Ba, Pw (V1-2)	Sili(in), Argi, Py diss(in)
11	H2-246.80m	157	118.2	Ba, Pw (V1-2)	Sili(in), Py diss(in)
12	S1-64.20m	101	5.0	Ba, Dy	Sili(sl), Py diss(sl)
13	S1-93.45m	130	2.8	Ba, Dy	Sili(sl)
14	S1-109.90m	103	95.7	Ba, Pw (V1-2)	Sili(sl), Py diss, Py vein
15	S1-135.25m	39	9.4	Ba, Dy	Sili, Py diss(in), Py vein
16	S1-213.00m	272	2.4	Ba, Pw (V1-2)	Sili(sl)
17	S1-248.40m	862	10.3	Ba, Dy	Sili(in), Py diss(in)
18	S2-48.30m	370	47.1	Ba, Dy	Sili(in), Py diss, Py-Epi-Qz vein
19	S2-99.90m	307	23.6	Ba, Ma (V1-2)	Sili, Py diss, Py-Epi-Qz vein
20	S2-169.20m	155	151.2	Ba, Ma (V1-2)	Sili(in), Py diss(in), Py vein
21	S2-220.70m	175	6.2	Ba, Pw (V1-2)	Sili, Py diss
22	MQ-1	7,600	1.6	Ba, Dy	
23	MQ-2	10,856	3.1	Ba, Dy	
24	MQ-3	1,720	33.6	Me	Magnetite, Hematite
25	MQ-4	2,095	7.3	Me	Magnetite, Hematite
26	HK-1	7,014	6.0	Ls (BO)	
27	HK-2	364	19.7	Ch (BO)	
28	HK-3	414	16.3	Ch (BO)	
29	HK-4	5,767	3.0	Ls (BO)	
30	SM-1	2,100	11.7	Ls (BO)	
31	SM-2	1,372	5.0	Ch (BO)	
32	SM-12	765	9.7	Tr	
33	SM-13	34,600	4.3	Gb	

Remarks:

H,HK : Hara Kilab
S,SM : Sarami
MQ : Maqail

V1-2 : Lower Extrusives 2
V2 : Middle Volcanic Rocks
BO : Batinah Olistostromes

Ba : Basalt
Pw : Pillow lava
Ma : Massive lava
Hy : Hyaloclastite
Pb : Pillow breccia
Dy : Dyke
Me : Metalliferous sediments
Ch : Chert
Tr : Trondhjemite
Gb : Gabbro
Ls : Limestone

Py : Pyrite
Epi : Epidote
Qz : Quartz
Argi : Argillization
diss : dissemination
Sili : Silicified
vein : veinlets

(sl) : slight
(in) : intense

No. 26 to No. 31, which are sedimentary rocks, generally indicated high resistivity. However, since there are seen abundant joints in these sediments on the site, the sediments are probably classified as a low resistivity feature.

Among the rock samples from the outcrop, metalliferous sediments, limestone, dyke and gabbro indicated extremely high resistivity of more than a few kΩ-m .

The chargeability values determined in the samples ranged from 0.5 to 151mV/V. Samples with intense pyrite dissemination presented high chargeability. Among them, the samples with high resistivity and associated with pyrite veinlet mineralization showed in particular high chargeability values. Metalliferous sediments also indicated a relatively high chargeability above 30mV/V, while some sediments showed high chargeability values.

2-5-2 Ghuzayn area

(1) Lines location

A total of 11 lines, from 1000E to 1000W, along N14°W direction were surveyed around the main gossan during the 1995 field survey season. Additionally, a total of 10 lines, from 1200E to 2000E and from 1200W to 2000W, were surveyed around the last survey area during the 1997 field survey season. During this field survey, a total of 4 lines (1000W to 1600W) were extended towards south 1.0km each. New 5 lines (2200W to 3000W) of 2.5km each were located on the western side of this area.

Fig.II-2-4 shows the location of all the IP lines surveyed in Ghuzayn.

(2) Results

Pseudo sections of apparent resistivity, chargeability and metal factor values are presented from Fig.II-2-5(1) to Fig.II-2-7(2). Compiled contour maps of apparent resistivity, chargeability and metal factor for N=1 to 4 are presented in Figs.II-2-8 to II-2-11.

According to the investigation carried out this year; the following results were obtained:

The apparent resistivity in the south side (from station No.-7) of the line 1000W to 1600W shows an N-S structure, with apparent resistivity values of more than 50Ω-m distributed around 1200W and becoming higher toward E-W direction (Fig.II-2-9).

The chargeability related to the above distribution, shows also an N-S structure with a value of about 6mV/V seen in 1000W and increasing gradually to about 13mV/V in 1600W in the western side.

The metal factor shows relatively high values around the lines 1200W and 1400W, however the chargeability shows low values.

In relation to the results in the west side, the apparent resistivity shown in the plane maps, indicates low values in the north side (Fig.II-2-10) from the lines 2200W to 3000W, but high values in the south side.

The chargeability distribution shows anomaly values of more than 15mV/V in the center of the stations No.24 to 25 in line 2600W. This anomaly presents a width of about 400m around the lines 2400W to 2800W, however this value becomes very low in the east. The chargeability values in the

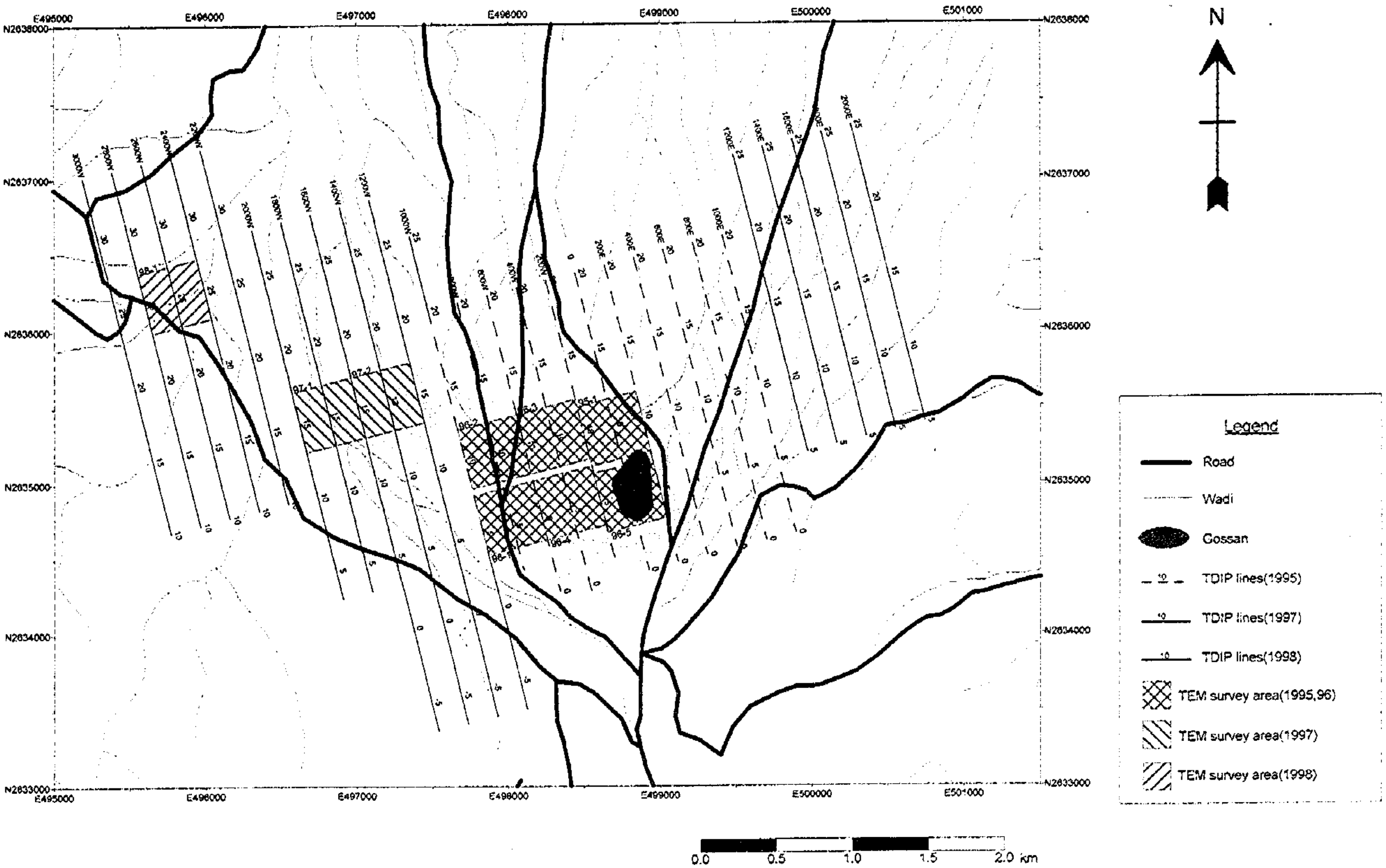

Fig. II -2-4 Geophysical survey location in Ghuzayn area

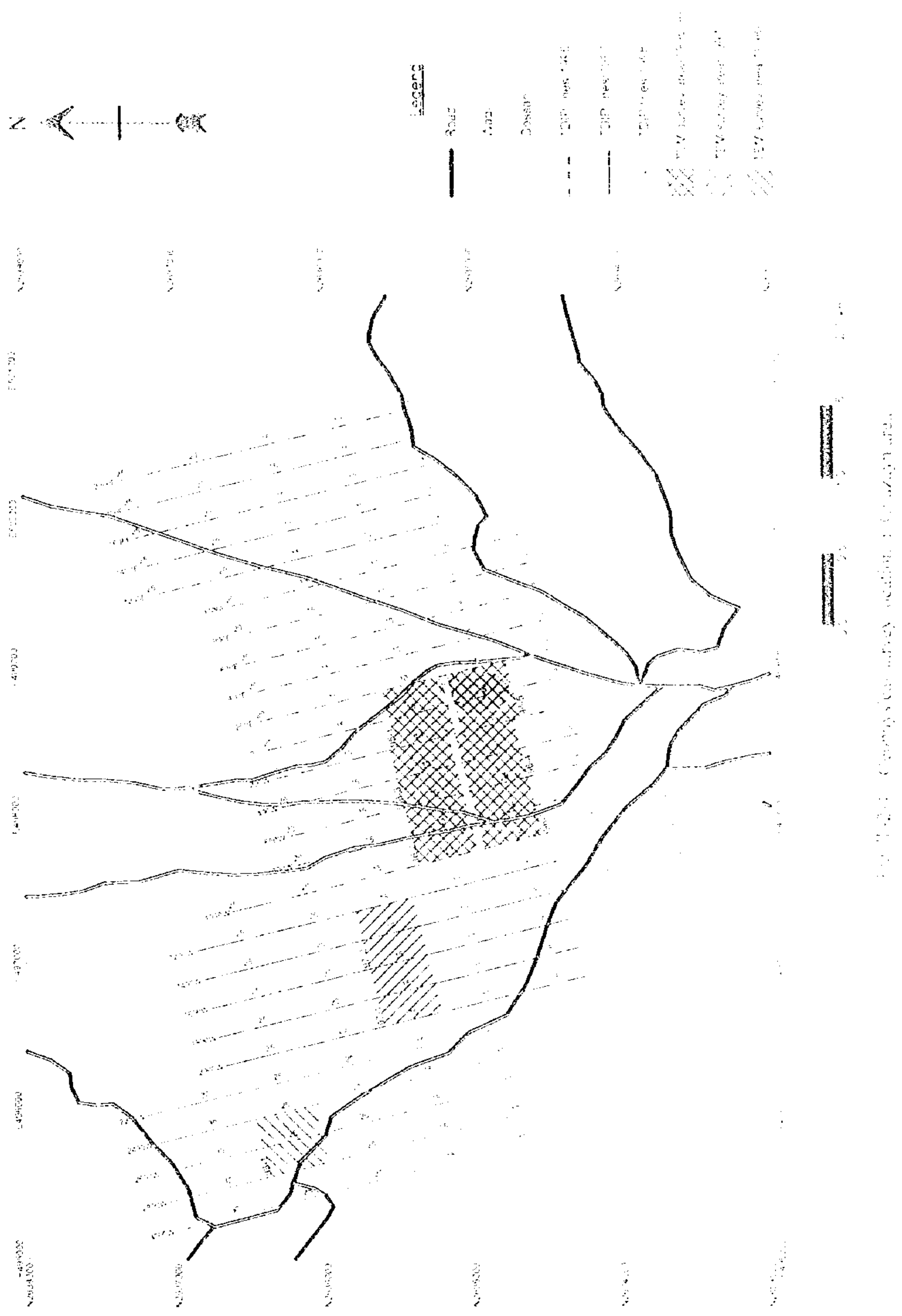

Fig. II -2-5(1) Apparent resistivity pseudo-sections in Ghuzayn area

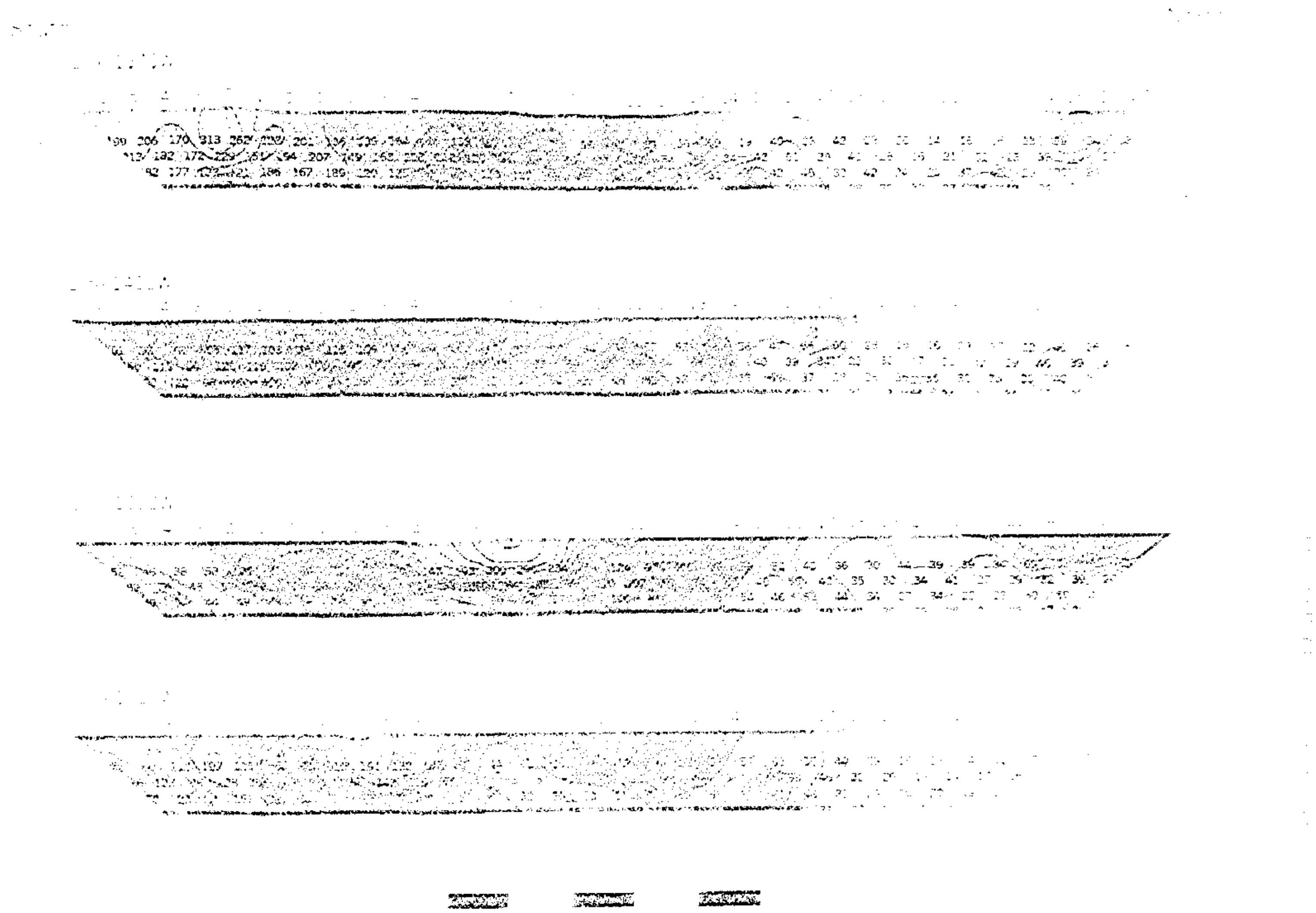

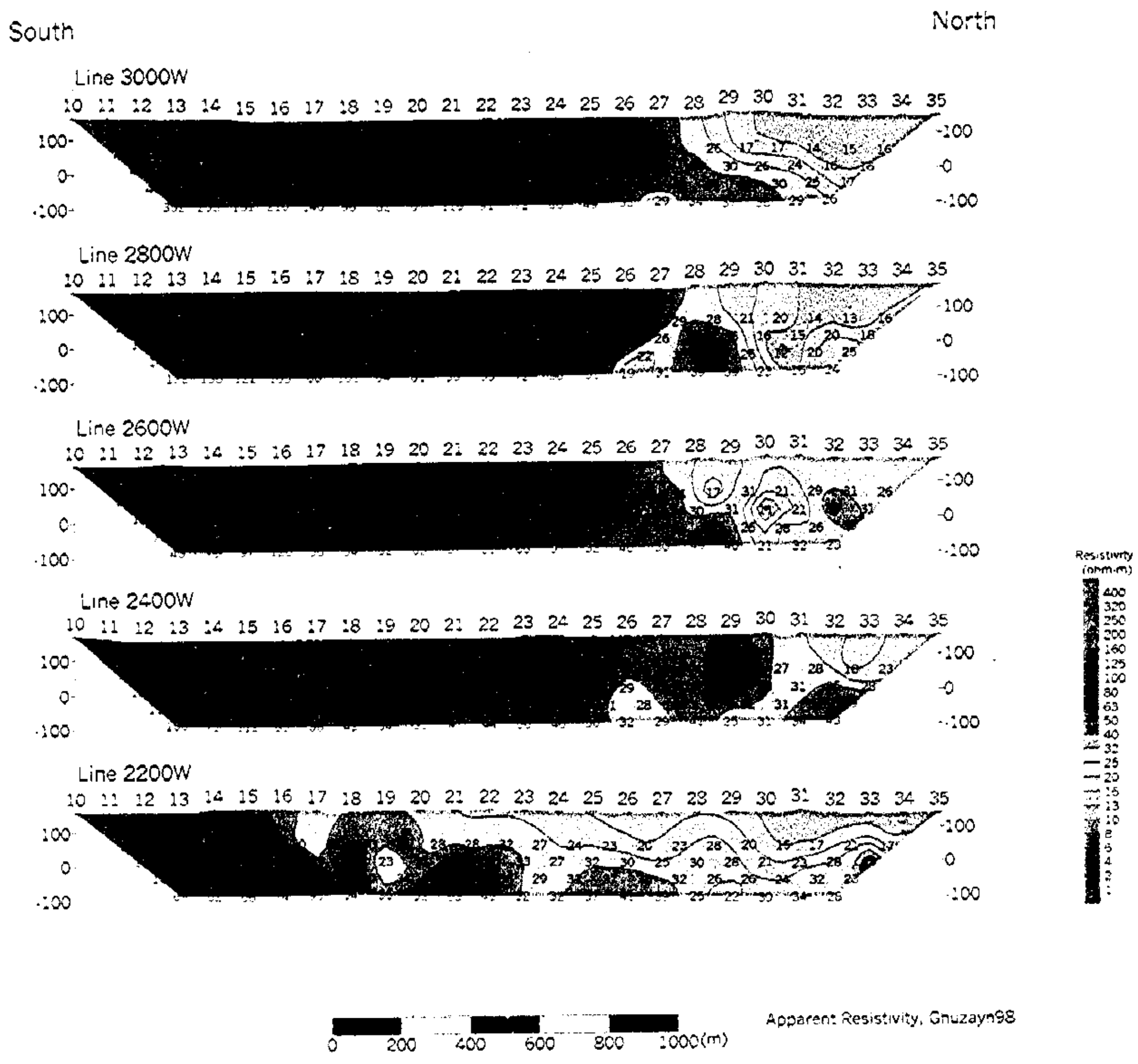

Fig. II-2-5(2) Apparent resistivity pseudo-sections in Ghuzayn area

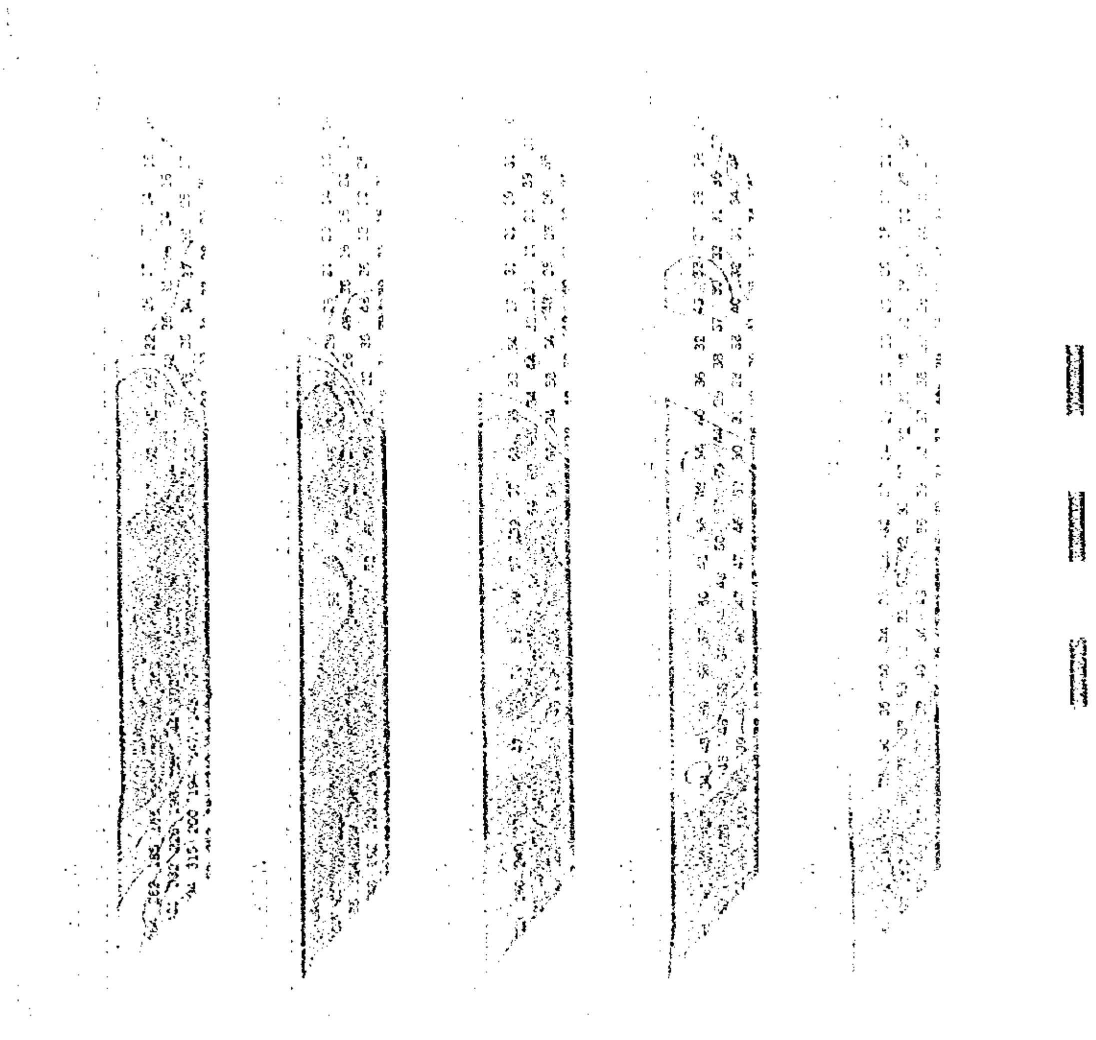

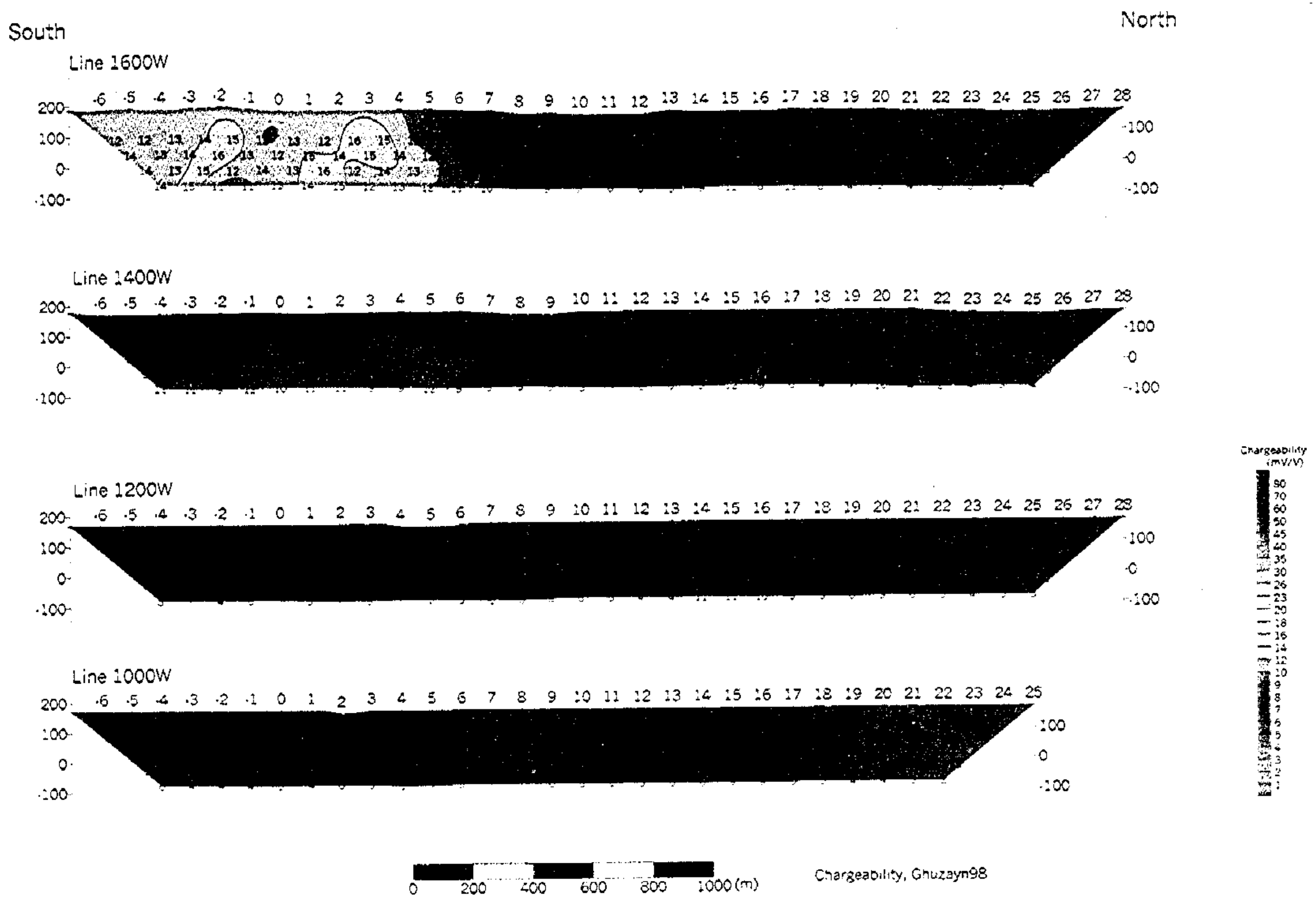

Fig. II -2-6(1) Chargeability pseudo-sections in Ghuzayn area

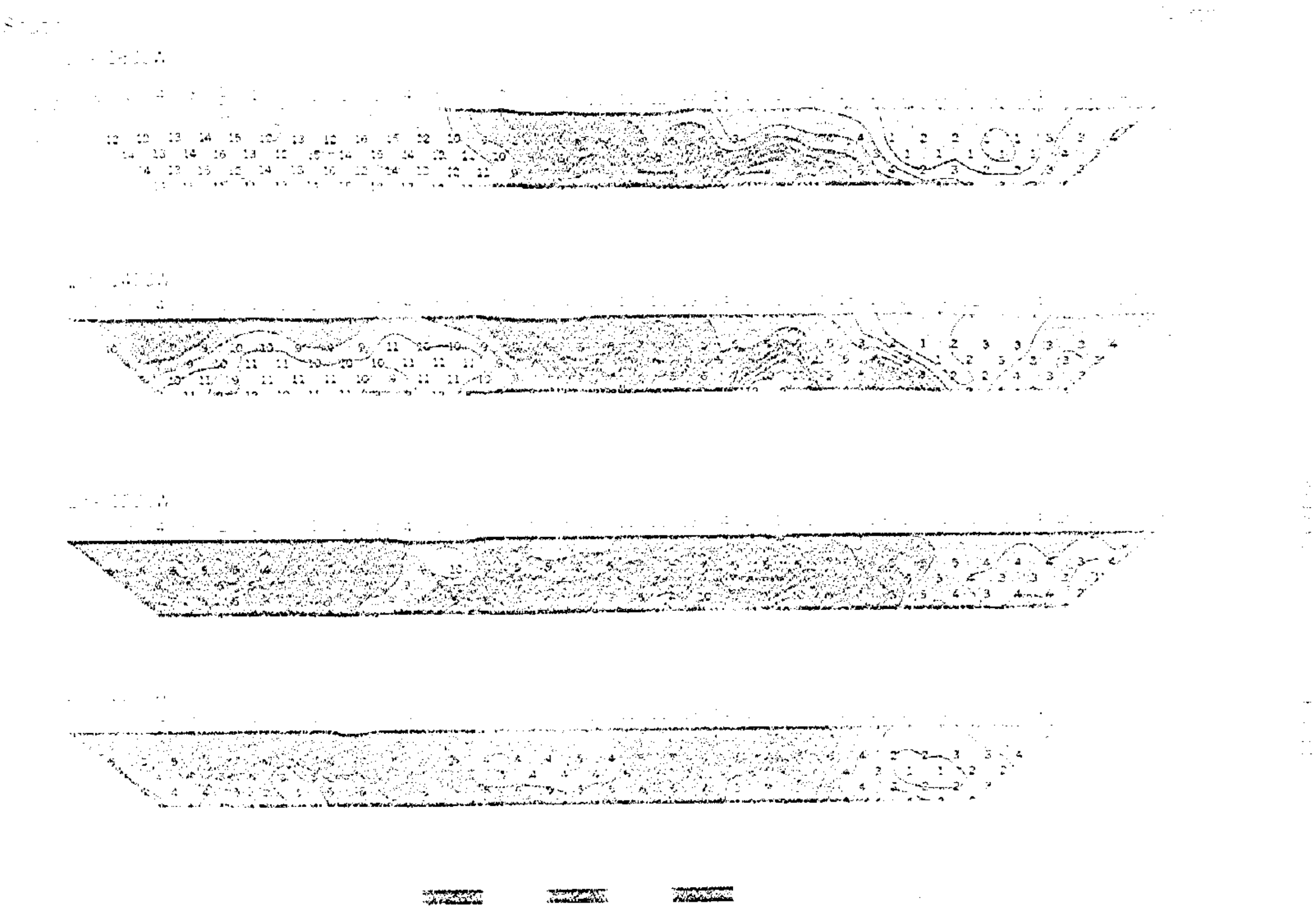

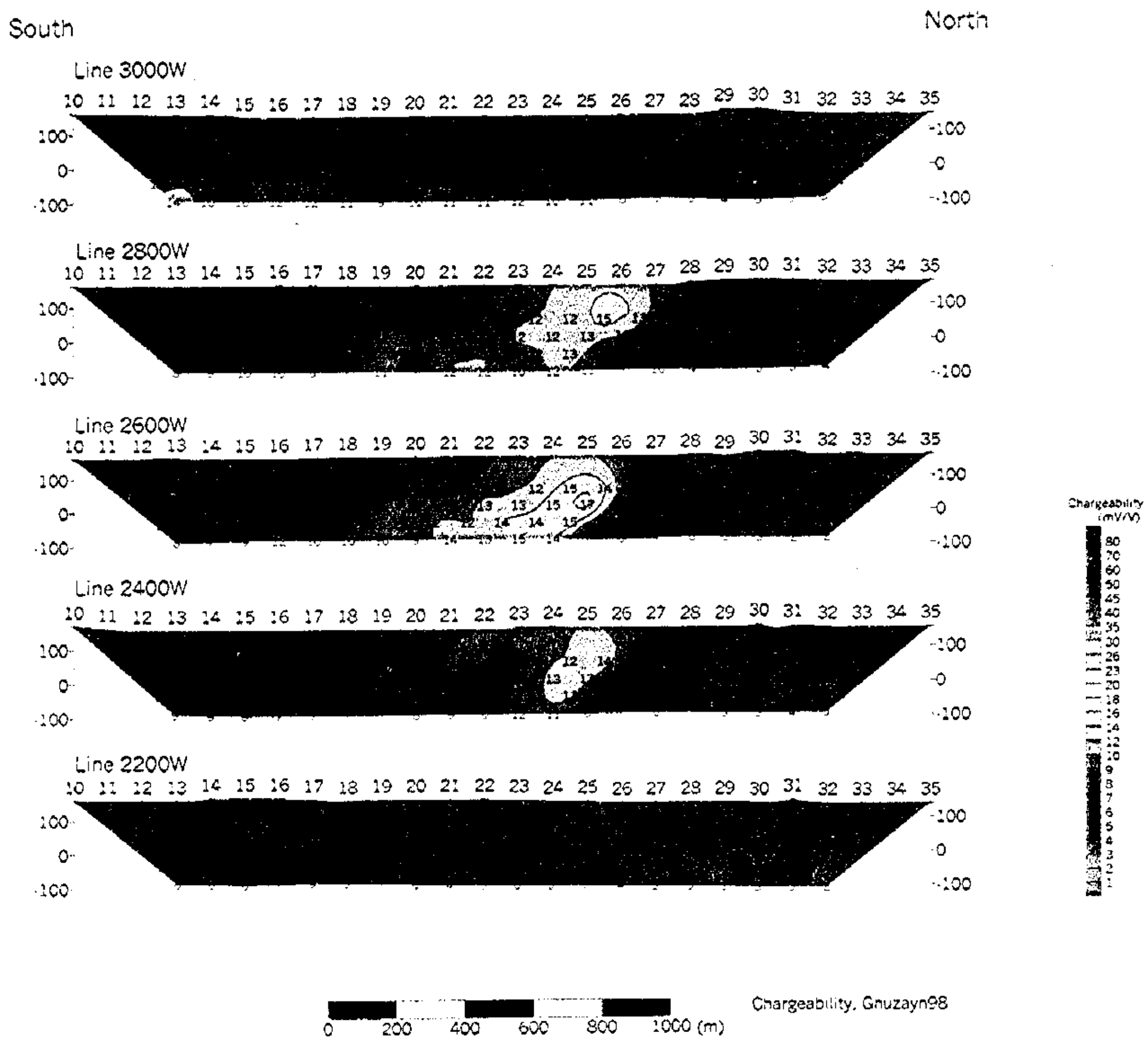

Fig. II-2-6(2) Chargeability pseudo-sections in Ghuzayn area

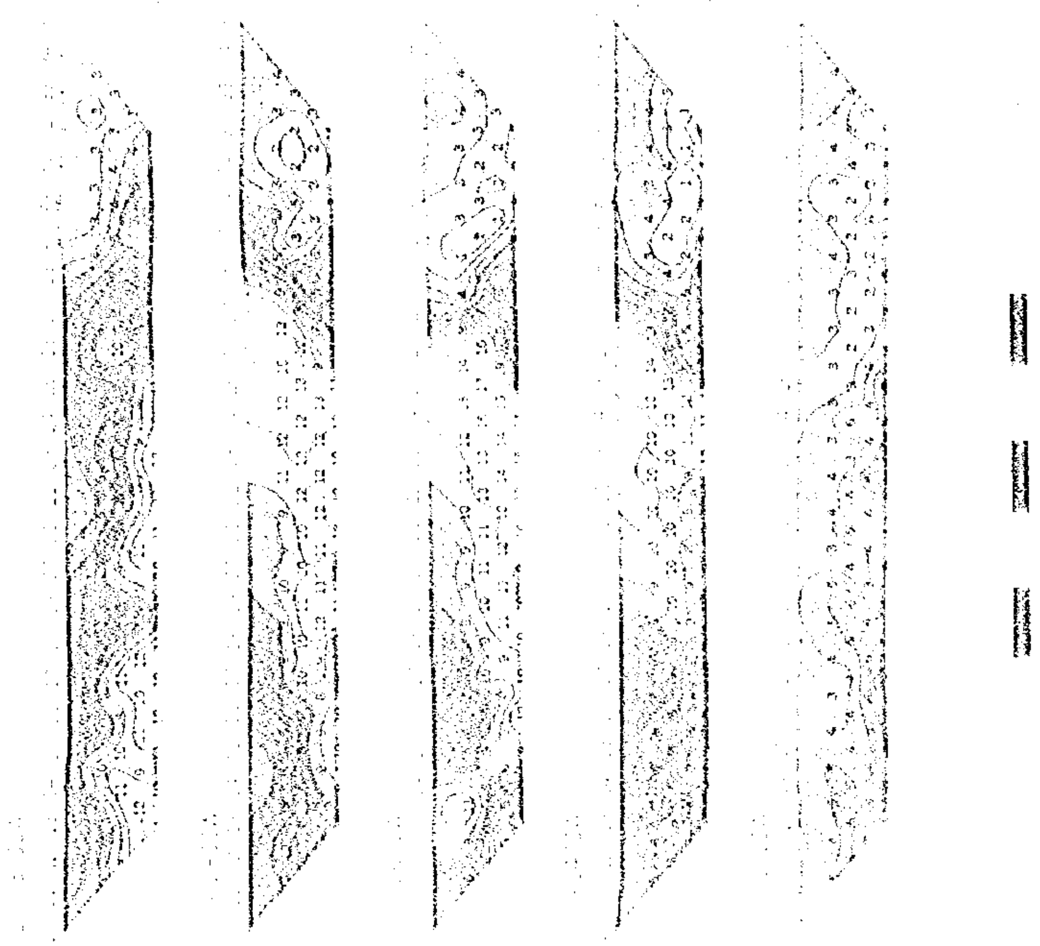

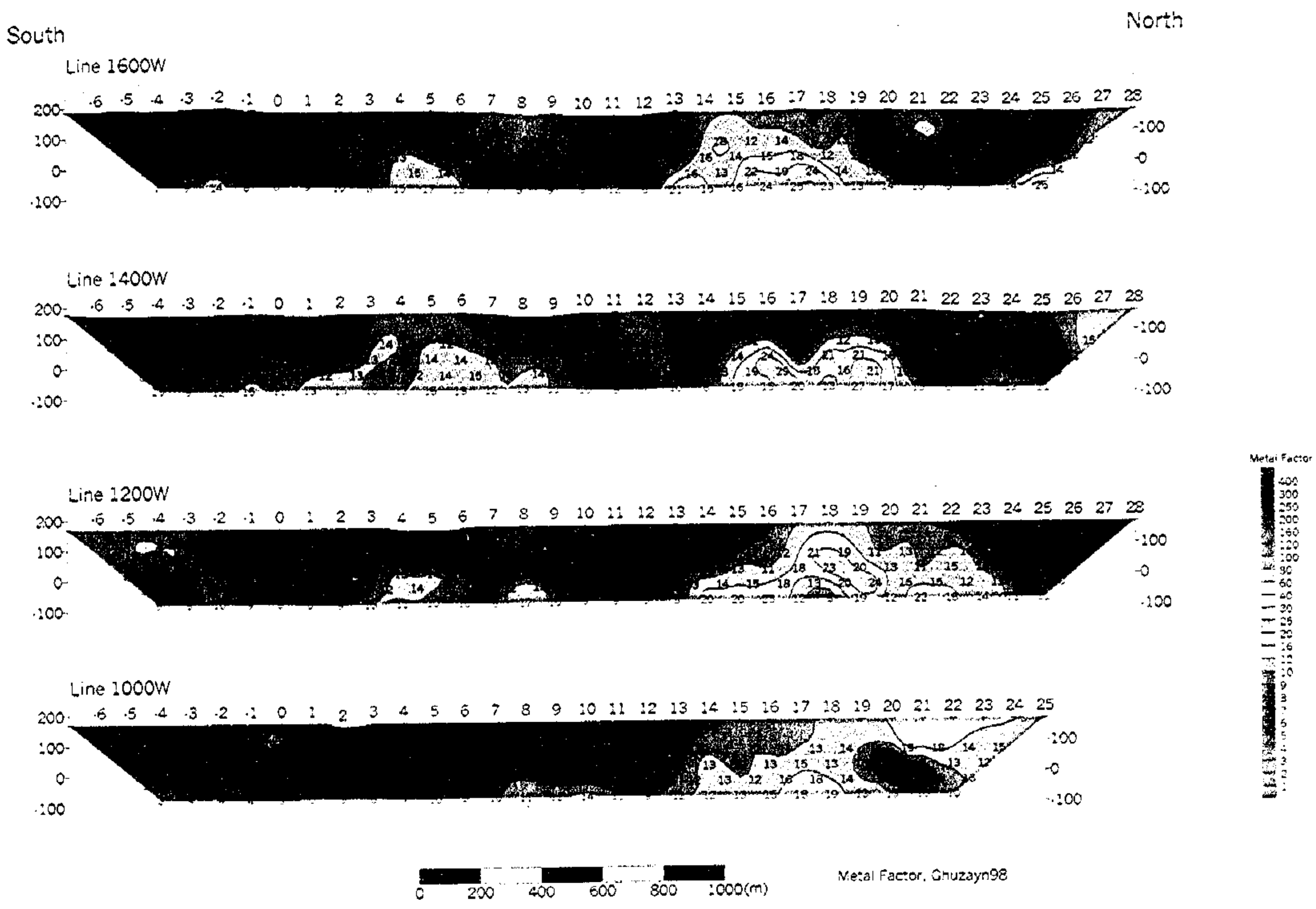

Fig. II-2-7(1) Metal factor pseudo-sections in Ghuzayn area

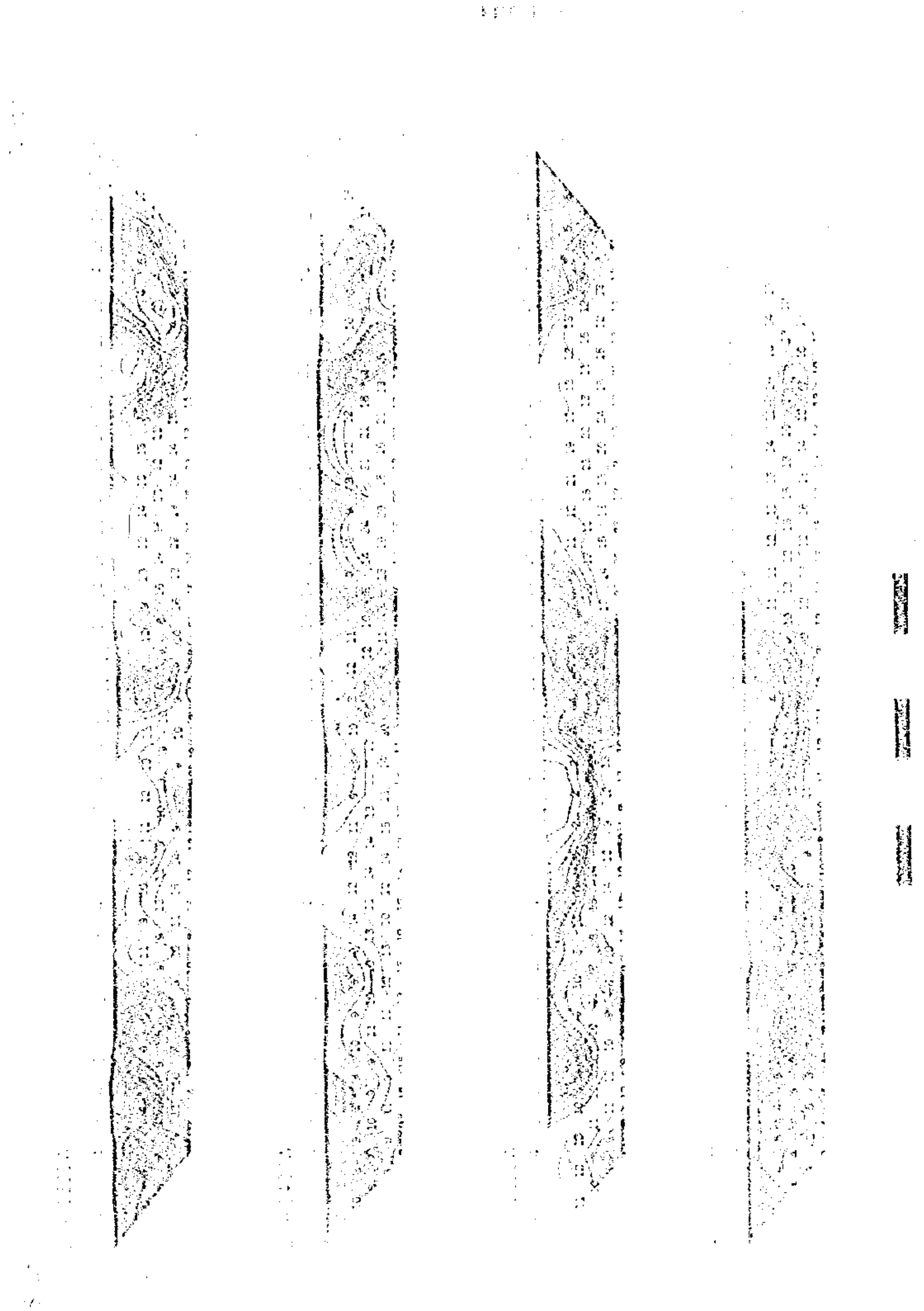

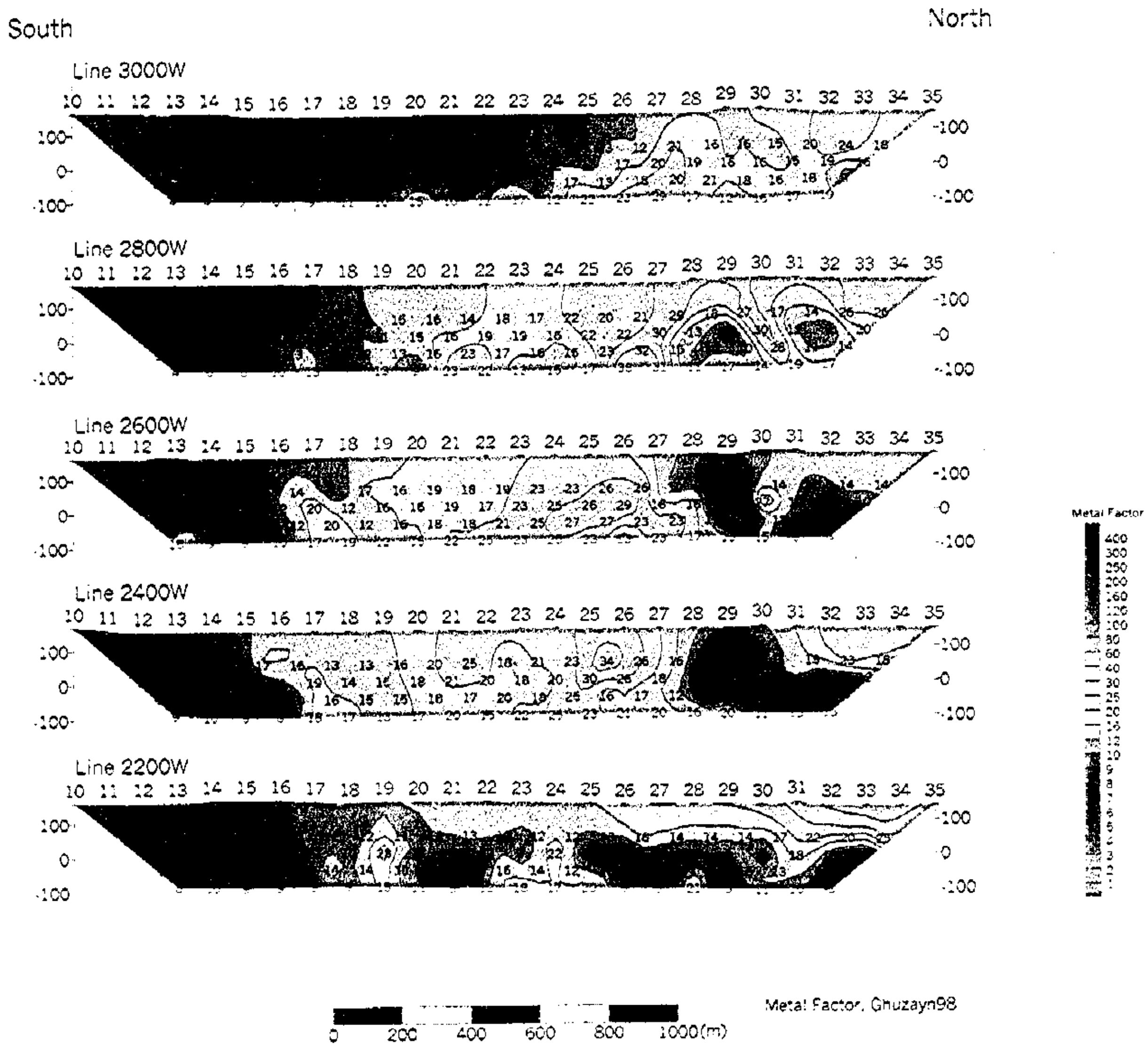

Fig. II-2-7(2) Metal factor pseudo-sections in Ghuzayn area

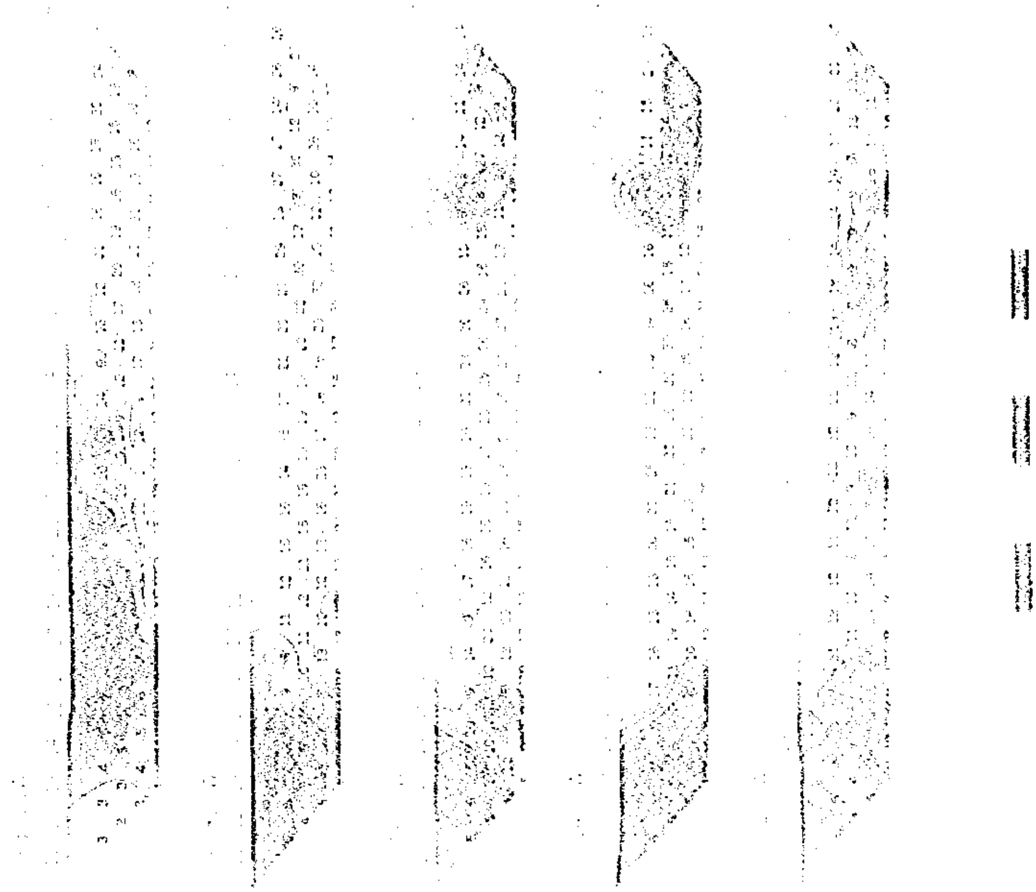

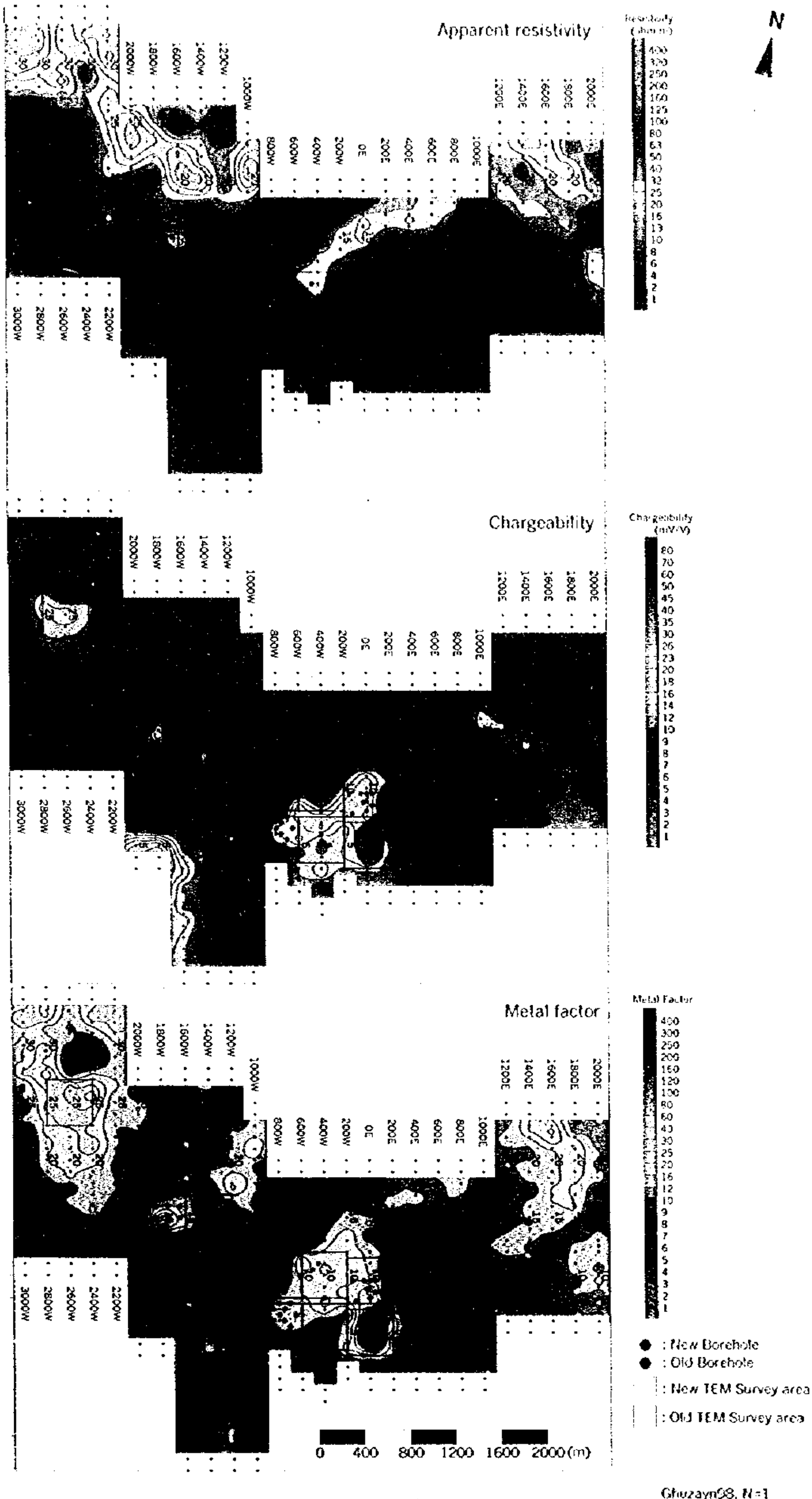

Fig. II-2-8 IP plane map of n=1 in Ghuzayn area

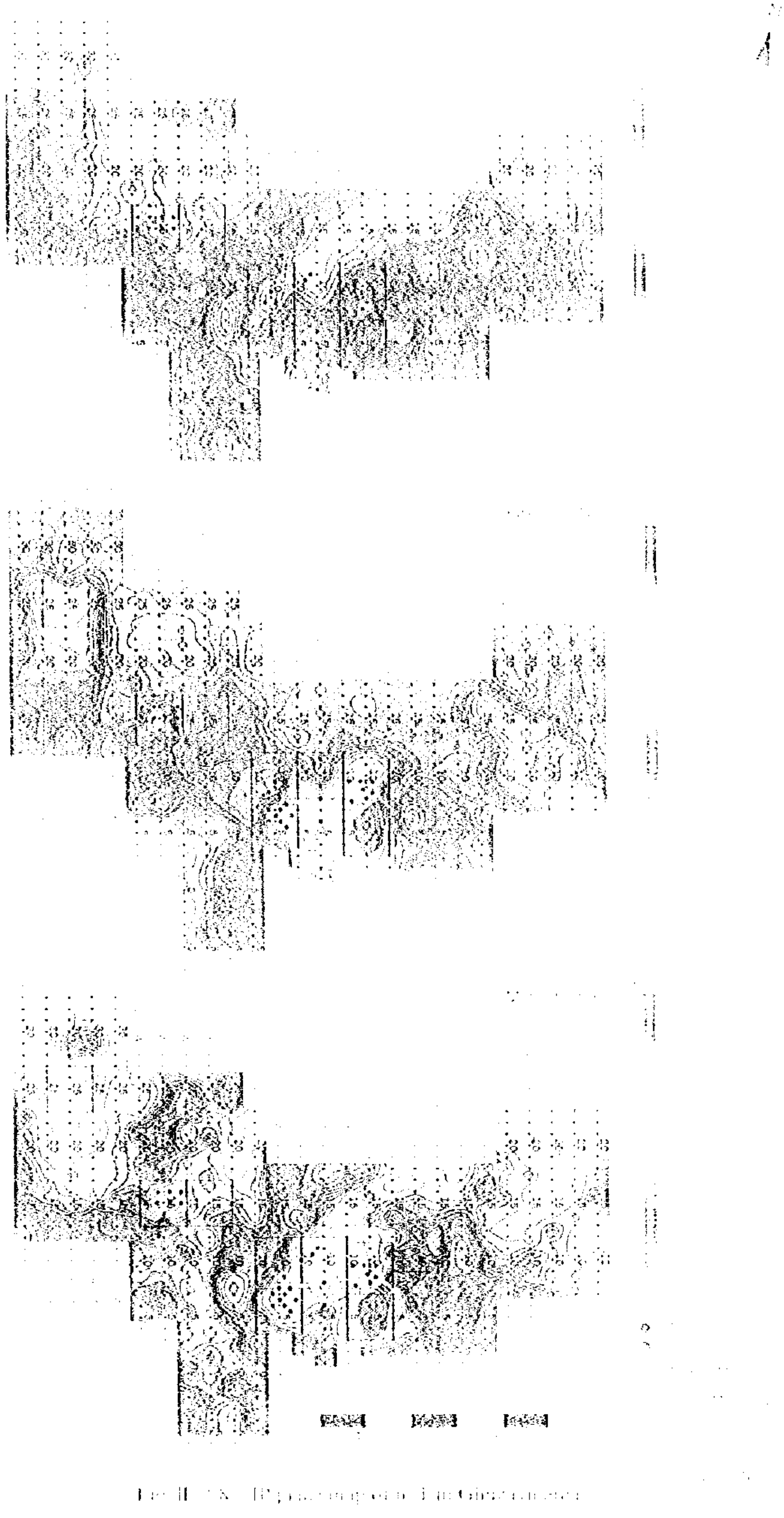

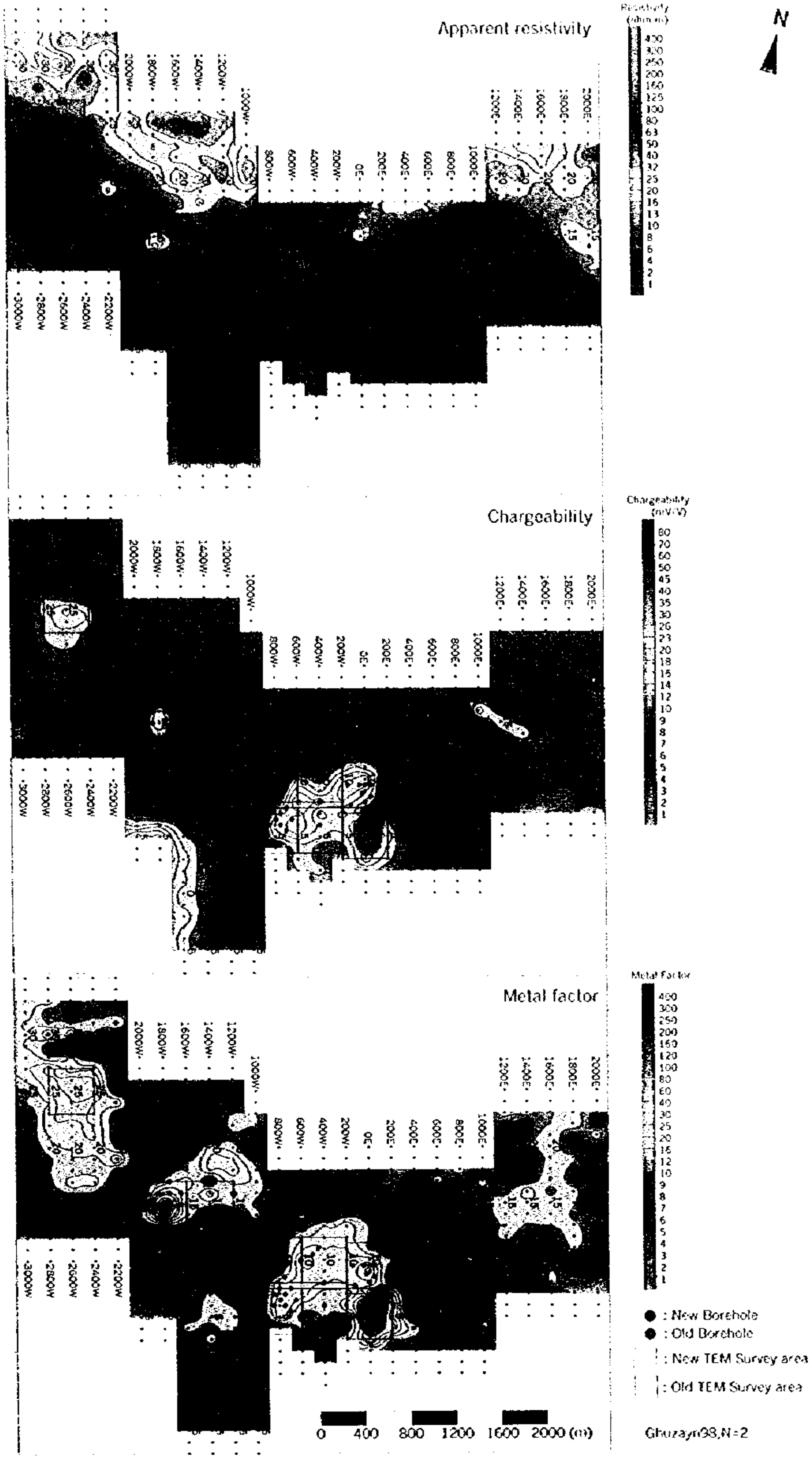

Fig. II -2-9 IP plane map of n=2 in Ghuzayn area

Fig. II. 2.9 IP plane maps of ... [illegible]

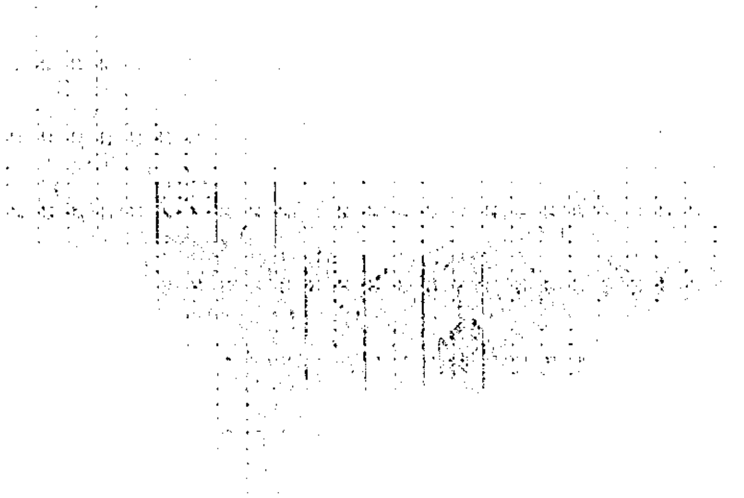

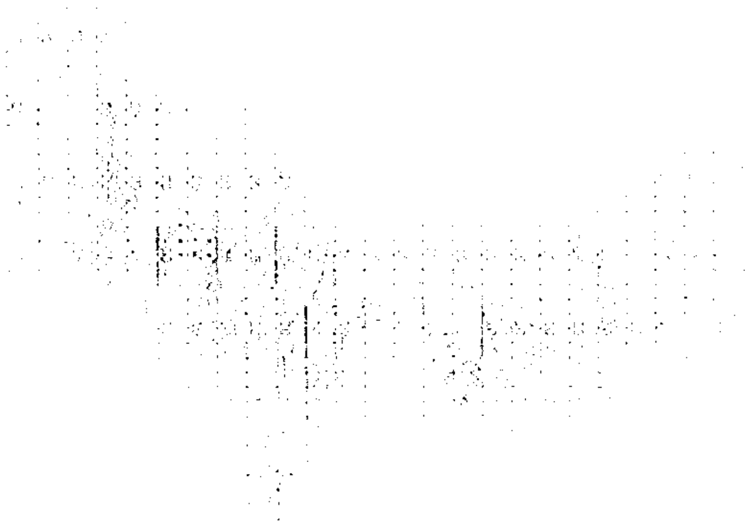

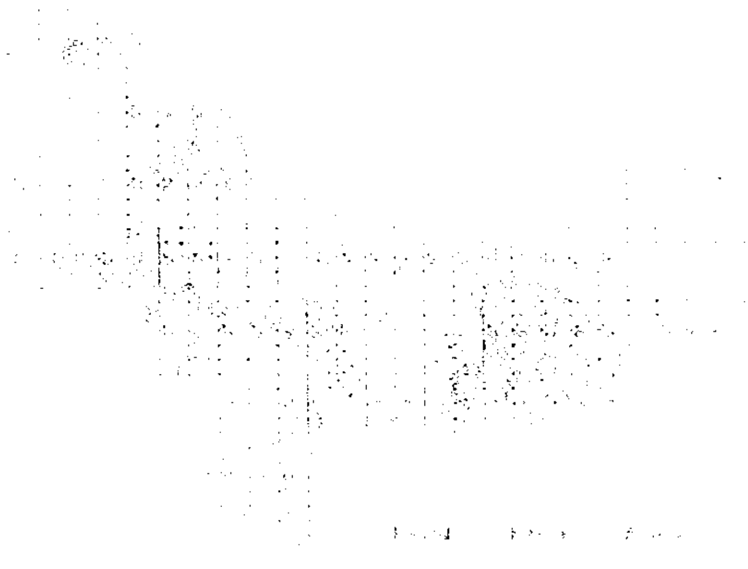

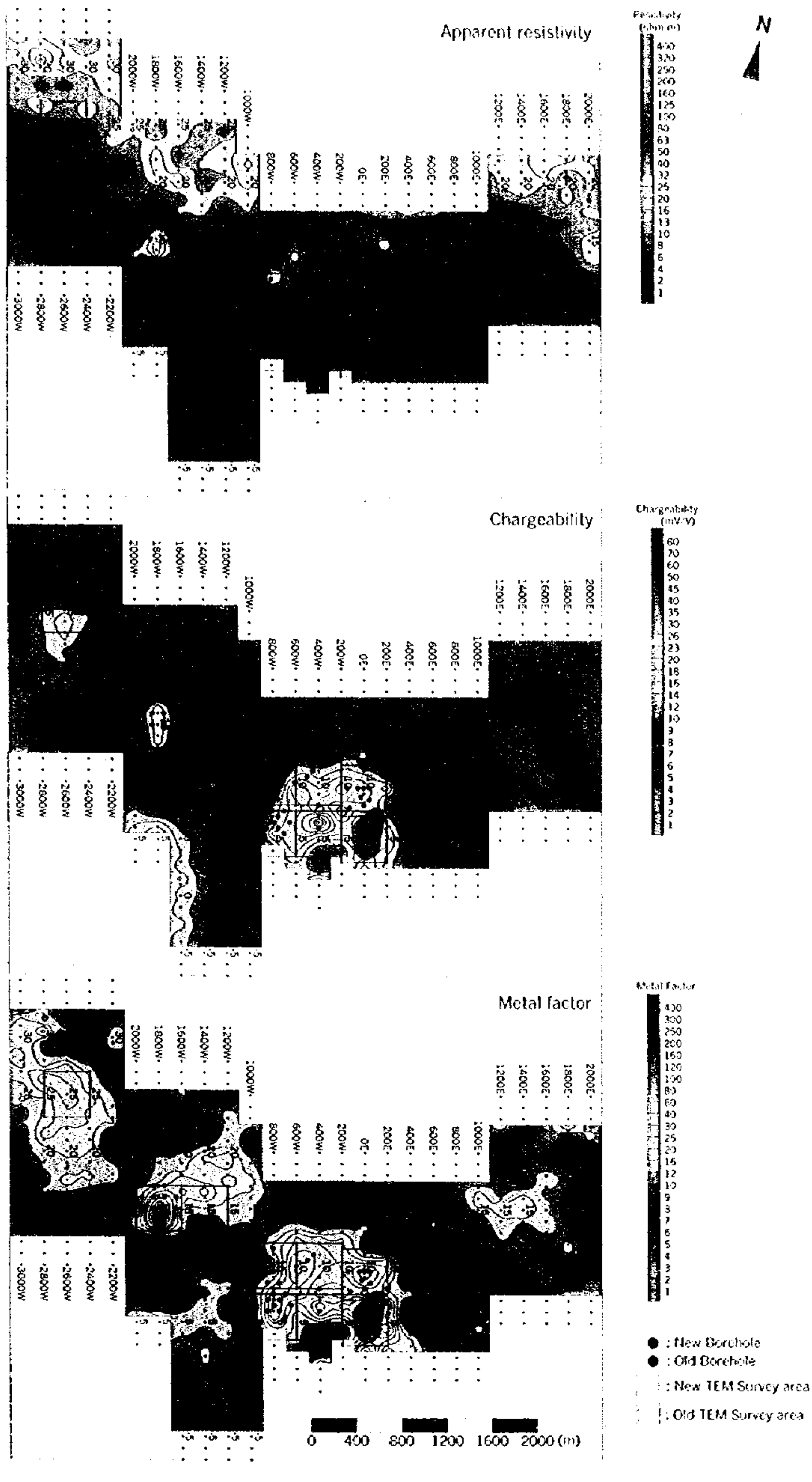

Fig. II-2-10 IP plane map of n=3 in Ghuzayn area

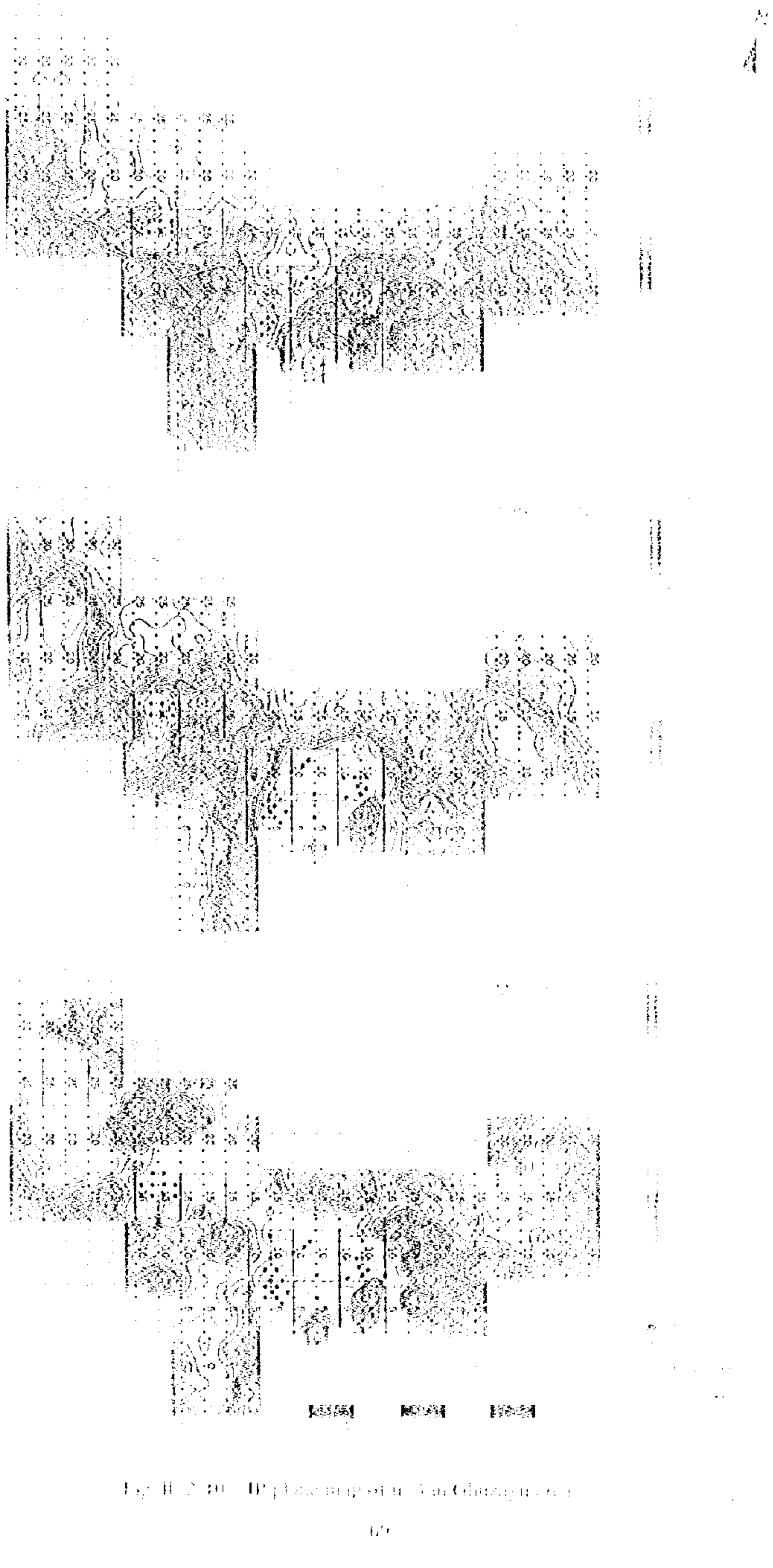

Fig. II.2.10 [illegible]

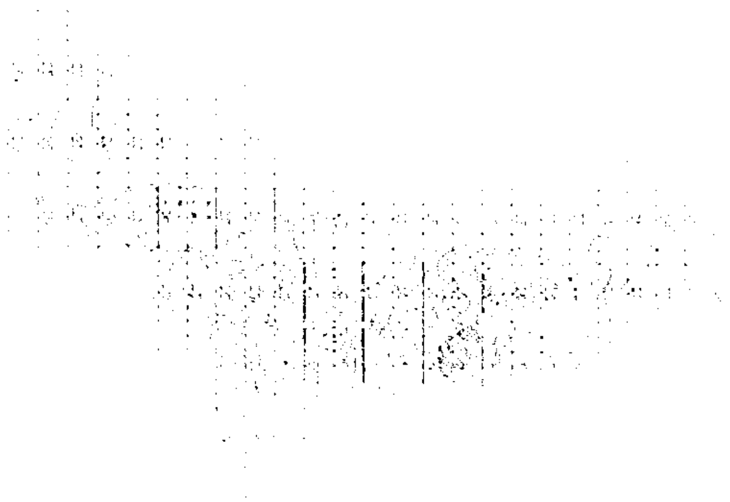

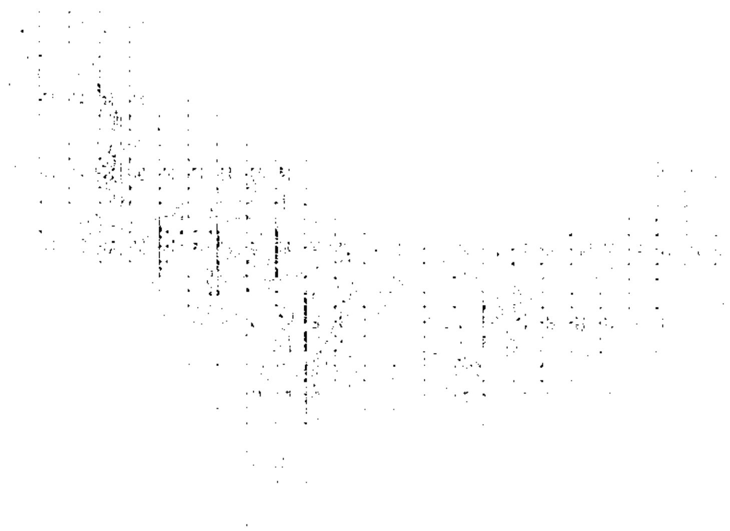

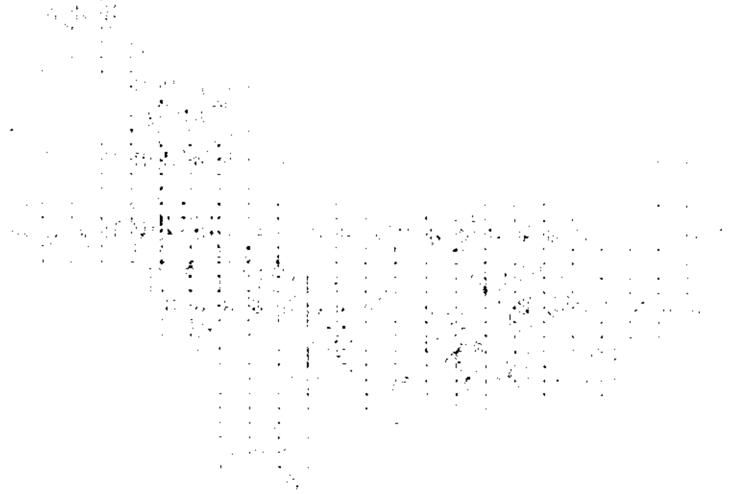

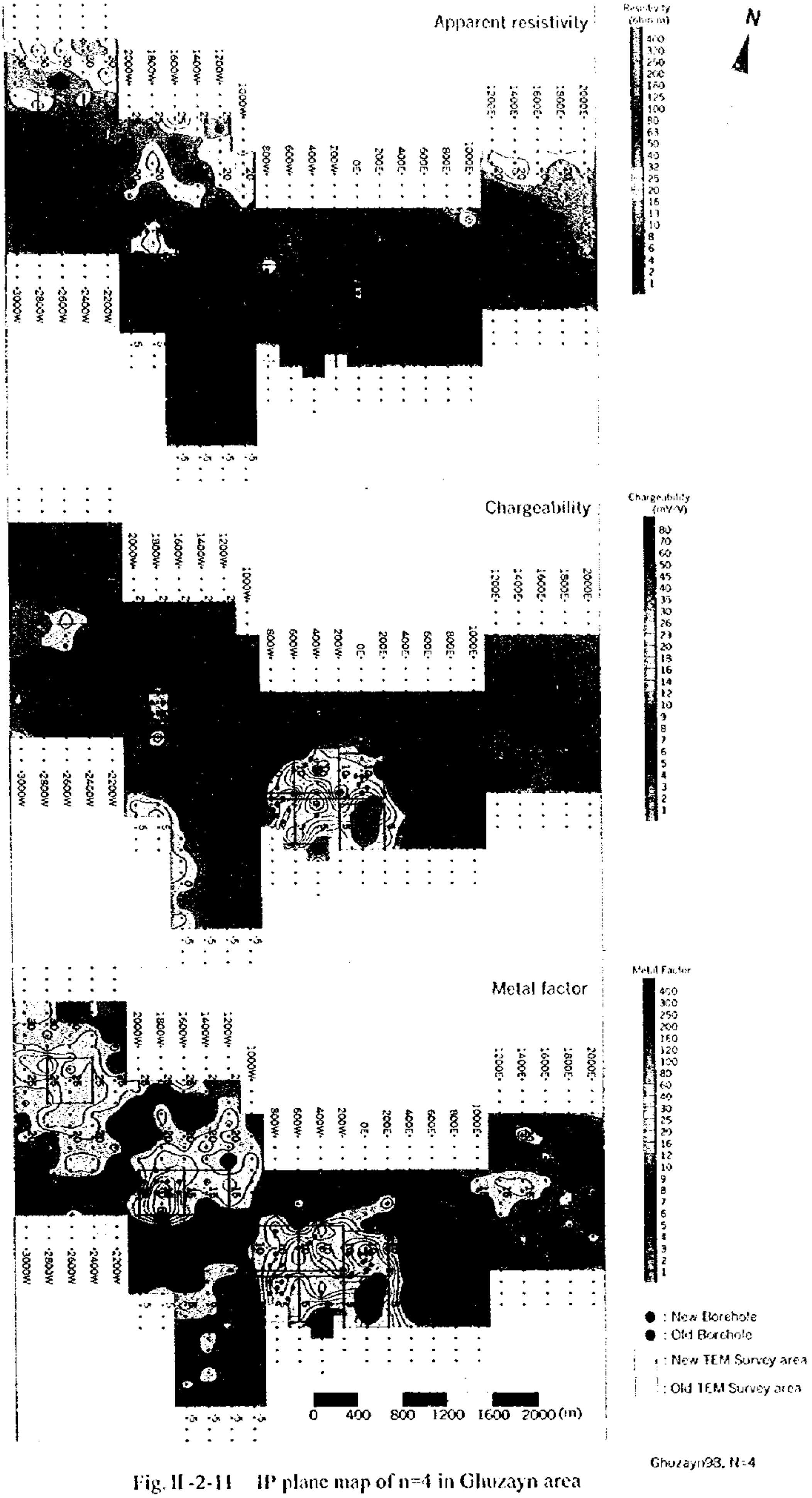

Fig. II-2-11 IP plane map of n=4 in Ghuzayn area

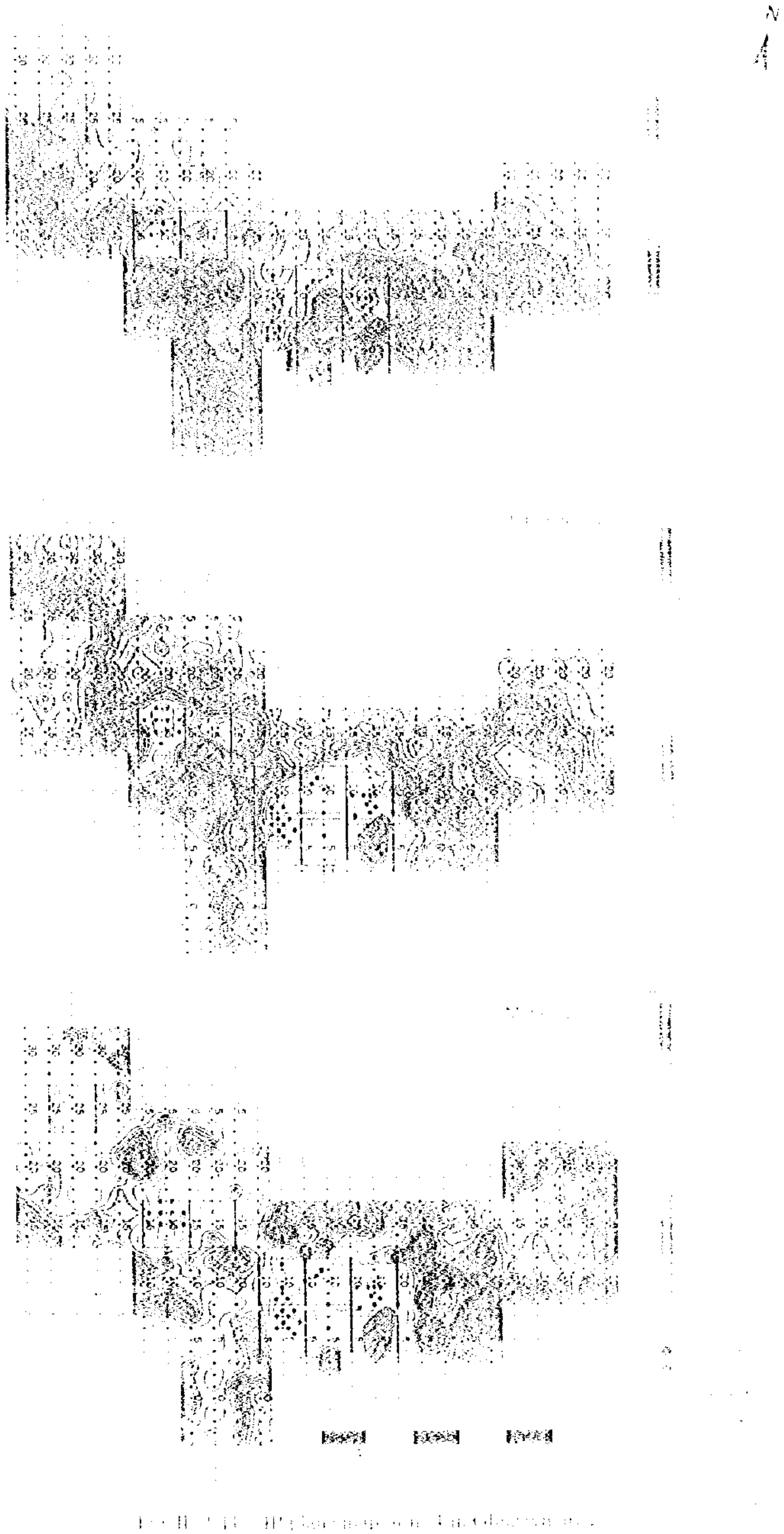

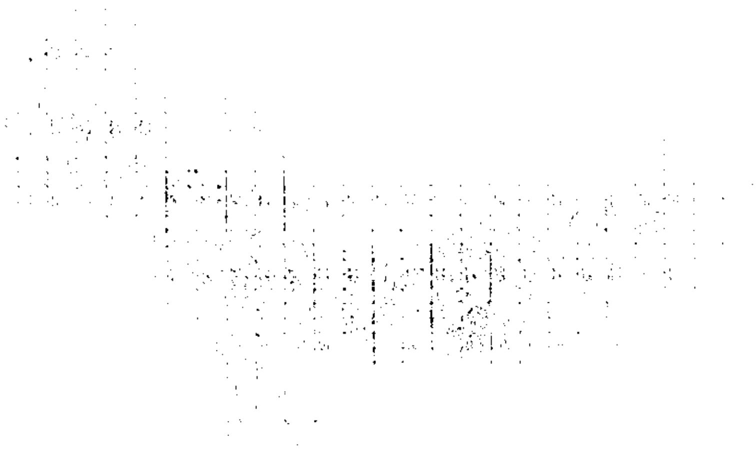

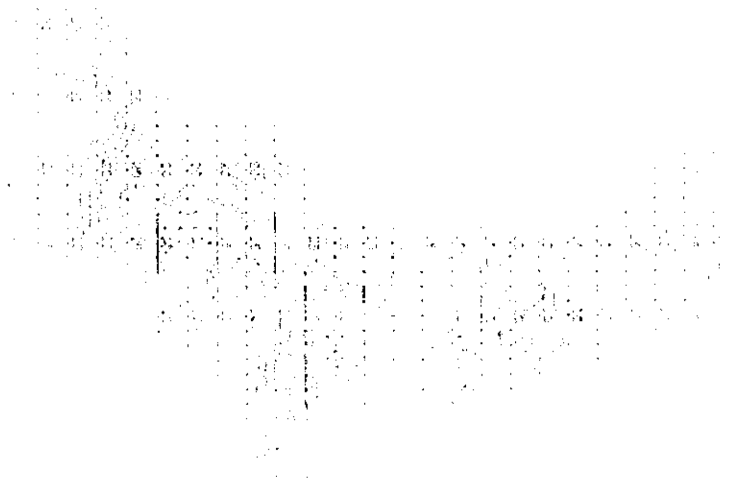

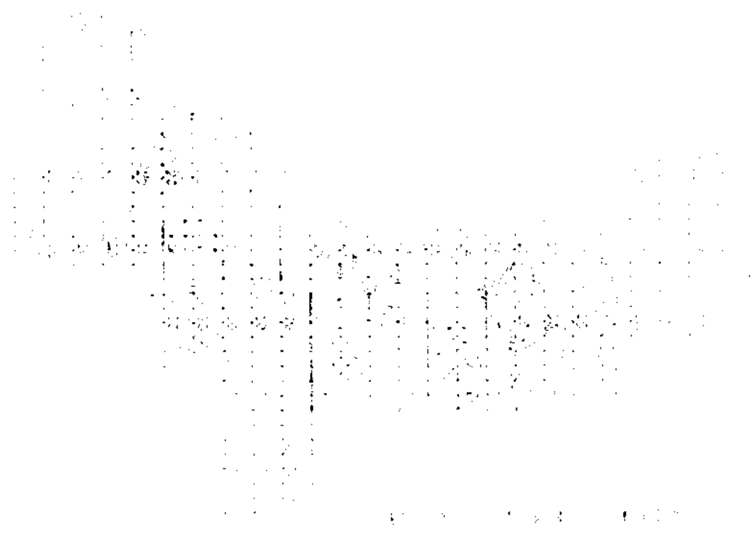

north side become quite low in the station No.26, however towards the south, it decreases in a gradual manner (Fig.II-2-6(2)).

In relation to the metal factor, although evident metal factor anomalies were not detected, an anomaly of relative size is seen widely distributed between the lines 2400W and 2800W, with its anomaly center located around station No. 25 (Fig. 2-7(2)).

(3) 2D analysis

2D analysis was performed for all the lines, but here for matter of convenience, only the sections containing representative anomalies will be described. On these regards, only the 2D results of the lines 1600W and 2600W will be briefly described (Fig.II-2-12 and Fig.II-2-13).

In relation to the line 1600W, the apparent resistivity shows at depth of station No 14, a resistivity distribution of medium values around 60Ω-m, while the chargeability shows relative high values of 10mV/V. At depth of the stations Nos. 26 to 27, a high chargeability anomaly with values as high as 19mV/V are seen. In relation to the metal factor, relatively high values are interpreted at intermediate depths (N=2 to 4) in the vicinity of the station No 14 as well as in the vicinity of station No. 26.

In relation to the line 2600W and in the vicinity of the station No. 25, high chargeability values with a maximum of about 19mV/V are seen at depth, but they are accompanied by relatively high resistivity values. This chargeability anomaly spreads widely towards the south around the surroundings of the station No 19, however this anomaly seems to drop drastically to low values as the distribution goes to the south towards the station No 26. In relation to the metal factor, it shows somewhat a high anomaly pattern distribution similar to the indicated by the chargeability anomaly around the stations Nos. 18 to 27.

2-5-3 Sarami area

(1) Lines location

During this field season, a total of 25 lines were surveyed along N45°E direction with a line spacing of 200m, as follow: 10 lines (200S to 1600N) of 1.7km each and 15 lines (1800N to 4600N) of 1.8km each. Fig.II-2-14 shows the location of all the IP lines surveyed in Sarami.

(2) Results

The results of the TDIP survey in Sarami are presented here as pseudo sections of apparent resistivity (Fig.II-2-15(1) to Fig.II-2-15(3)), chargeability (Fig.II-2-16(1) to Fig.II-2-16(3)) and metal factor (Fig.II-2-17(1) to Fig.II-2-17(3)). Compiled plan maps of apparent resistivity, chargeability and metal factor for N=1 to 4 are also presented in Figs.II-2-18 to II-2-21.

The apparent resistivity distribution presents a NW-SE tendency, for which the apparent resistivity values increase gradually from low values in the southeast side to about 100Ω-m in the northwest side of this area. In the region where V1-2 is distributed, around the central part of the lines 1600N to 2400N, medium resistivity values of about 20Ω-m and not so high resistivity values of about 60Ω-m are

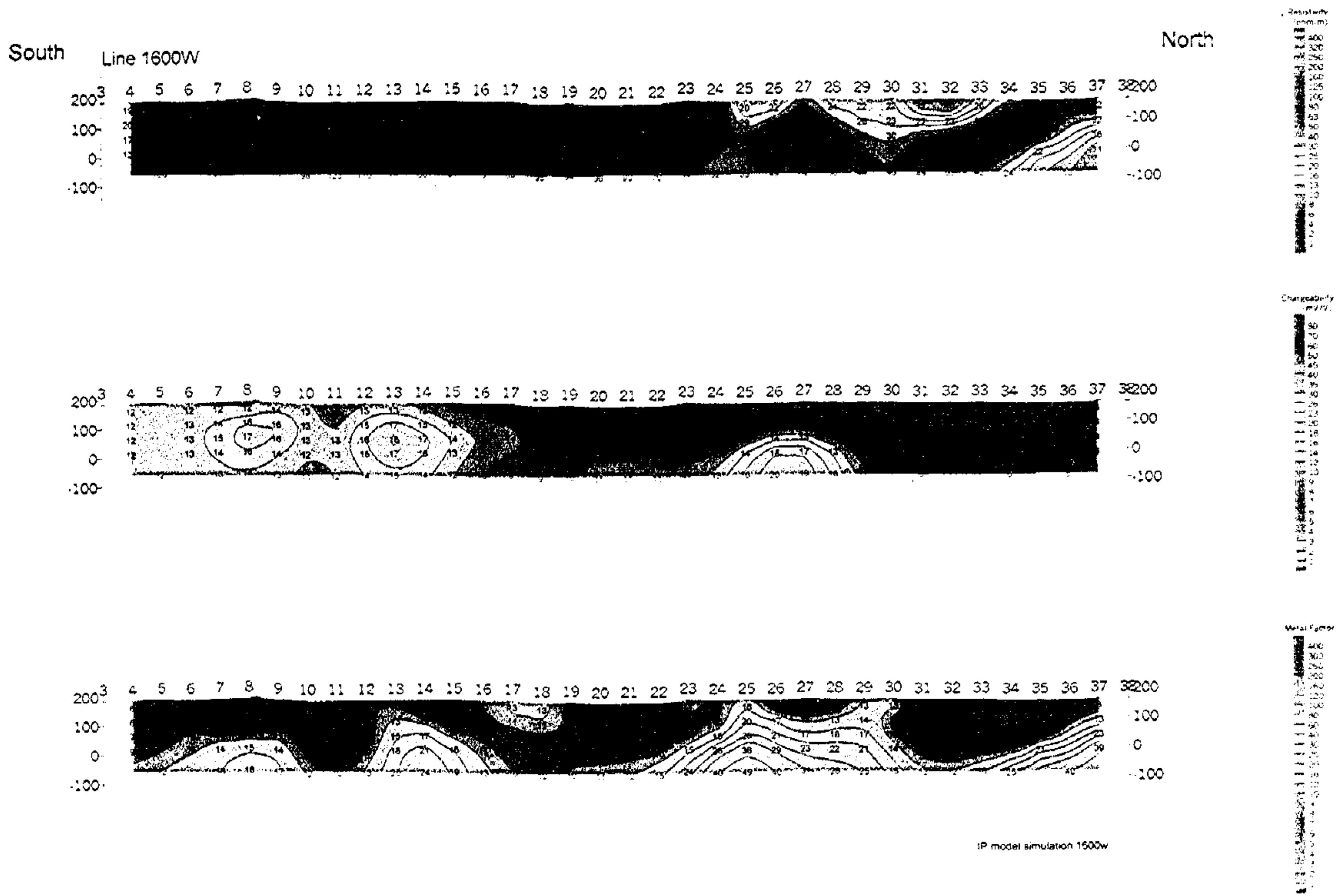

Fig. II-2-12 IP 2D model simulation on line 1600W in Ghuzayn area

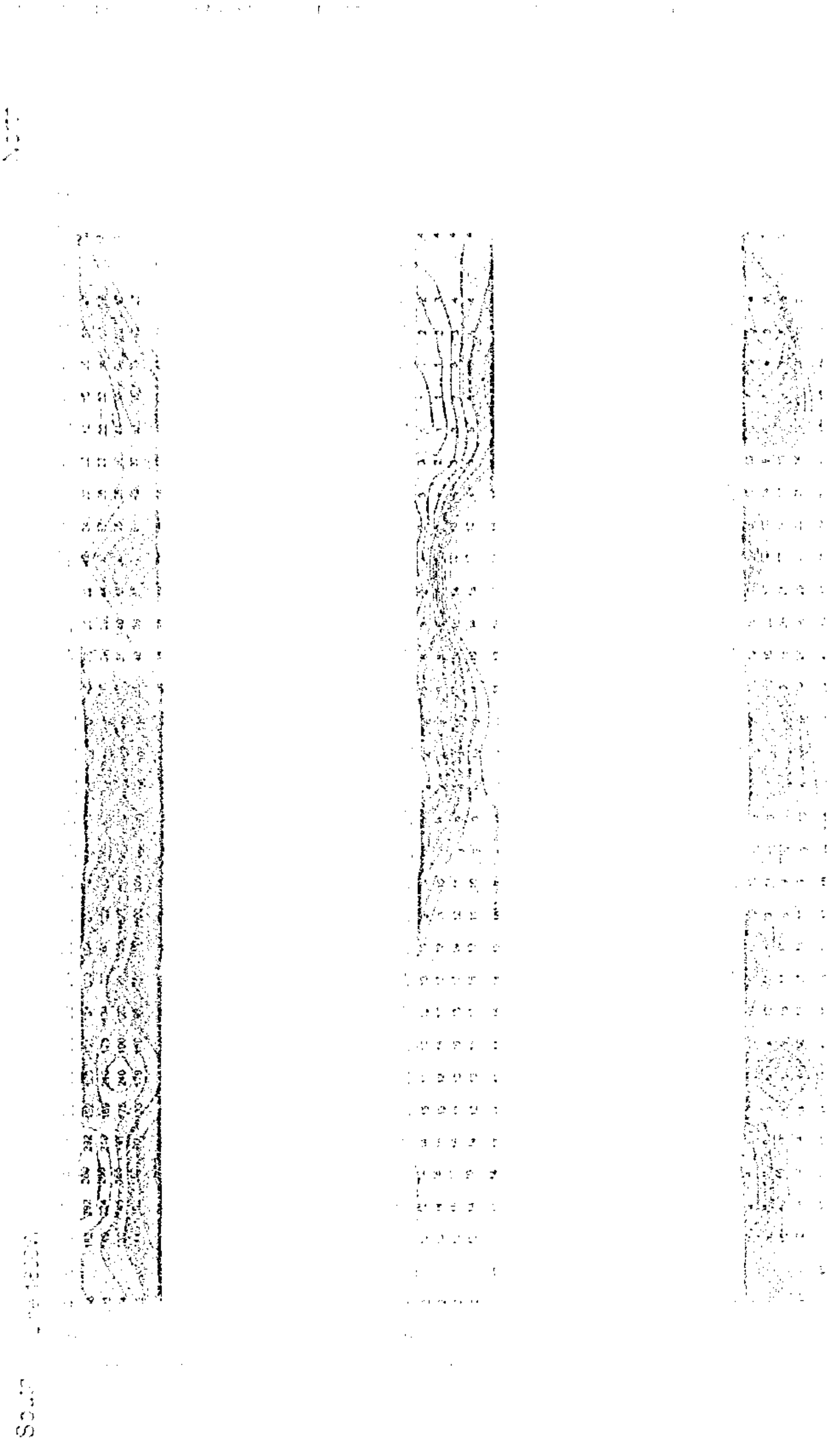

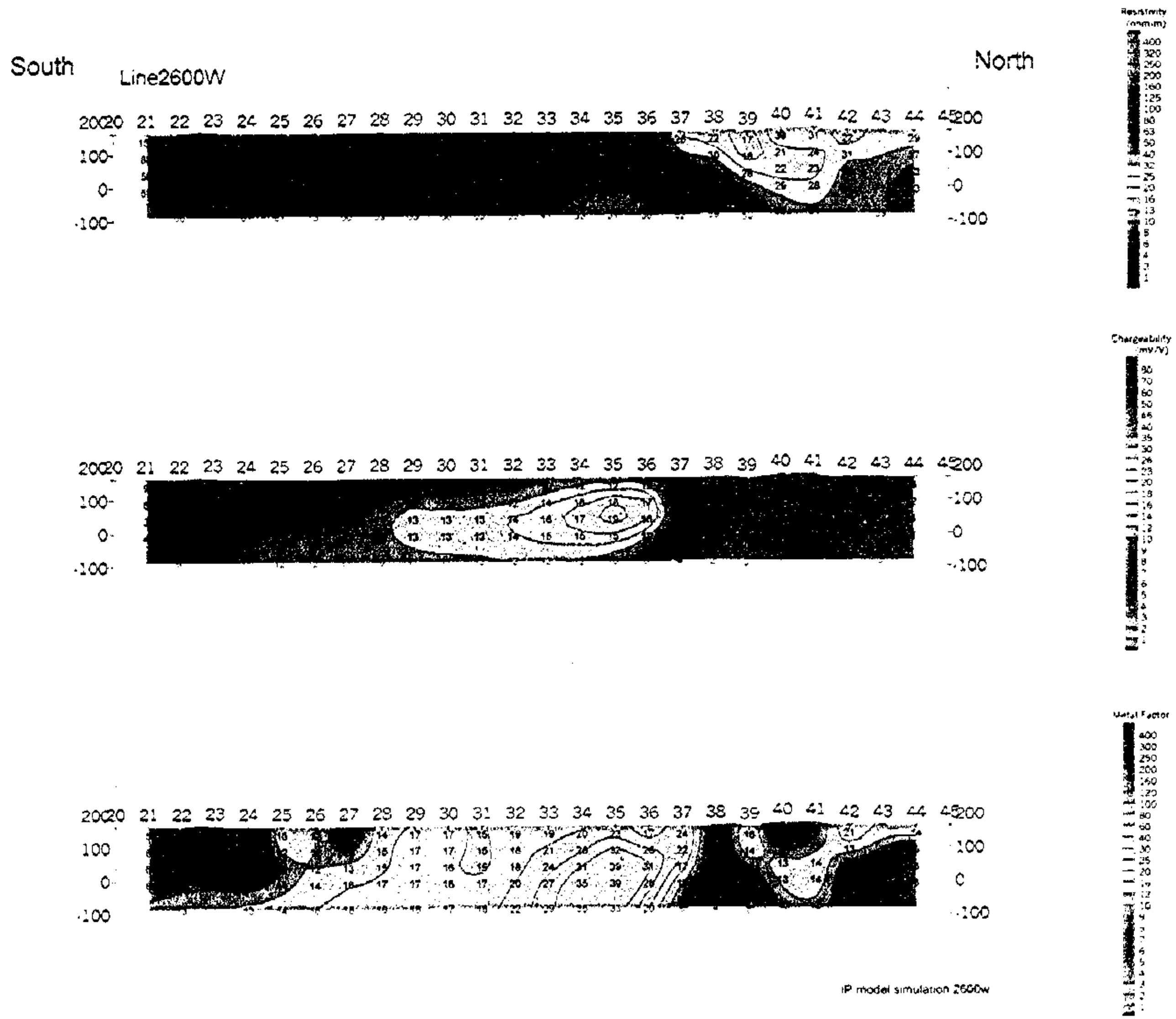

Fig. II-2-13 IP 2D model simulation on line 2600W in Ghuzayn area

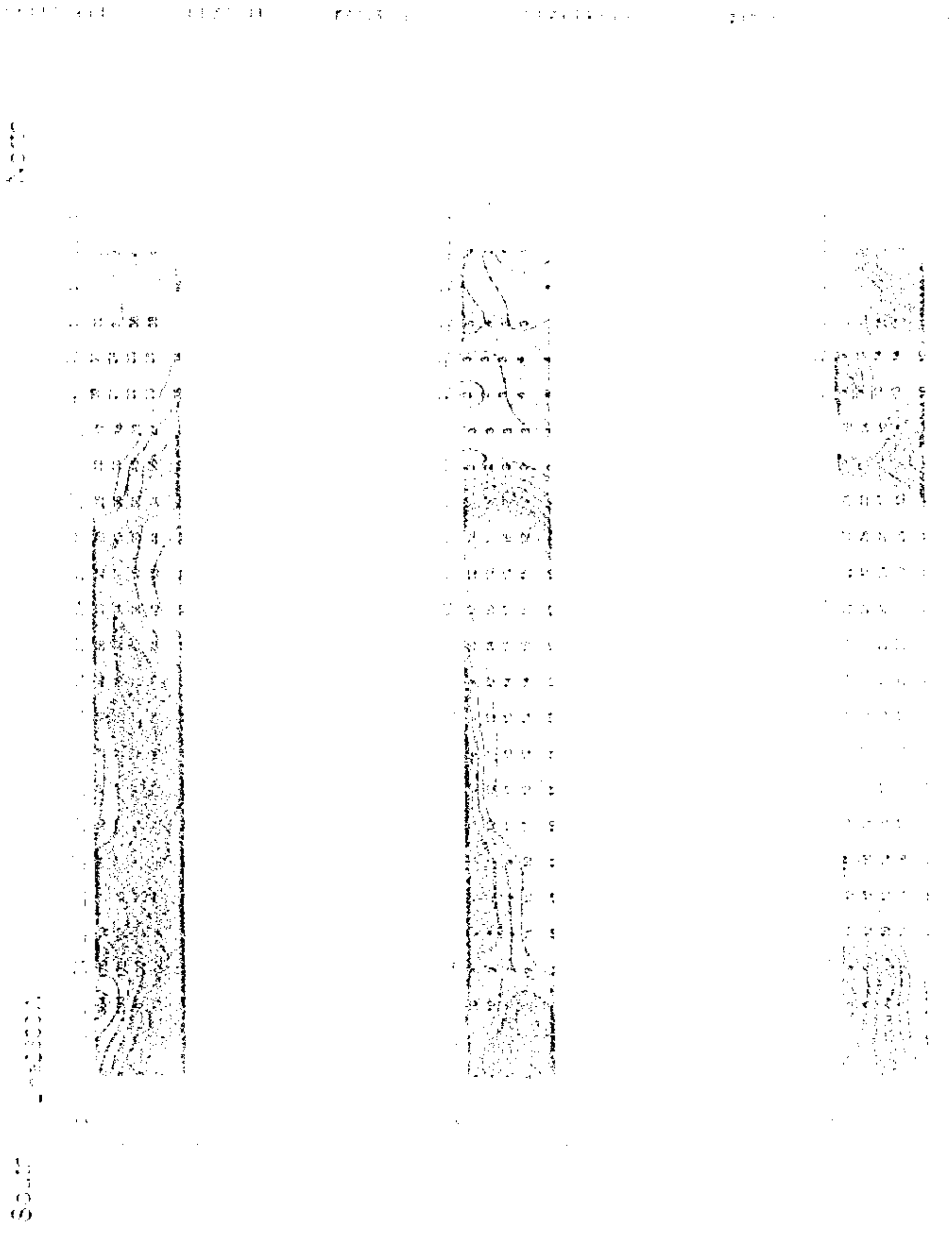

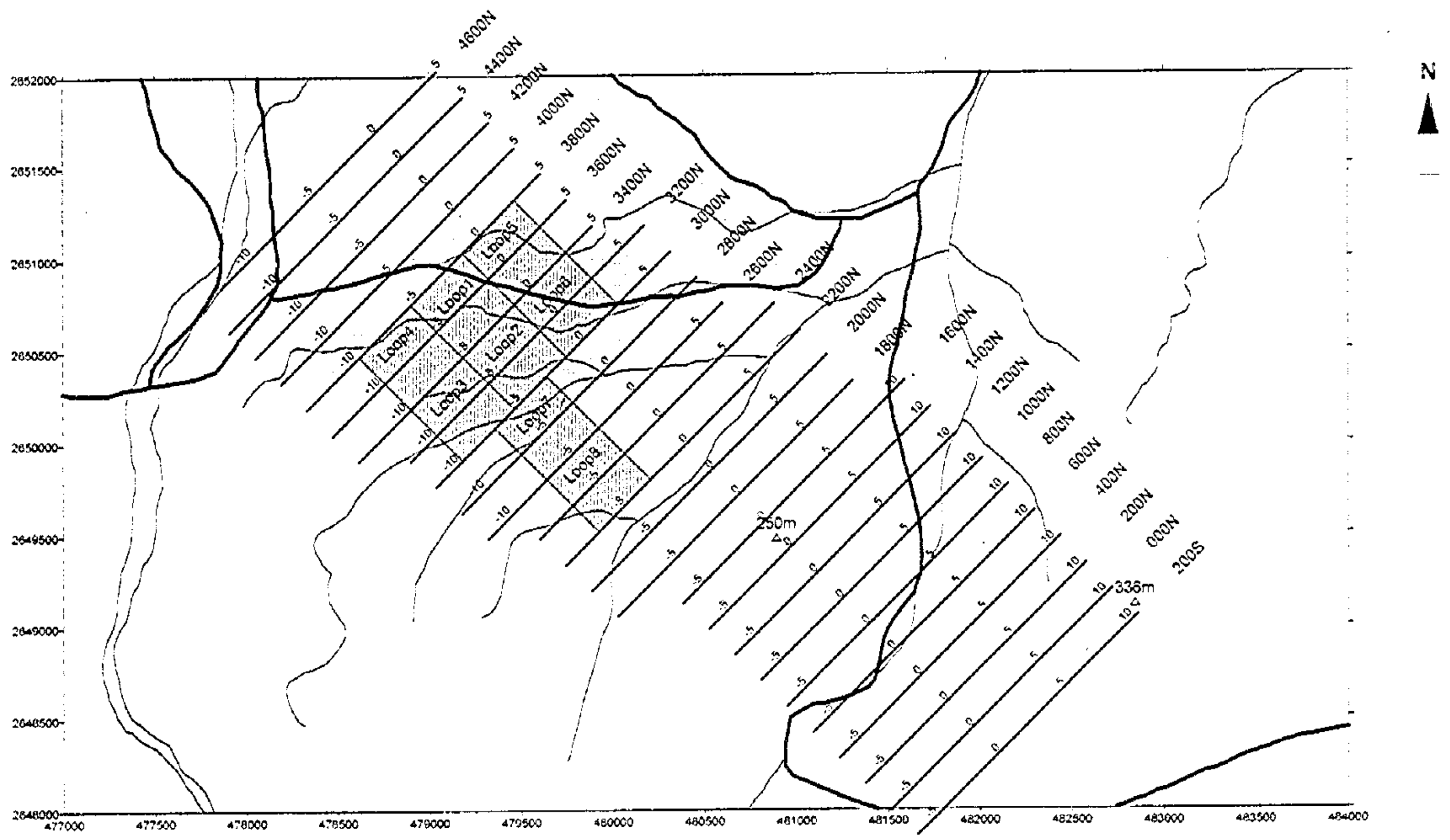

TEM survey area
Road
Wadi
TDIP lines

Fig. II-2-14 Geophysical survey location in Sarami area

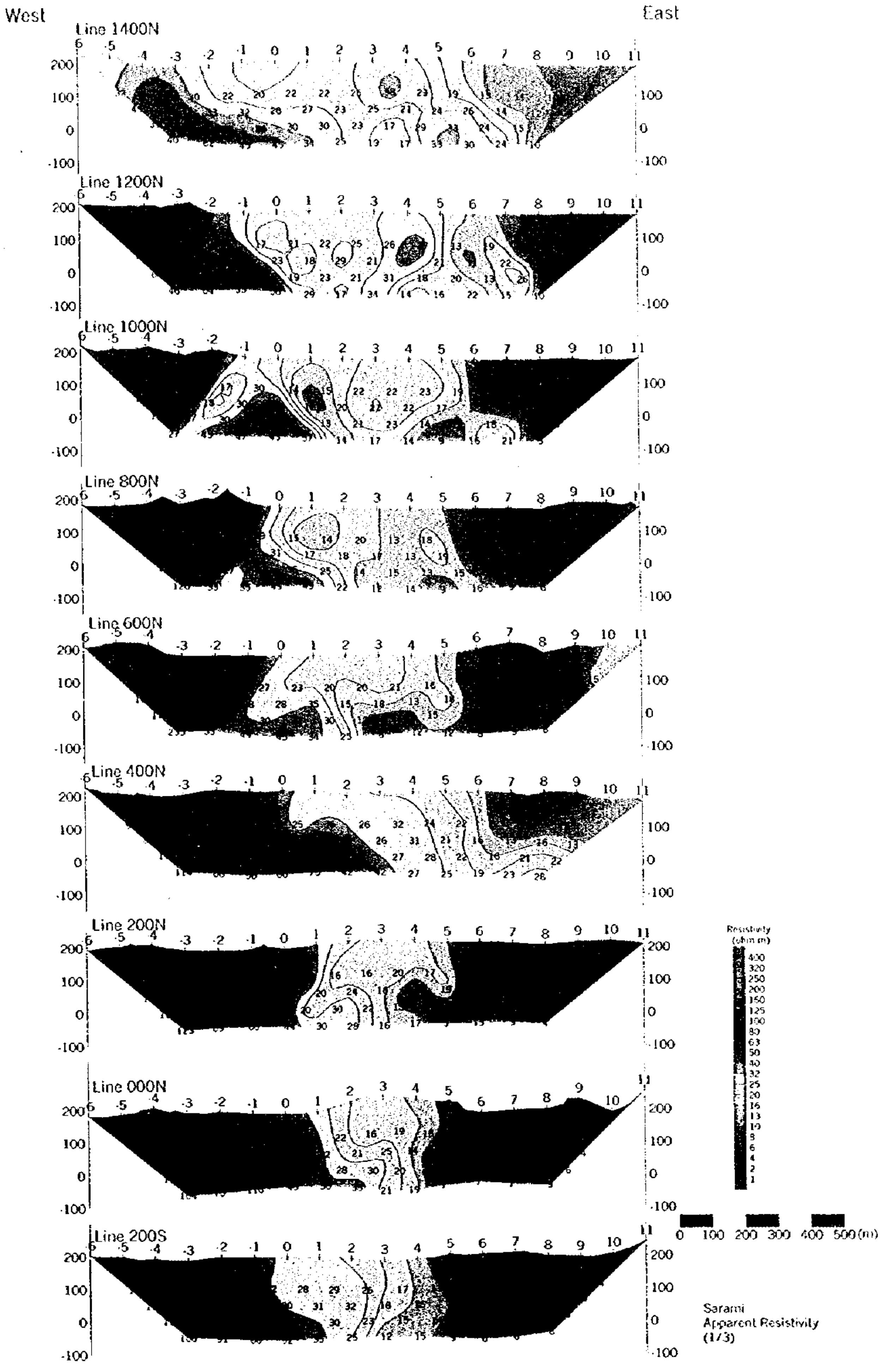

Fig. II-2-15(1) Apparent resistivity pseudo-sections in Sarami area

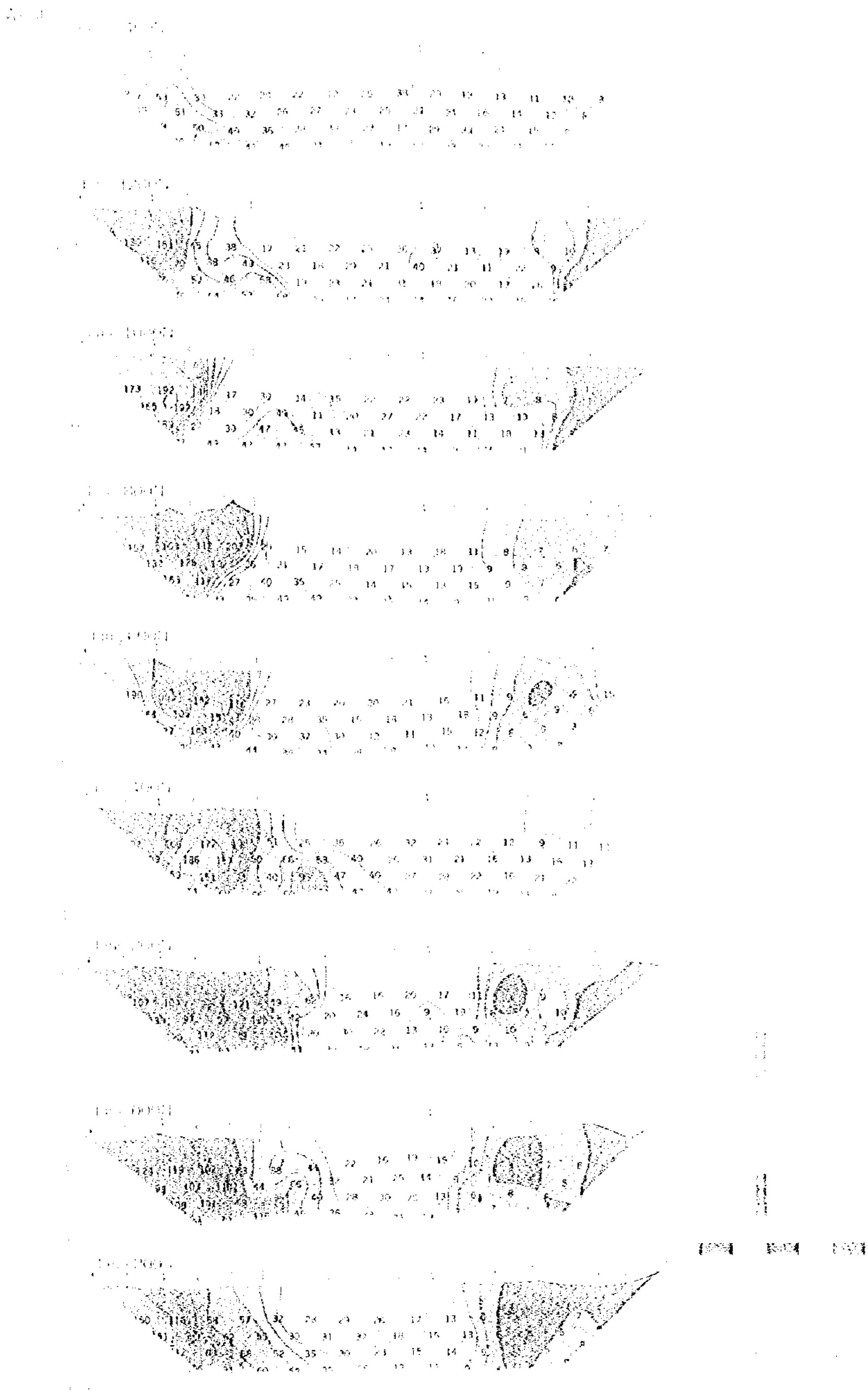

Fig. II. 2-[illegible] Apparent resistivity pseudo section in S[illegible]

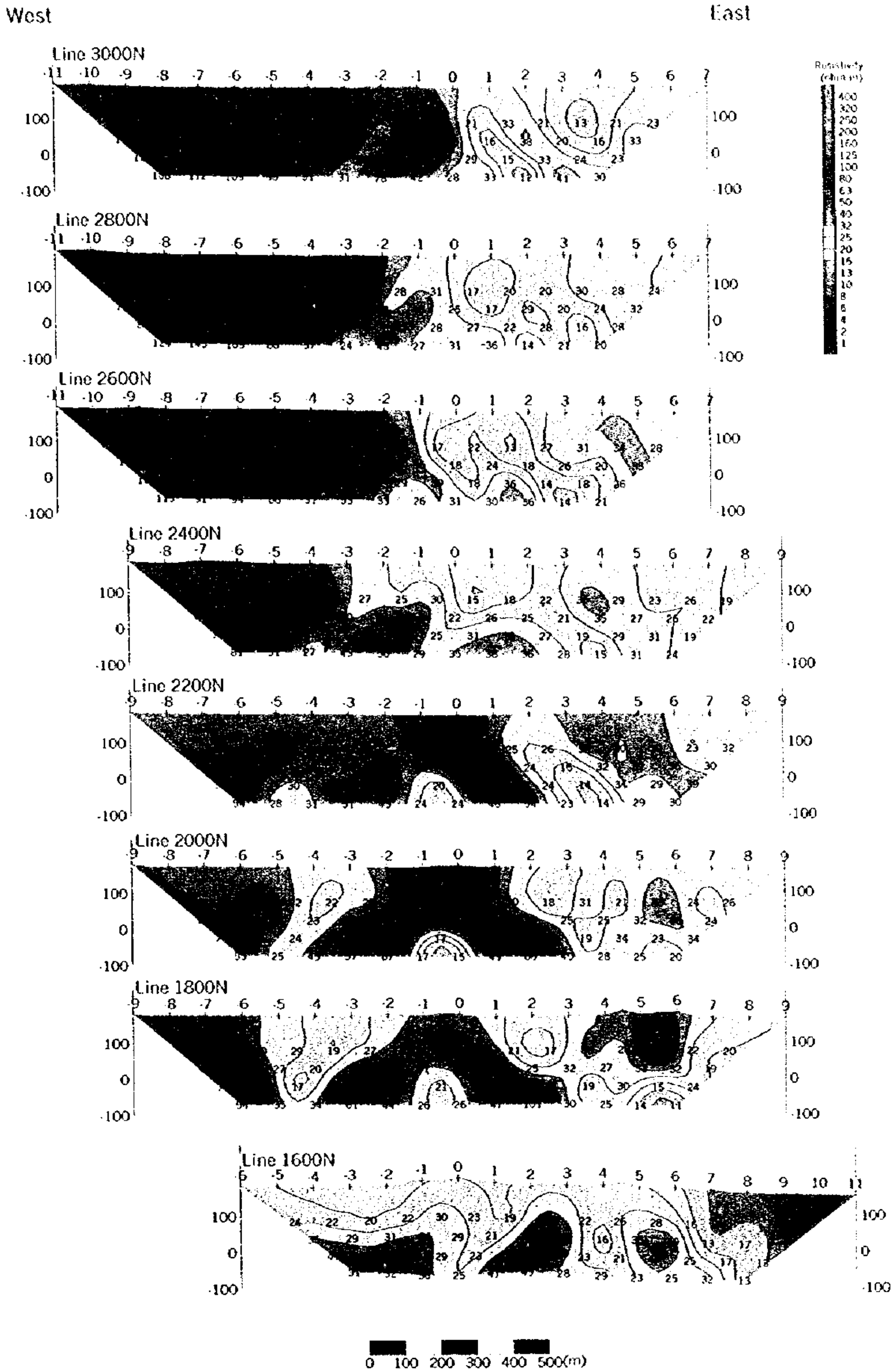

Fig. II-2-15(2) Apparent resistivity pseudo-sections in Sarami area

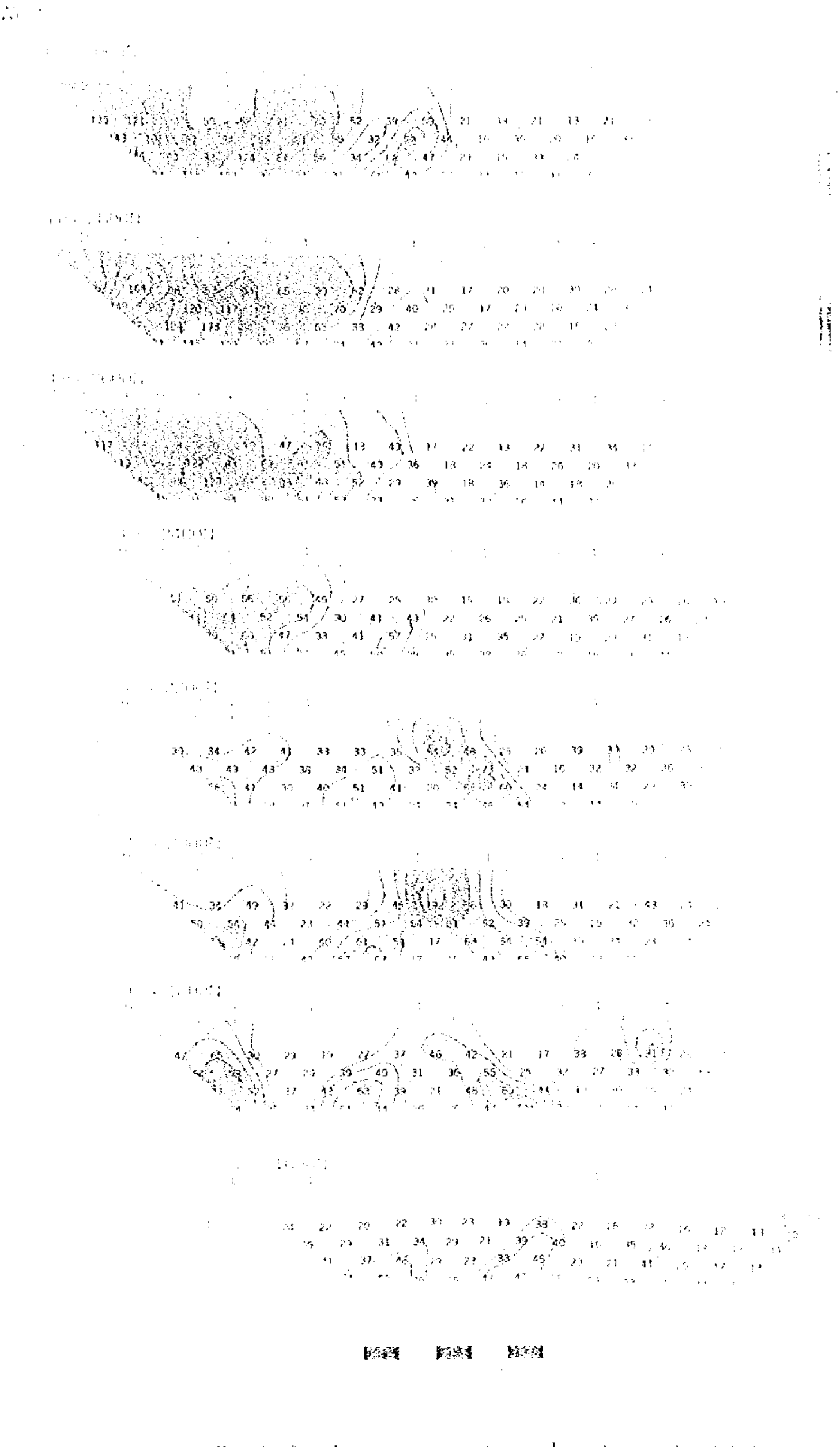

Fig. II-[illegible] Apparent [illegible] activity [illegible]

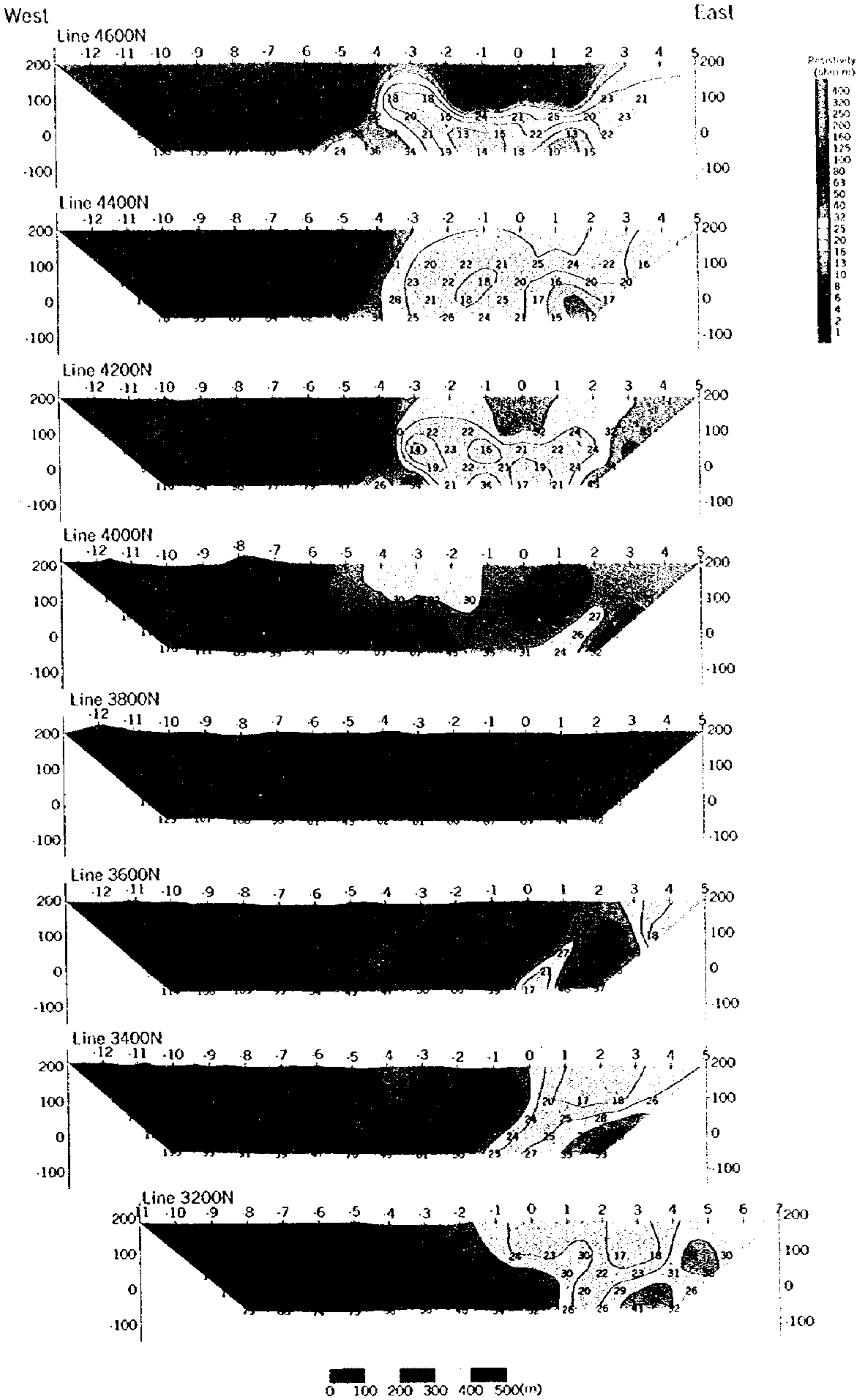

Fig. II-2-15(3) Apparent resistivity pseudo-sections in Sarami area

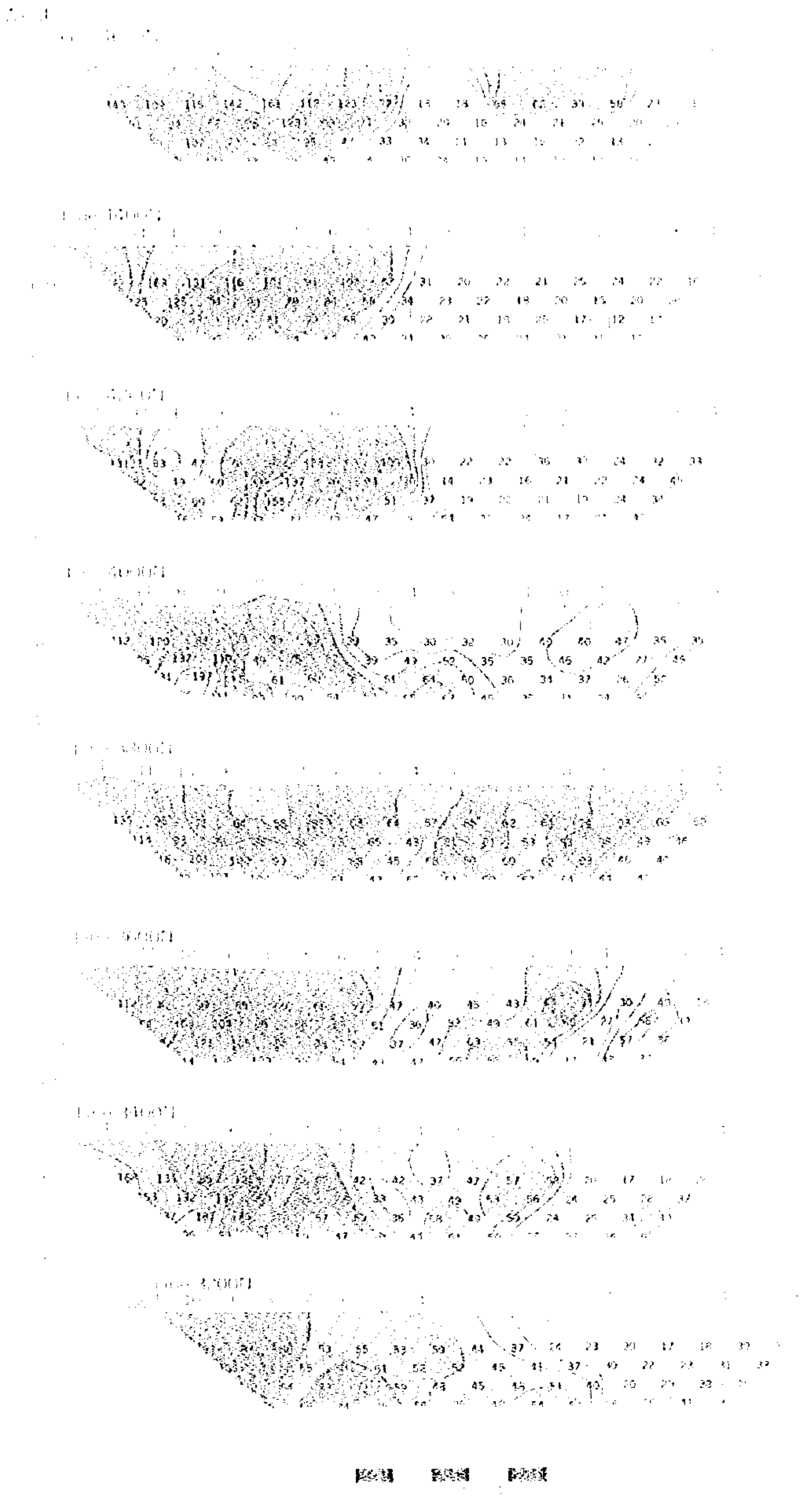

Fig. II.2 [illegible] Apparent [illegible]

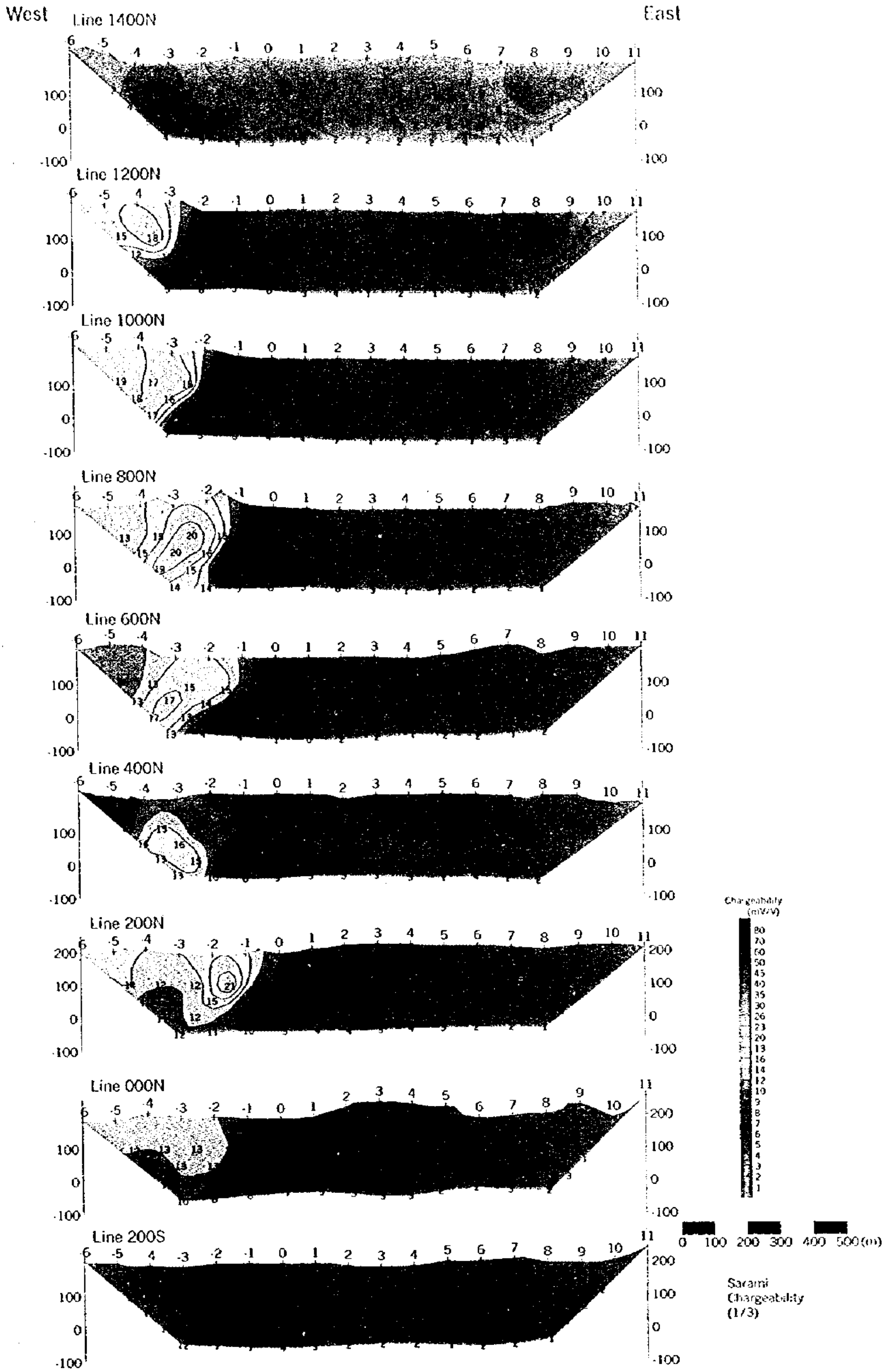

Fig. II-2-16(1) Chargeability pseudo-sections in Sarami area

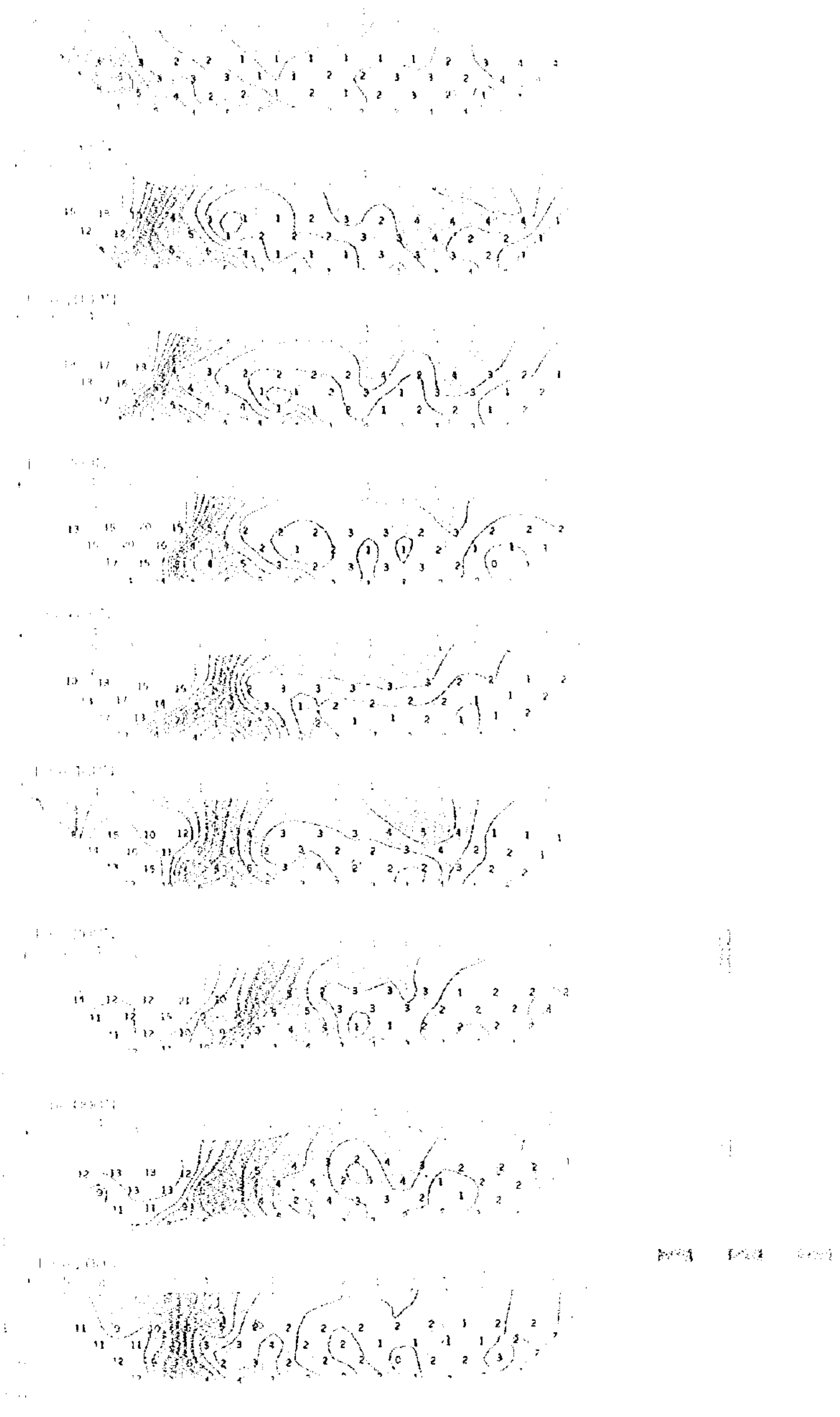

Fig. 11. [illegible] Chlorophyll [illegible] in Saanich Inlet

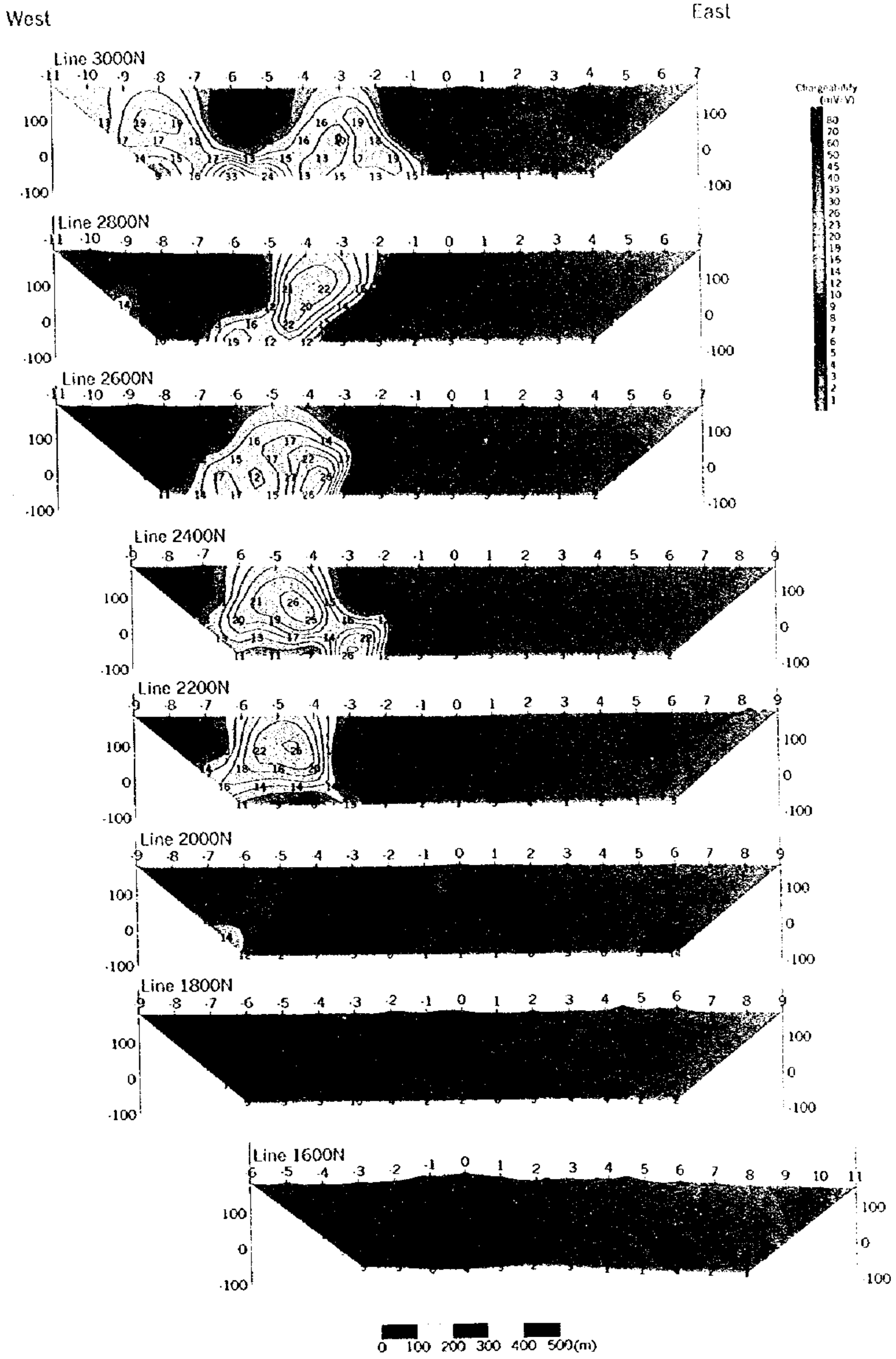

Fig. II -2-16(2) Chargeability pseudo-sections in Sarami area

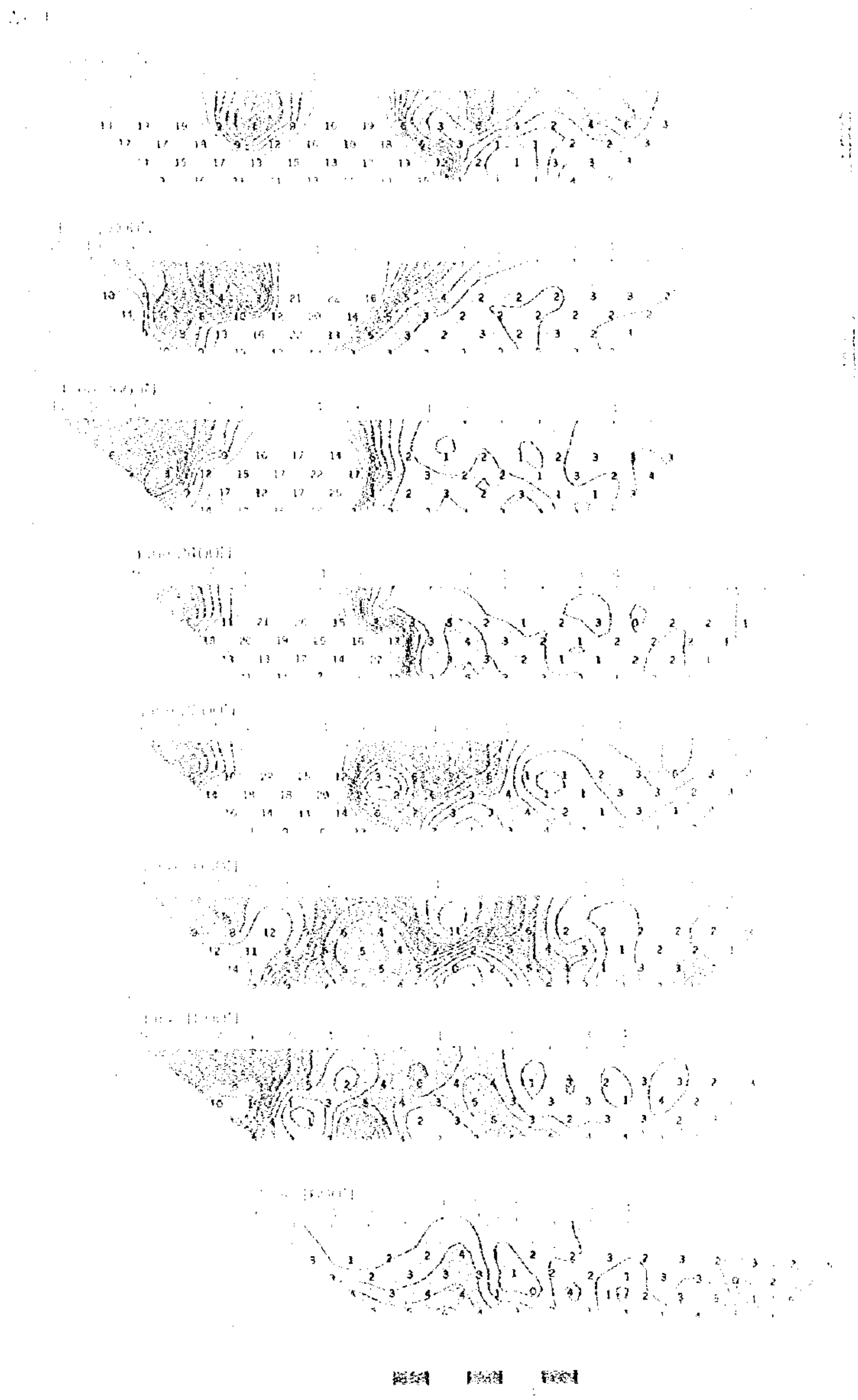

Fig. II [illegible]

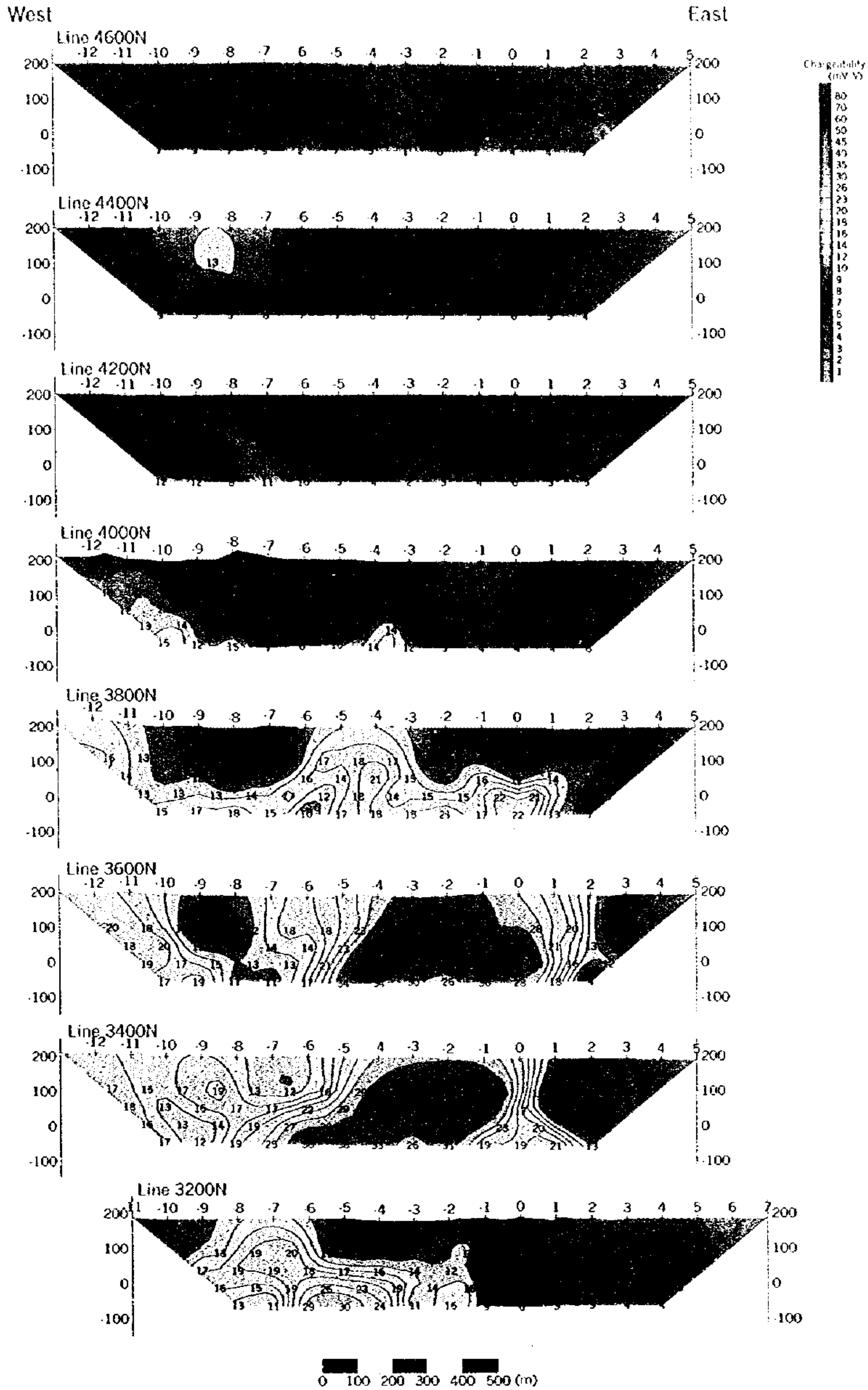

Fig. II-2-16(3) Chargeability pseudo-sections in Sarami area

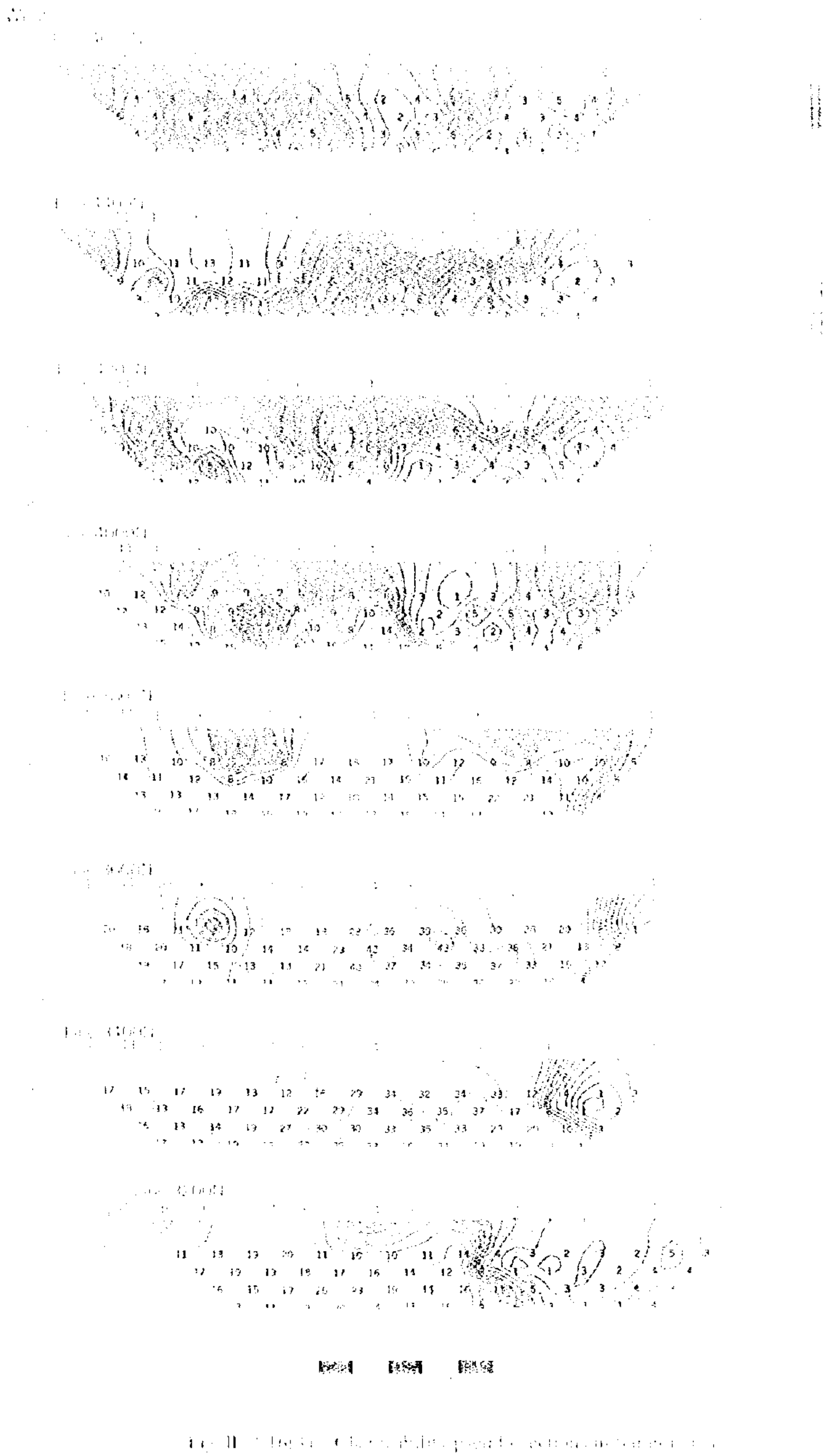

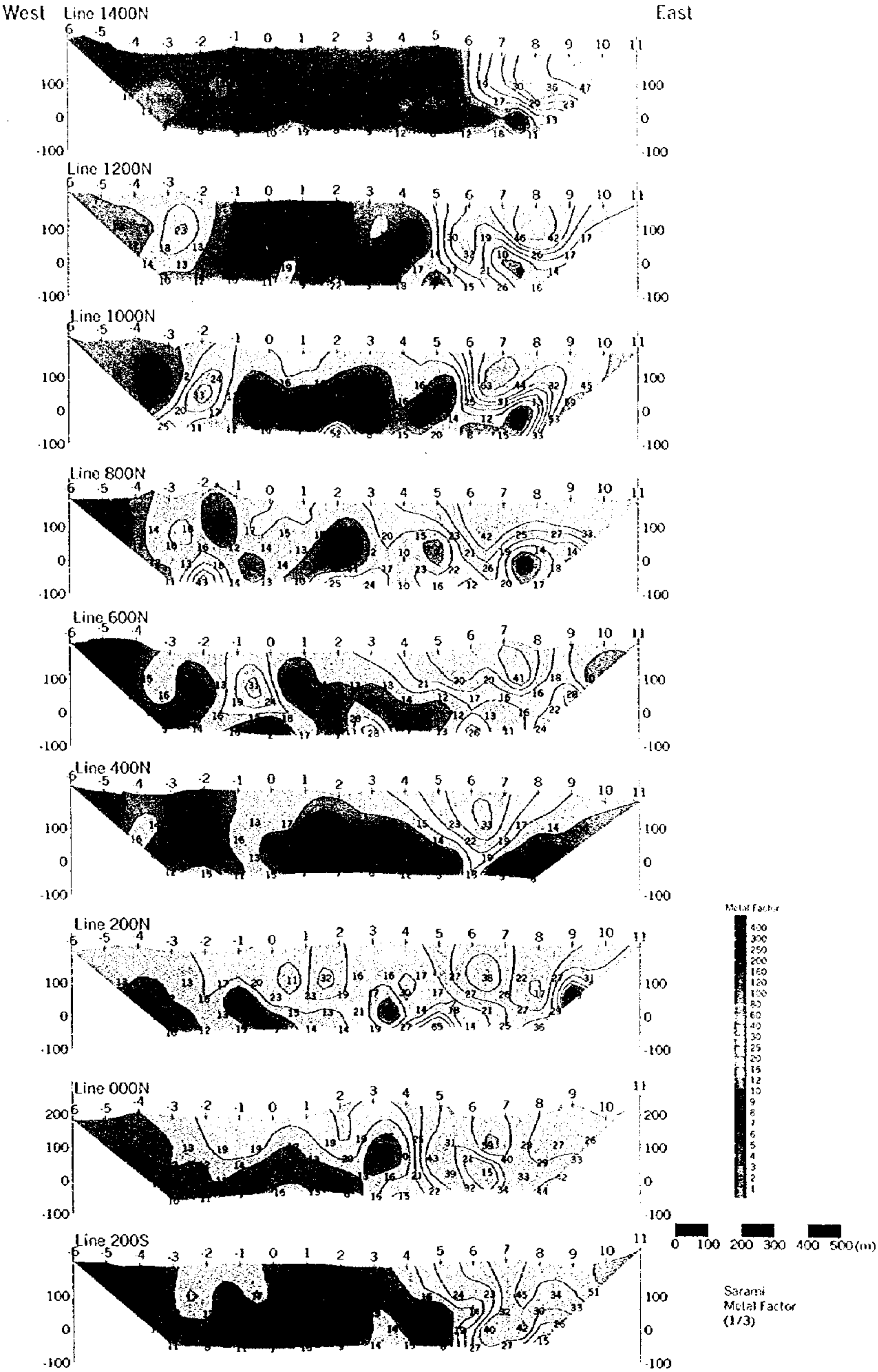

Fig. II-2-17(1) Metal factor pseudo-sections in Sarami area

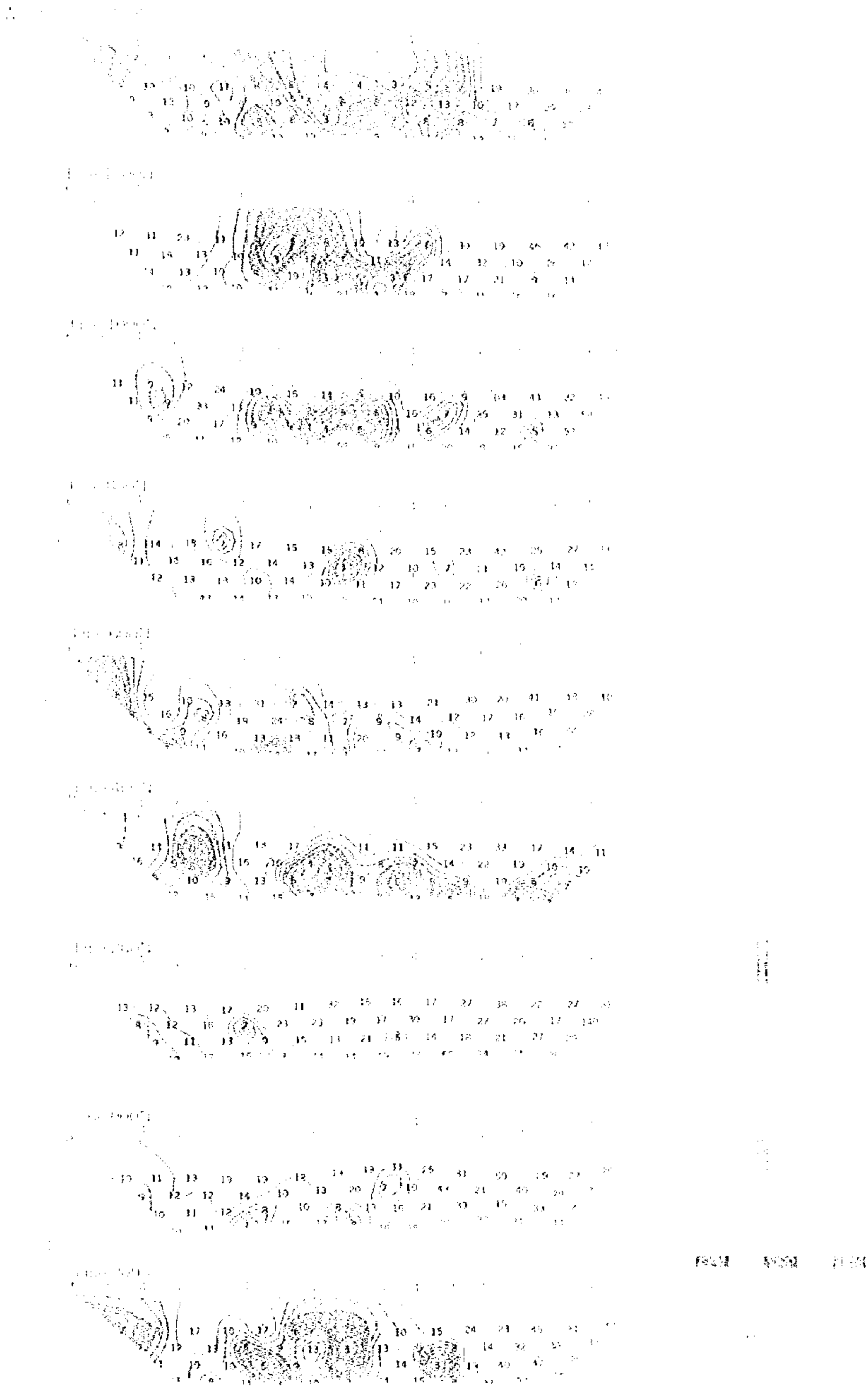

Fig. II.2.1.7(6) Metal factor pseudo-sections in Saona area

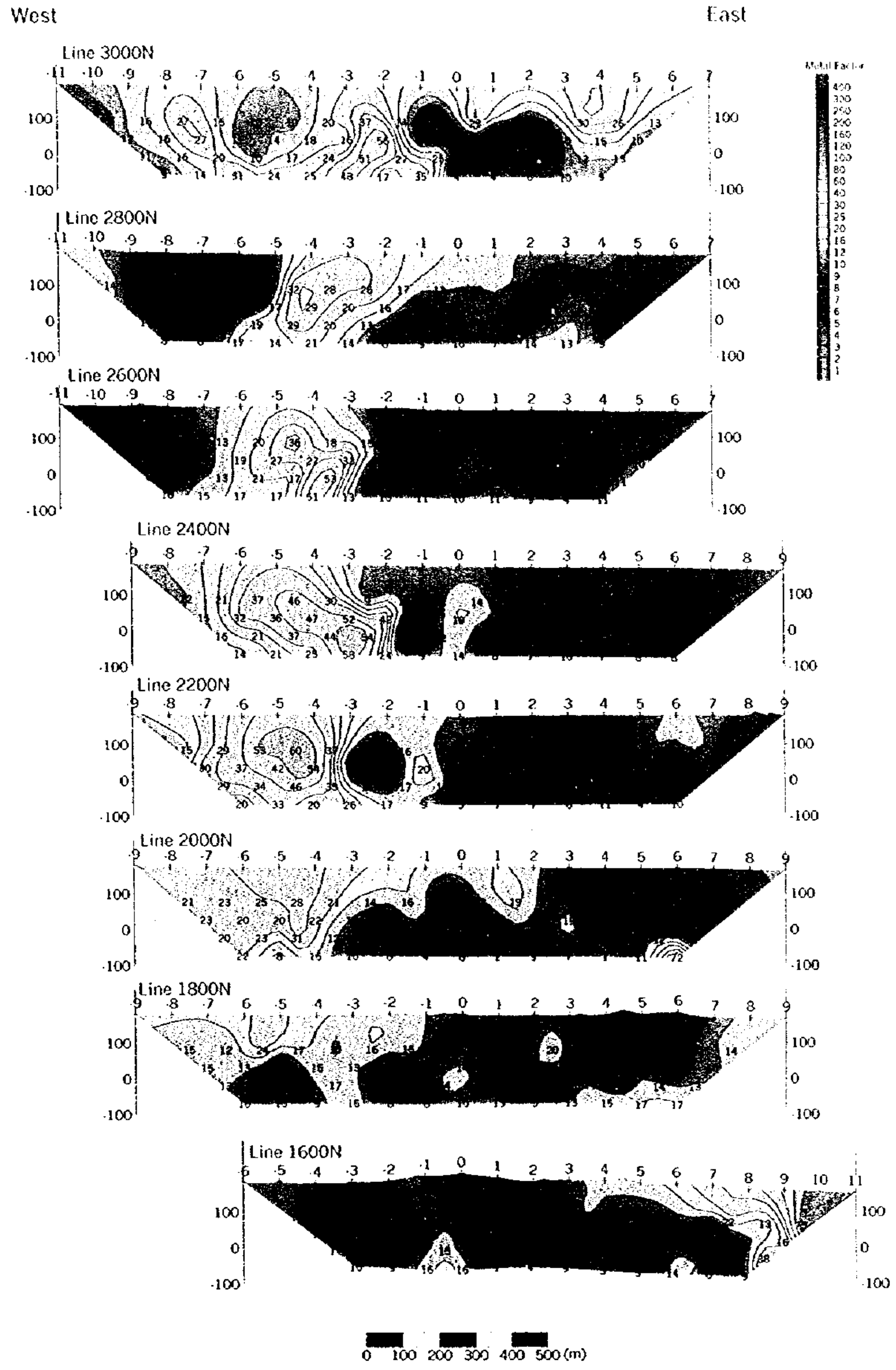

Fig. II-2-17(2) Metal factor pseudo-sections in Sarami area

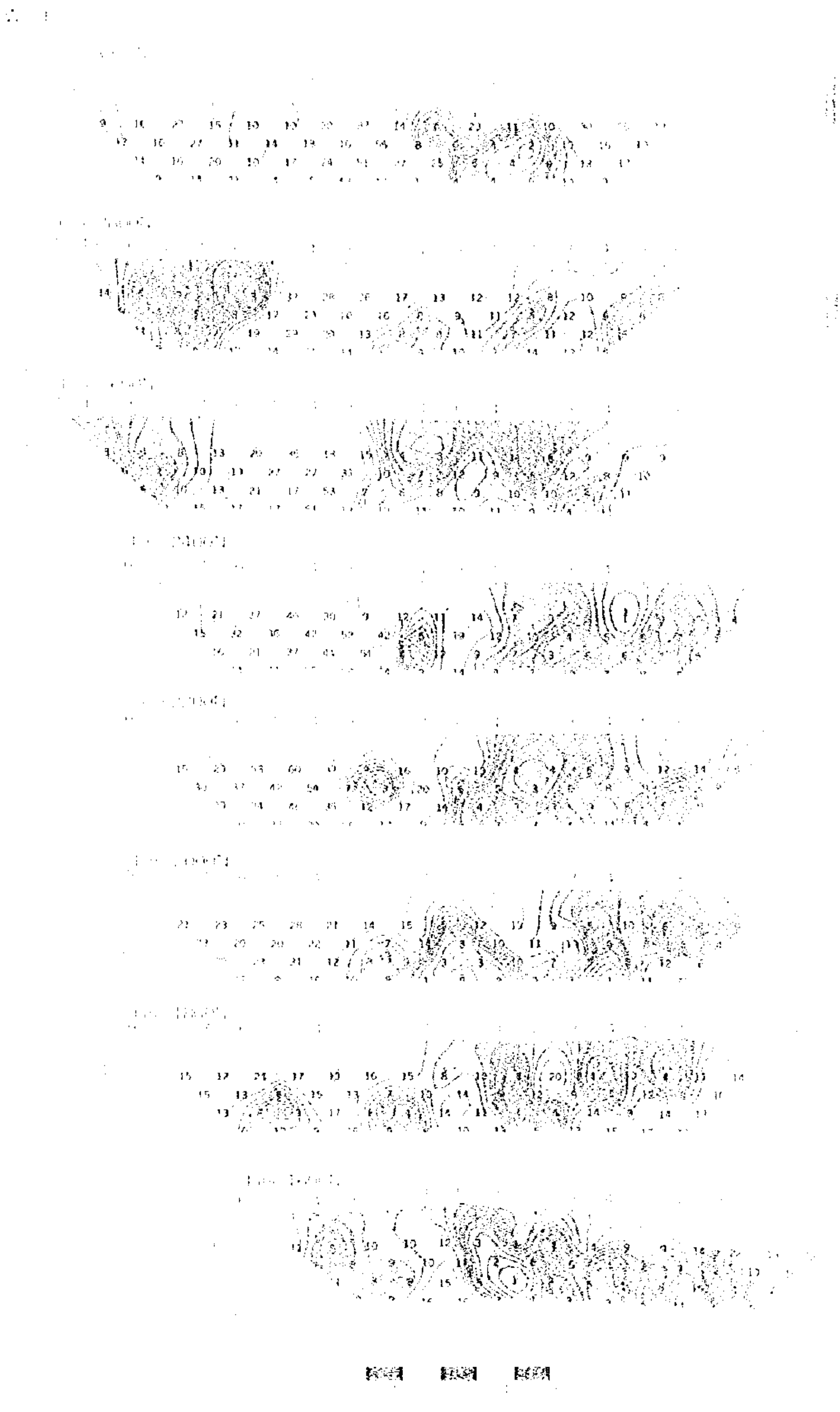

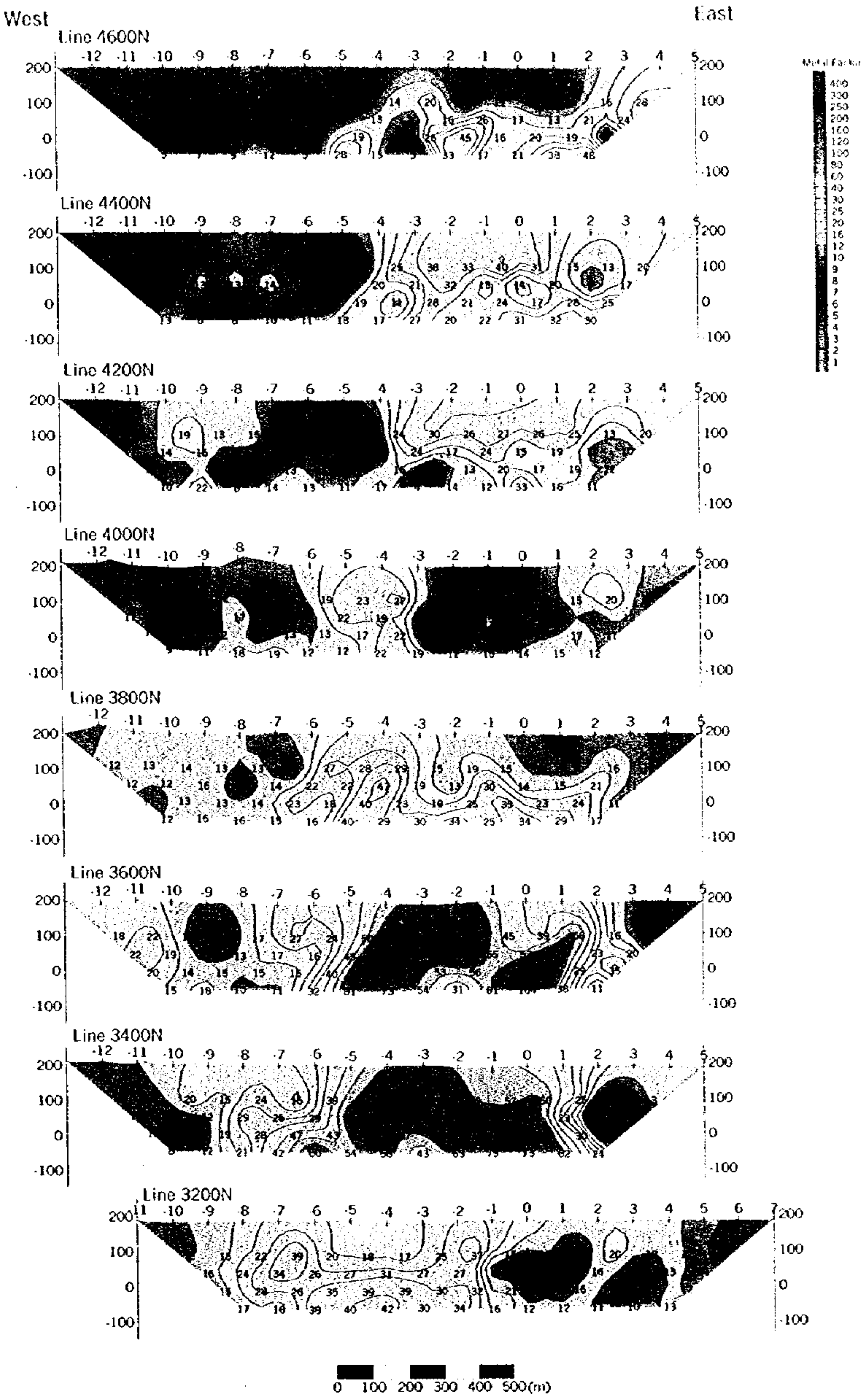

Fig. II-2-17(3) Metal factor pseudo-sections in Sarami area

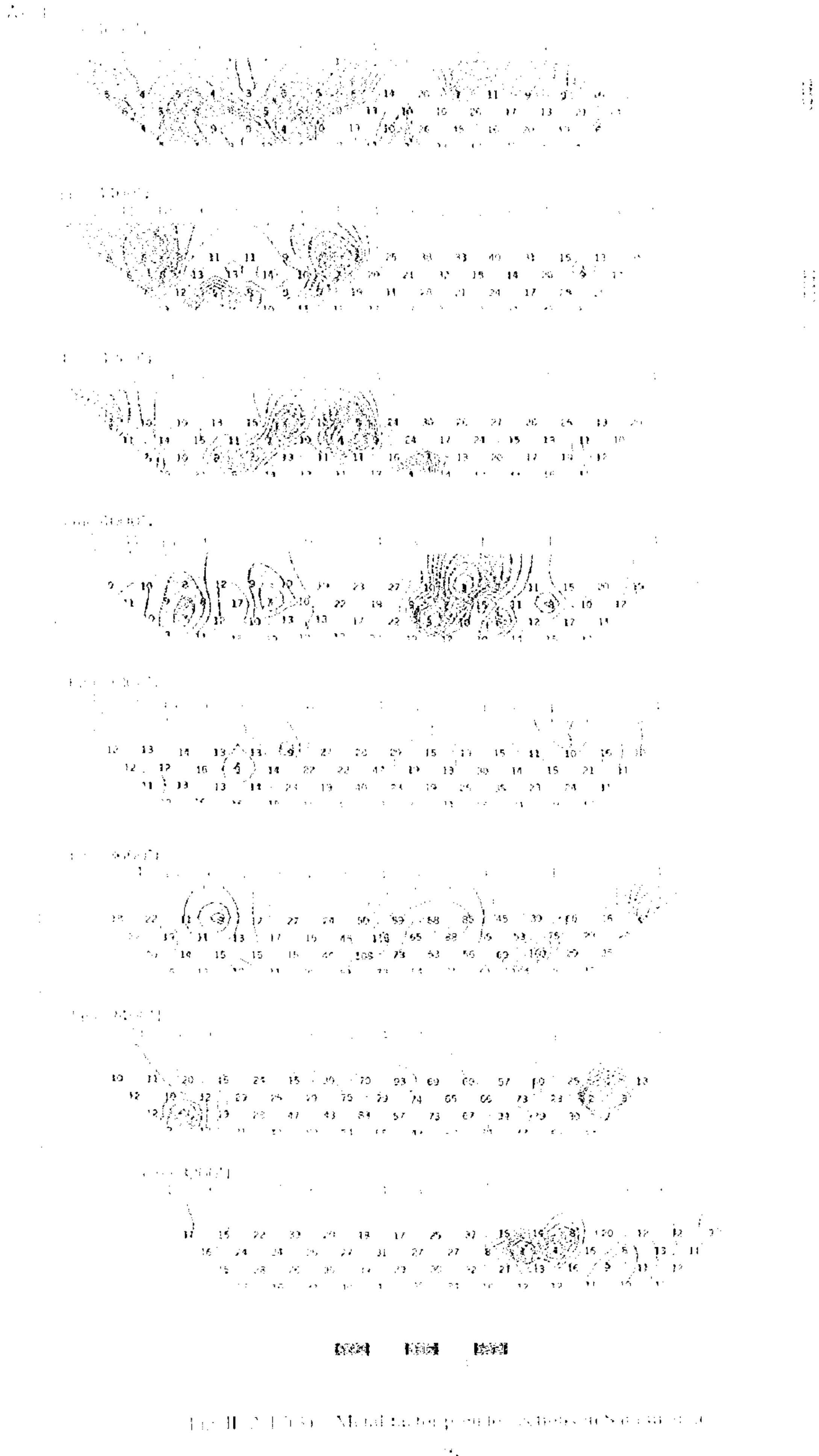

Fig. II. [illegible] Metal factor [illegible]

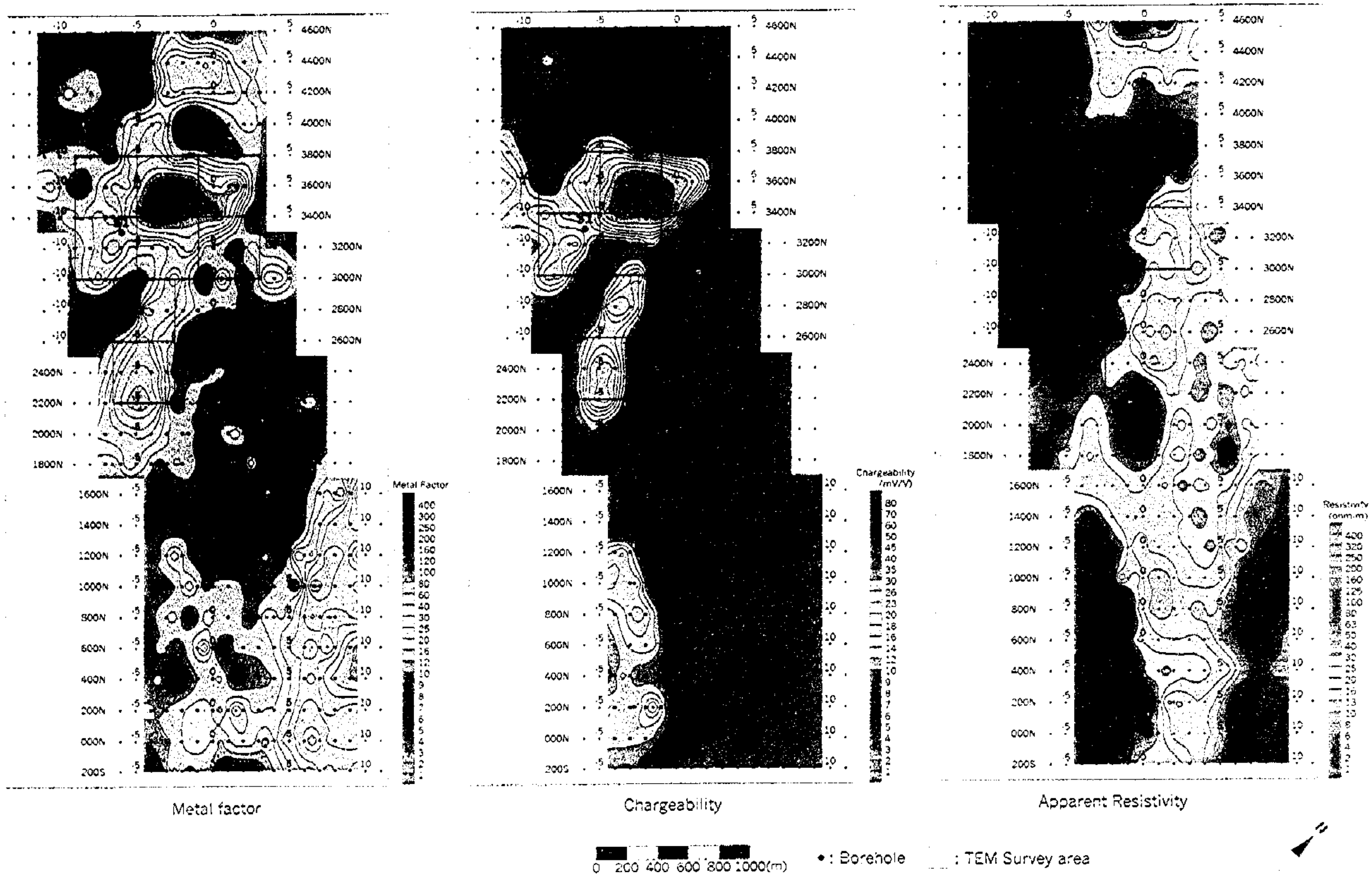

Fig. II-2-18 IP plane map of n=1 in Sarami area

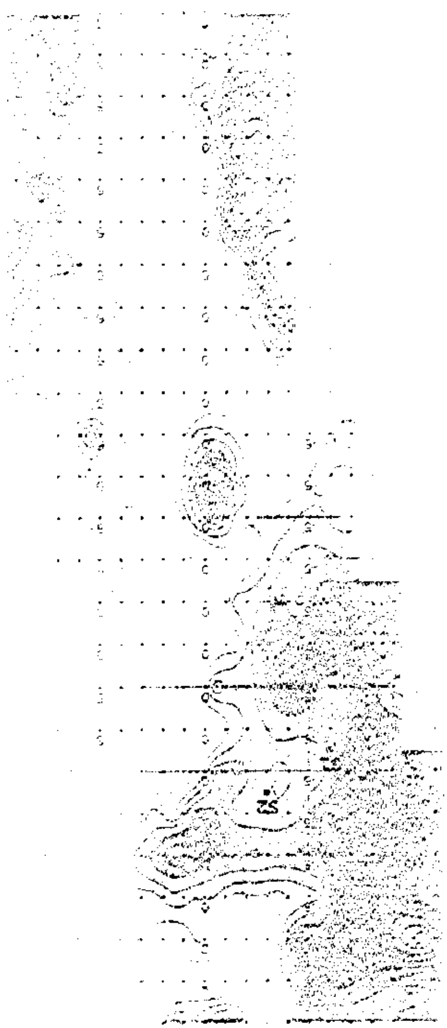

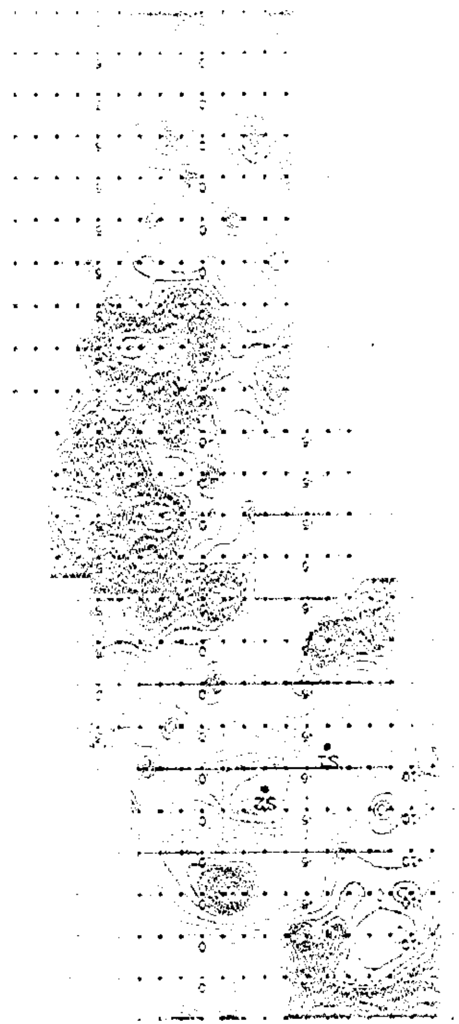

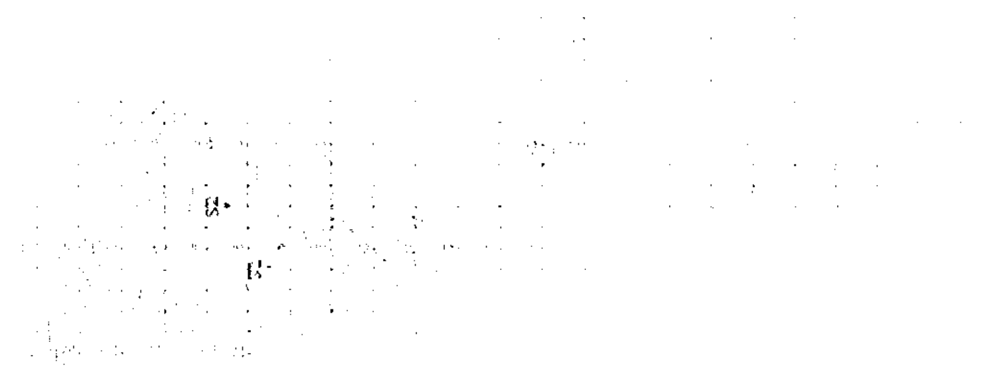

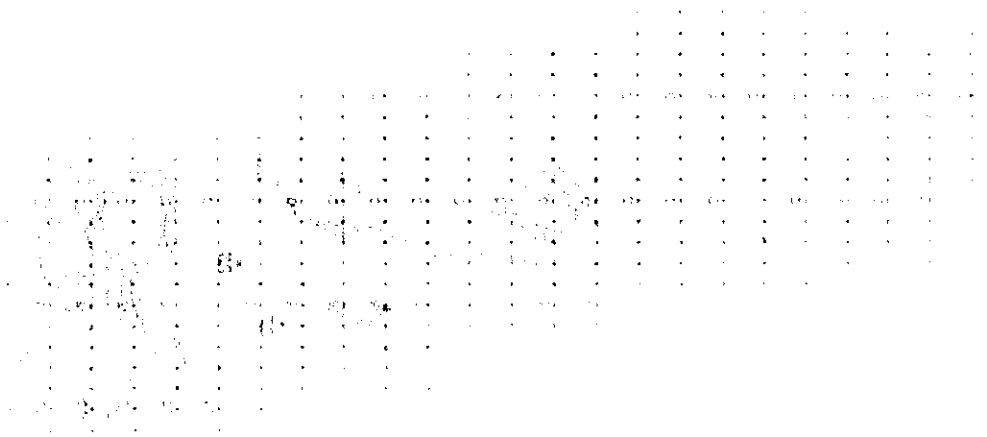

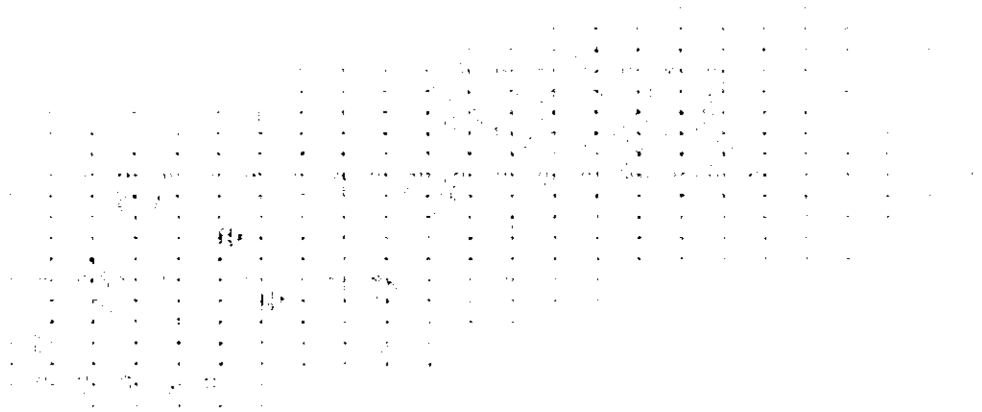

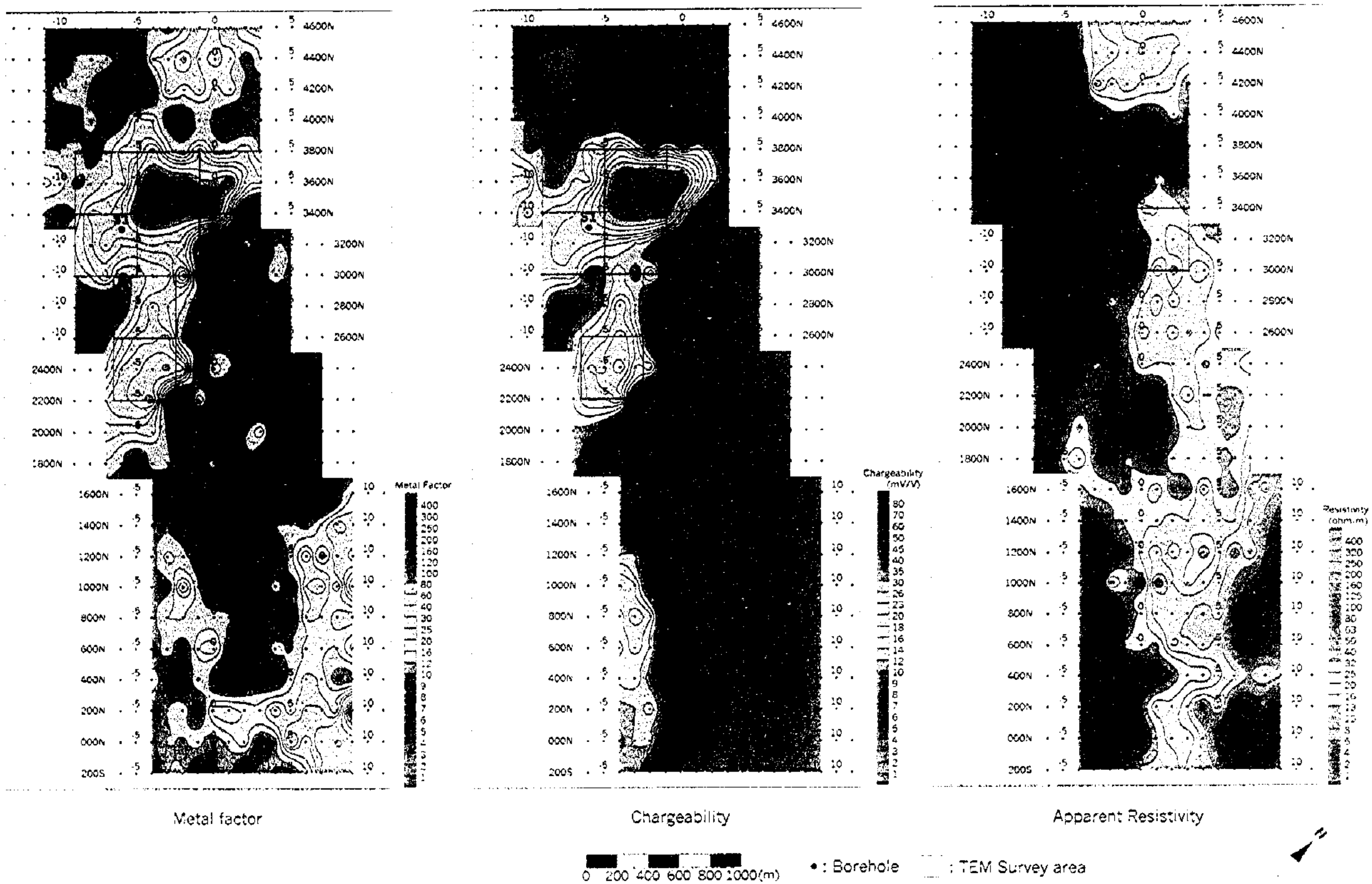

Fig. II-2-19 IP plane map of n=2 in Sarami area

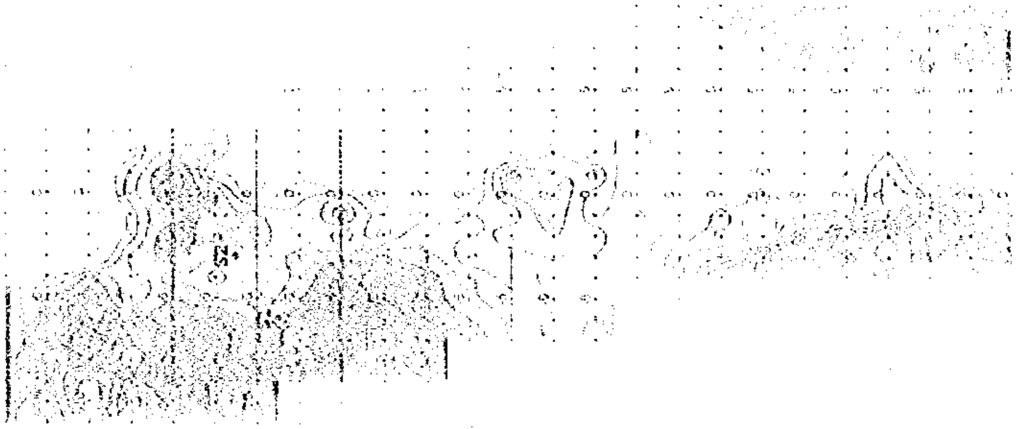

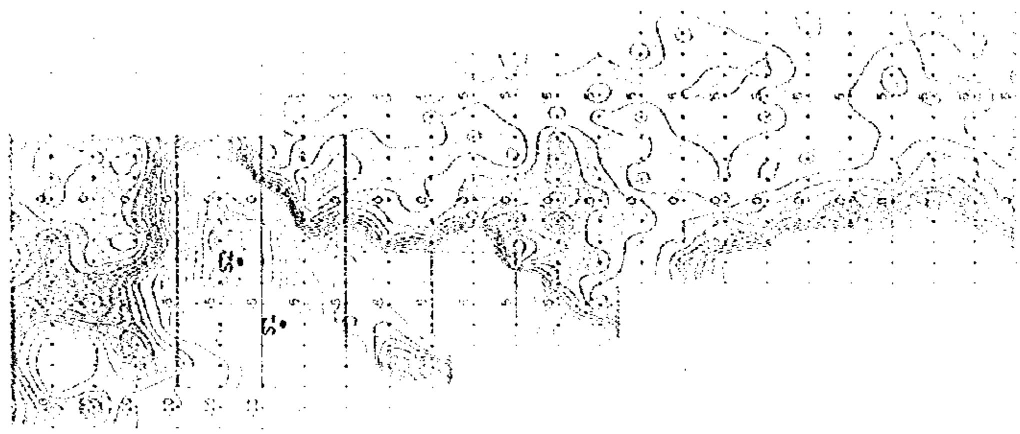

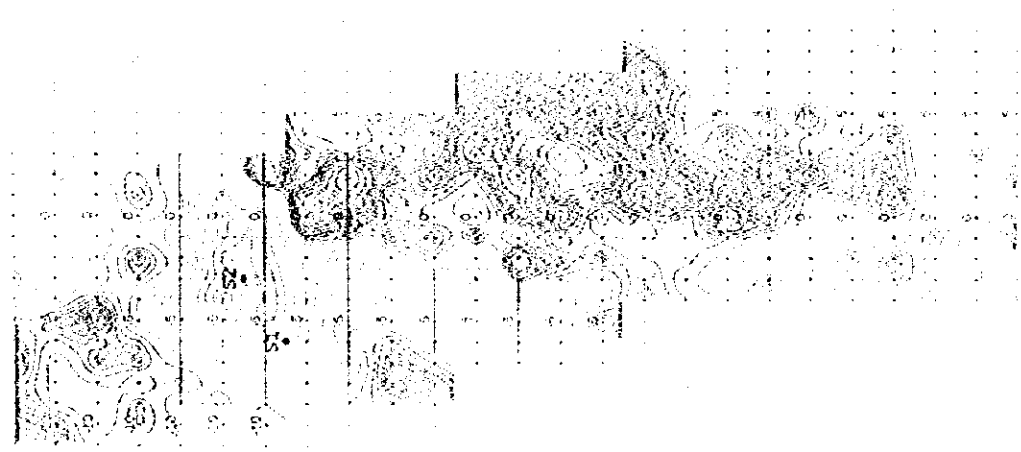

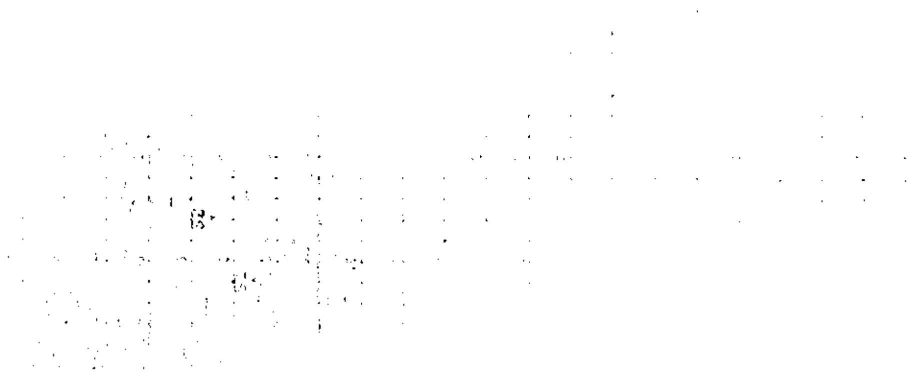

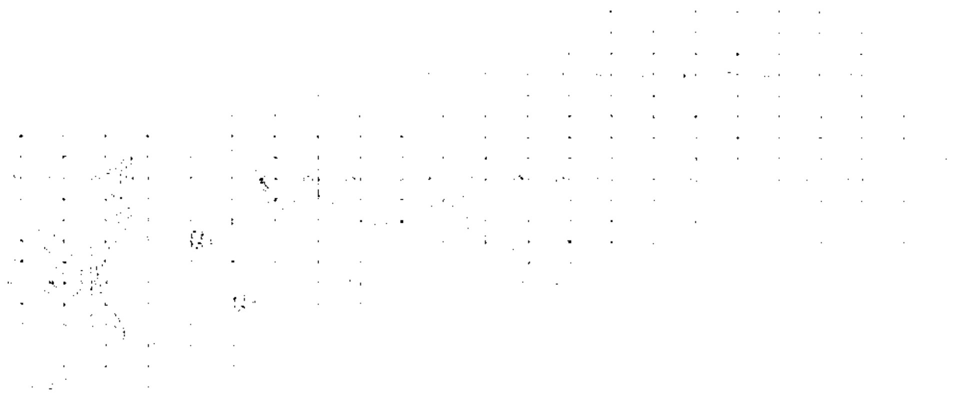

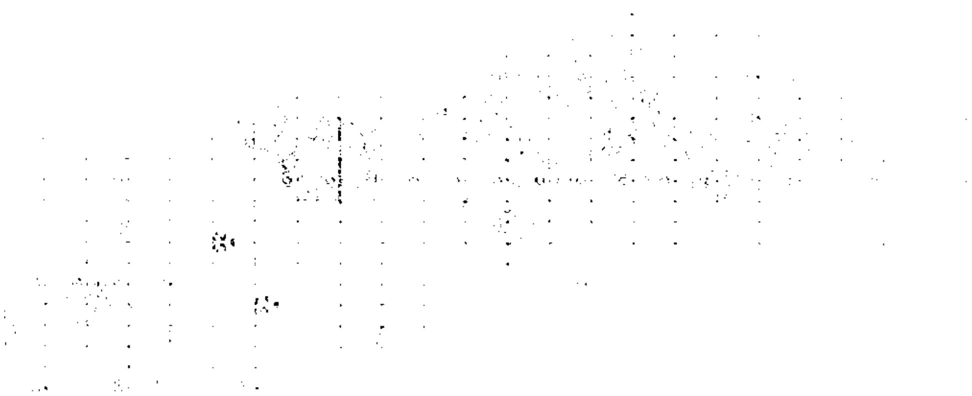

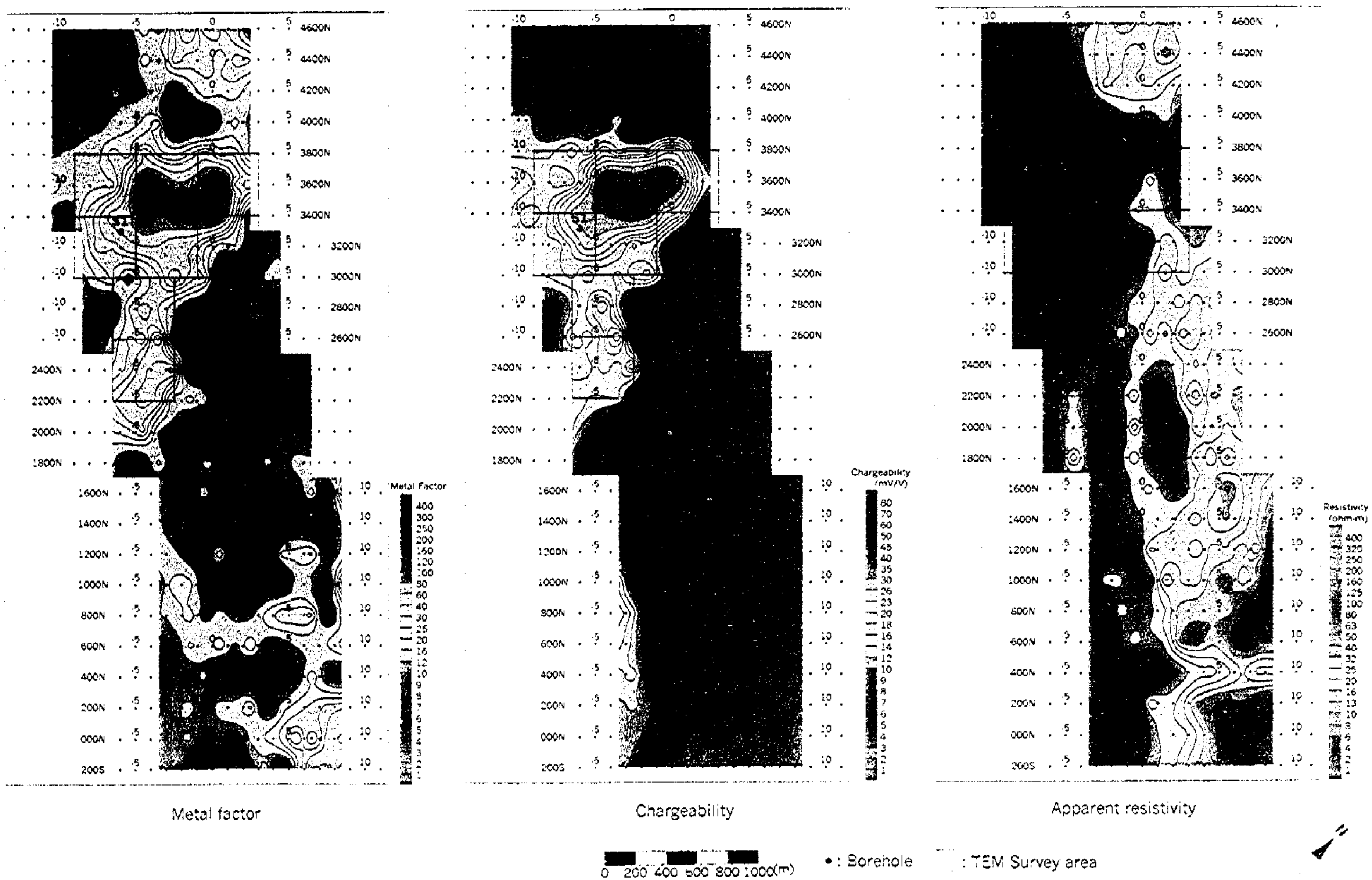

Fig. II-2-20 IP plane map of n=3 in Sarami area

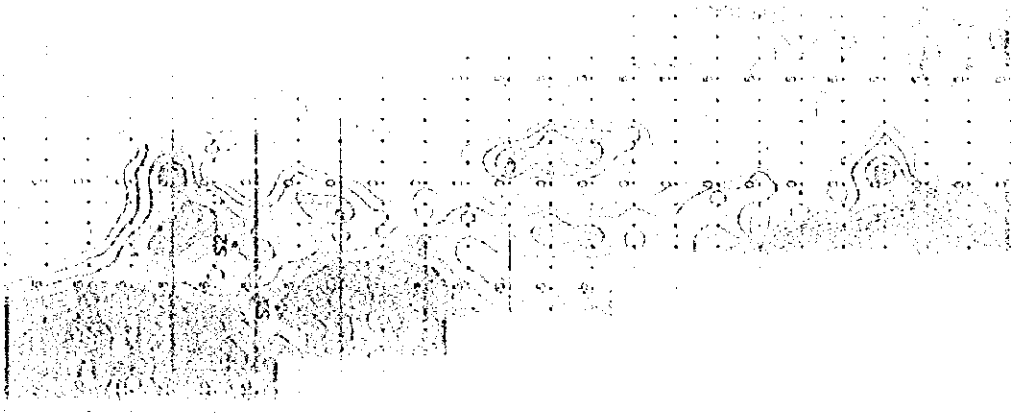

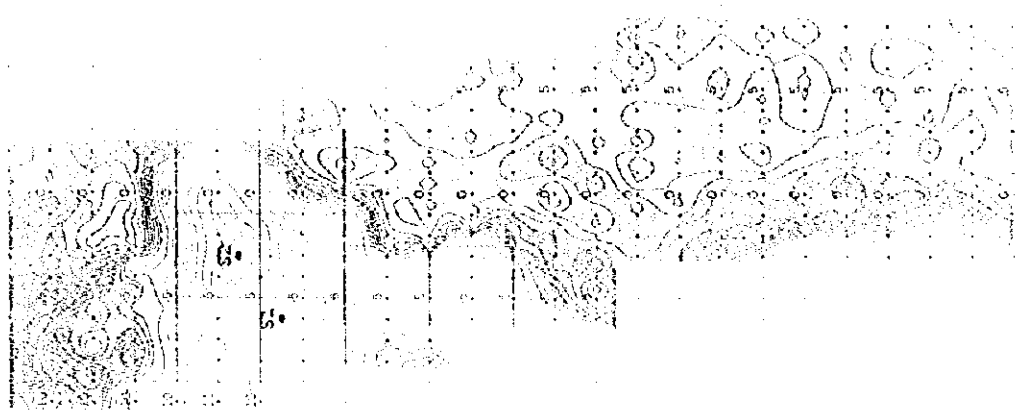

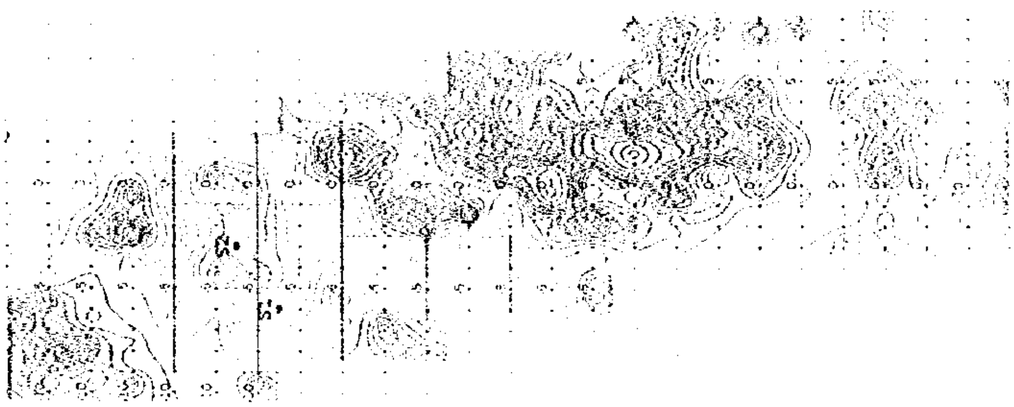

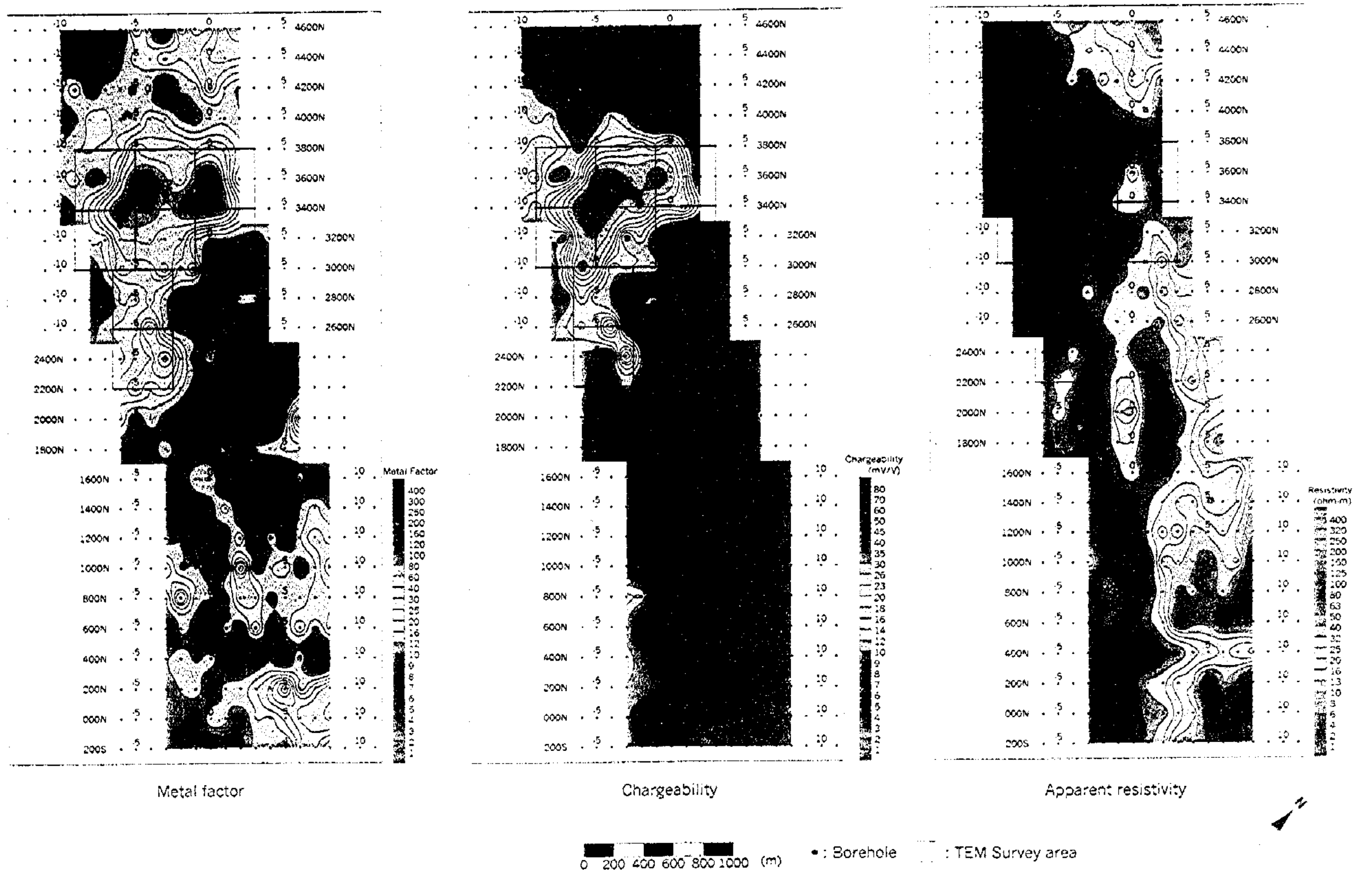

Fig. II-2-21 IP plane map of n=4 in Sarami area

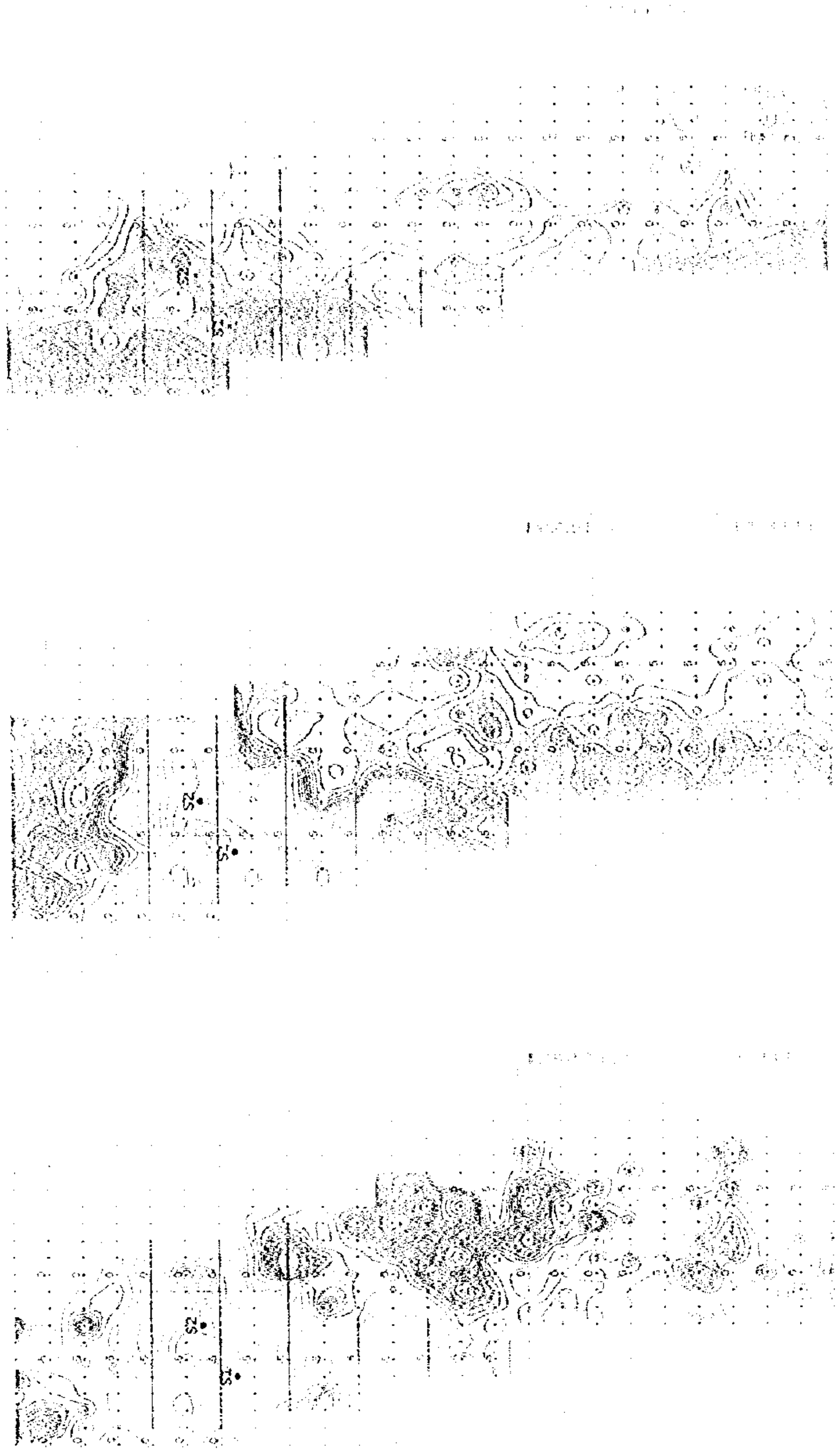
S2
S1

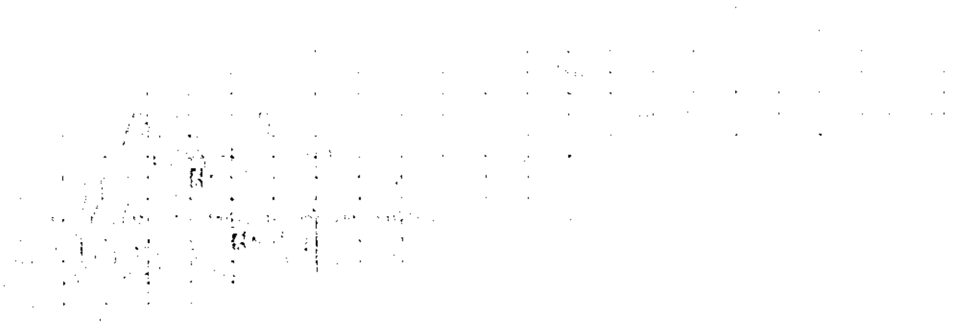

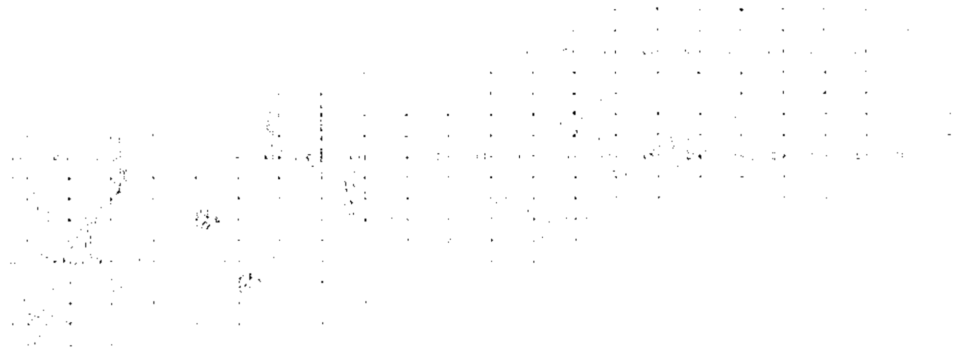

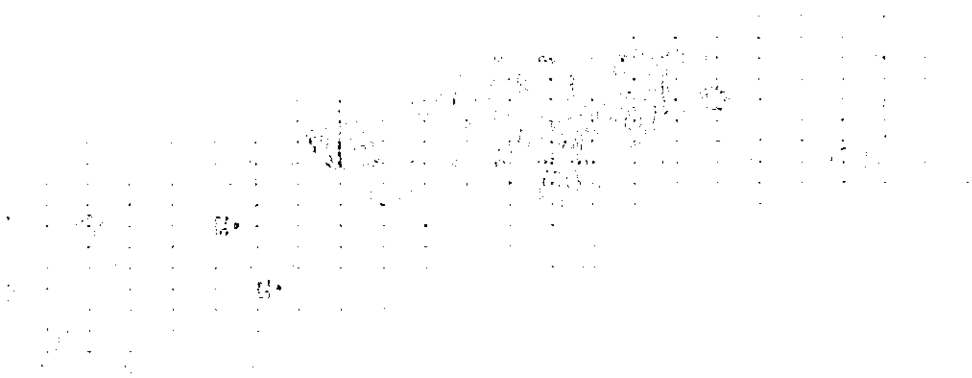

observed at depth (N=3 to 4) along the NW-SE direction. In lines 3600N to 3800N, a not so high resistivity distribution of about 60Ω-m is seen continuously distributed from west side to east end of this area.

According to the chargeability results, the chargeability distribution shows almost same pattern as the resistivity distribution (Fig.II-2-20). Relatively high values of about 20 mV/V are shown in the west end of the lines 200S to 1000N. In the north side of this area, a high value of more than 10mV/V is distributed in the west side from station No.-6 of line 1800N to station No.3 of line 3600N and in the south side of line 3800N. Particularly high chargeability distribution with values of more than 20mV/V (maximum 43mV/V) is observed distributed with a width of 400m along N-S direction and with a width of 600m along E-W direction in the vicinity of station No.-3 of lines 3400N to 3600N. A relatively high chargeability distribution is observed in the vicinity of station No.-5 of line 2200N to 2800N (Fig.II-2-16(2)).

In relation to the metal factor, a high metal factor distribution coincides with a high chargeability distribution located in the north side of the area. Particularly, the anomaly around the vicinity of the stations Nos.0 to -5 of line 3600N shows high values, and additionally, their apparent resistivity values are relatively low (Fig.II-2-18).

(3) 2D Analysis

2D analysis was performed for all the lines, however, in this report only the sections containing representative anomalies will be described. On these regards, here only the 2D results of the lines 2400N and 3600N will be briefly presented (Fig.II-2-22).

In relation to the line 2400N, it is recognized a low resistivity distribution of about 30 Ω-m at depth below the stations No. -3 to -4 (N=3 to 4). In this vicinity, high chargeability distribution shows a maximum value of about 31mV/V, with an anomalous chargeability distribution of about 200m in width along E-W direction. Low resistivity zone is seen widely distributed on the surface to the east of the station No -3, however due to the presence of low chargeabilities, this zone can not be related to mineralization. The metal factor becomes quite clear below the stations Nos. -2 to -3, showing a vertical-like pattern with anomaly values as high as 70.

As far as the line 3600N is concerned, low resistivity values of about 30 Ω-m are seen distributed at depth (N=3 to 4) of station No -4, as well as at shallow levels of stations Nos. -3 to -4. This distribution coincides with a high chargeability anomaly zone, however it is very narrow as compared to the high chargeability distribution which shows a wide zone of about 800m along E-W direction and showing especially high values (maximum 46mV/V) in its center. Metal factor anomaly distribution shows almost the same pattern as the chargeability distribution, where high values are seen in station No. -4 at depth as well as in stations Nos. -2 to -3 at shallow depth.

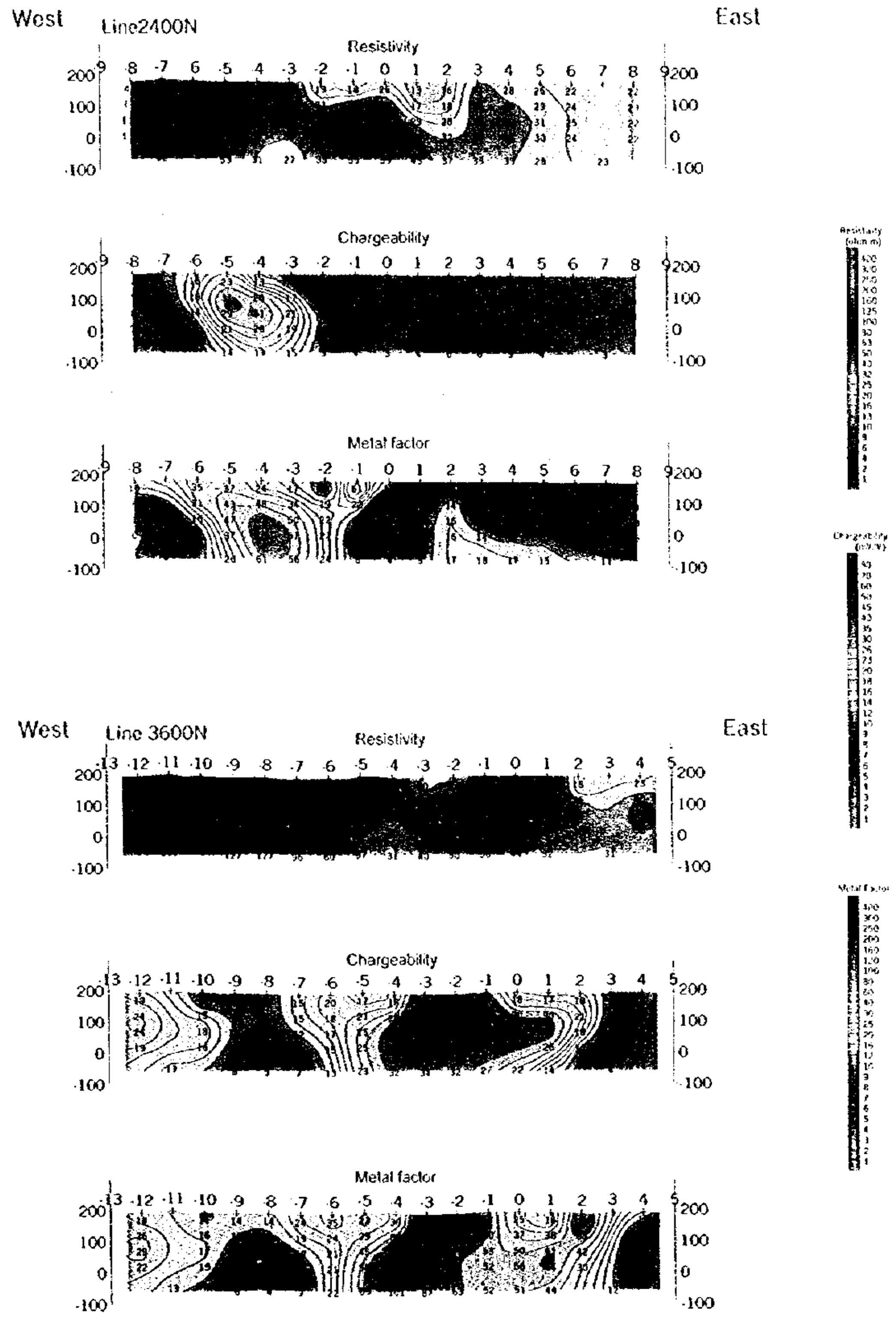

Fig. II-2-22 IP 2D model simulation on lines 2400N and 3600N on Sarami area